



ΕΘΝΙΚΟ ΜΕΤΣΟΒΙΟ ΠΟΛΥΤΕΧΝΕΙΟ  
Σχολή Πολιτικών Μηχανικών  
Τομέας Υδατικών Πόρων και Περιβάλλοντος

## **Modeling Hydrodynamics and Sediment Transport in Kremasta Reservoir**

---

**Μαθηματική Προσομοίωση της Ροής και της Στερεομεταφοράς  
στον Ταμιευτήρα Κρεμαστών**



Markos Pitsios

**Supervisor:** A. I. Stamou, Professor N.T.U.A.

**Co-supervisor:** D. Koutsoyiannis, Professor N.T.U.A.

Athens, July 2020



## Ευχαριστίες | Acknowledgments

Με την περάτωση αυτής της διπλωματικής εργασίας κλείνει ένας μεγάλος και σημαντικός κύκλος για εμένα. Παράλληλα όμως ανοίγονται κάποιες νέες πόρτες και προσφέρονται συναρπαστικές ευκαιρίες για πρόοδο και δημιουργικότητα.

Αρχικά, θέλω να ευχαριστήσω θερμά τους καθηγητές μου κ. Αναστάσιο Ι. Στάμου (Επιβλέπων καθηγητής) και κ. Δημήτριο Κουτσογιάννη (Συνεπιβλέπων καθηγητής) οι οποίοι αποτέλεσαν πηγή στήριξης, έμπνευσης και αδιάκοπης βοήθειας για εμένα. Ήταν εκεί σε κάθε βήμα, από το Σεπτέμβριο μέχρι και σήμερα, λύνοντας όλες τις απορίες και θέματα που ανά περιόδους εμφανίζονταν και καθοδηγώντας με σε κάθε νέο βήμα.

Εν συνεχεία, νιώθω την ανάγκη να τονίσω την αδιάκοπη στήριξη και συνδρομή που δέχτηκα από τον καθηγητή μου κ. Νικόλαο Μαμάση σε ζητήματα θεωρητικά αλλά και πρακτικά. Δεν θα μπορούσα ακόμη να μην αναφερθώ στους Γερμανούς καθηγητές και ερευνητές: Dr. Minh Duc Bui και Dr. Markus Reisenbuechler από το Πολυτεχνείο του Μονάχου (TUM) οι οποίοι, με δεδομένο ότι η εργασία αυτή διεξήχθη στα πλαίσια του προγράμματος ΙΚΥΔΑ σε συνεργασία με το Πολυτεχνείο του Μονάχου, υπήρξαν ιδιαίτερα βοηθητικοί σε όλο αυτό το ταξίδι.

Ακόμη ένα μεγάλο ευχαριστώ οφείλω στους υποψήφιους διδάκτορες Παναγιώτη Δημητριάδη και Γεωργία Παπαδονικολάκη που χωρίς τη συμβολή και παρακίνησή τους σε όλα τα επίπεδα αυτή η εργασία θα ήταν αδύνατον να έρθει εις πέρας. Επιπλέον, θα ήθελα να ευχαριστήσω τους διδάκτορες κ. Δημήτριο Ζαρρή και κα. Ευδοξία Λυκούδη για την παροχή σημαντικών δεδομένων, καθώς και τον ερευνητικό συνεργάτη κ. Αντώνιο Κουκουβίνο για την πολύτιμη βοήθειά του.

Τέλος, ένα ξεχωριστό ευχαριστώ ανήκει στην οικογένεια μου για όλη την ψυχολογική και υλική υποστήριξη σε κάθε βήμα αυτής της πορείας και στους φίλους μου οι οποίοι στη διάρκεια των φοιτητικών μας χρόνων μου προσέφεραν αμέτρητες αναμνήσεις, μοναδικές στιγμές, και με βοήθησαν να βελτιωθώ και να εξελιχθώ ως φοιτητής και άνθρωπος.

Πίτσιος Μάρκος

Αθήνα, 2020

## Abstract

The calculation of the sediment yield inside a reservoir is critical for the design and the operation of a dam or a hydroelectric station. More specifically, for the present thesis the estimation of soil loss is carried out using the Revised Universal Soil Loss Equation (RUSLE) and Koutsoyiannis & Tarla (1987) methods by gathering precipitation, geomorphological and topographical data, and maps. Another way to estimate the soil loss of the watershed, is to collect maps from the European Soil Data Centre (ESDAC) in grid form for every factor of the RUSLE equation, and estimate the soil loss using Geographic Information Systems. All these methods result in a mean annual value of soil loss and the use of Vanoni (1975) equation afterwards leads to the computation of the sediment yield. However, the use of flow-sediment load rating curves, based on field measurements, seems to be a more direct and precise method for this purpose. What follows next is the application of a 1D hydrodynamic-sediment transport HEC-RAS model to estimate the bed changes of Kremasta reservoir throughout the years by inputting the computed rating curves, timeseries of inflow and stage data and the initial bathymetry of the reservoir. This study could assist in extracting some meaningful conclusions regarding the exact locations of sediment deposits, the changes in bathymetry and the hydrodynamic characteristics, and understand how the design and operation of the dam and the hydroelectric station is affected by sediment deposits.

## Περίληψη στα Ελληνικά | Abstract in Greek

Ο υπολογισμός της στερεοαπορροής που καταλήγει σε έναν ταμιευτήρα είναι κρίσιμος για το σχεδιασμό και τη λειτουργία ενός φράγματος, αλλά και ενός υδροηλεκτρικού έργου. Εν προκειμένω, για τον ταμιευτήρα των Κρεμαστών χρησιμοποιώντας την Παγκόσμια Εξίσωση Εδαφικής Απώλειας (RUSLE) και τη μέθοδο των Κουτσογιάννη και Τάρλα (1987) εκτιμάται η εδαφική απώλεια μέσω της συλλογής δεδομένων κατακρήμνισης, καθώς και μέσω γεωμορφολογικών και τοπογραφικών χαρτών. Ένας άλλος τρόπος για να υπολογιστεί η απώλεια εδάφους της λεκάνης απορροής, είναι χρησιμοποιώντας χάρτες από το Ευρωπαϊκό Κέντρο Δεδομένων Εδάφους (ESDAC) σε μορφή πλέγματος για κάθε παράγοντα της εξίσωσης RUSLE και στη συνέχεια κάνοντας χρήση Γεωγραφικών Συστημάτων Πληροφοριών (GIS). Όλες αυτές οι μέθοδοι καταλήγουν σε μια μέση τιμή για την απώλεια εδάφους, και εν συνεχεία ο υπολογισμός της στερεοαπορροής γίνεται μέσω της εξίσωσης Vanoni (1975). Ωστόσο, η χρήση καμπυλών παροχής-στερεοπαροχής, με βάση τις μετρήσεις πεδίου στη λεκάνη απορροής των Κρεμαστών, φαίνεται να προσεγγίζει καλύτερα και πιο άμεσα την πραγματική τιμή της στερεοαπορροής. Αυτό που ακολουθεί στη συνέχεια είναι η εφαρμογή ενός μονοδιάστατου μοντέλου στερεομεταφοράς σε περιβάλλον HEC-RAS για την εκτίμηση των μεταβολών του πυθμένα του ταμιευτήρα εισάγοντας στο πρόγραμμα ως δεδομένα την αρχική γεωμετρία του ταμιευτήρα, τις καμπύλες παροχής-στερεοπαροχής και τις χρονοσειρές εισροών και σταθμών. Η παρούσα μελέτη θα μπορούσε να συνδράμει στην εξαγωγή ορισμένων ουσιαστικών συμπερασμάτων σχετικά με την ακριβή απόθεση των φερτών υλικών στον ταμιευτήρα Κρεμαστών, τις αλλαγές στη βαθυμετρία του, τα υδροδυναμικά του χαρακτηριστικά και τον τρόπο με τον οποίο επηρεάζεται ο σχεδιασμός του φράγματος και του υδροηλεκτρικού σταθμού από την απόθεση φερτών υλικών.

## Table of Contents

Ευχαριστίες   Acknowledgments .....	i
Abstract.....	ii
Περίληψη στα Ελληνικά   Abstract in Greek.....	iii
Table of Contents.....	iv
1 Introduction .....	1
1.1 General .....	1
1.2 Objectives of the present study .....	2
1.3 Outline of the present study .....	2
2 Literature review.....	3
2.1 Study area.....	3
2.1.1 General.....	3
2.1.2 Technical characteristics .....	4
2.1.3 Geomorphological and geological characteristics .....	6
2.1.4 Hydrogeological characteristics.....	9
2.1.5 Natural characteristics and surrounding area.....	10
2.2 Soil loss and sediment transport.....	13
2.2.1 Definitions and basic meanings .....	13
2.2.2 Water erosion and soil loss .....	14
2.2.3 Types of sediment transport.....	15
2.2.4 Reservoir sediment deposition.....	16
2.3 Methods to estimate soil loss and sediment yield .....	18
2.3.1 General.....	18
2.3.2 RUSLE method.....	18
2.3.3 Other methods to estimate soil loss and sediment yield .....	32
3 Estimation of soil loss and sediment yield .....	33
3.1 First method: RUSLE equation .....	33
3.1.1 R-factor .....	33
3.1.2 K-factor .....	39
3.1.3 LS-factor .....	42
3.1.4 C-factor .....	43
3.1.5 P-factor.....	44
3.2 Second method: GIS modeling .....	46
3.2.1 Geometry of the surrounding area .....	47
3.2.2 Grids of RUSLE factors.....	48

3.2.3	Soil loss.....	51
3.3	Aggregated results of the two methods and further calculations .....	52
3.3.1	Comparison of the two methods .....	52
3.3.2	Estimation of sediment yield .....	52
3.4	Koutsoyiannis & Tarla (1987) method.....	53
4	Estimation of sediment yield using rating curves.....	55
4.1	Collection of data .....	55
4.2	Flow - sediment load rating curves .....	57
4.2.1	First case .....	57
4.2.2	Second case.....	60
4.2.3	Comparison with Zarris (2019) study .....	64
4.3	Comparison of the four methodologies developed .....	65
5	Sediment transport analysis in Kremasta reservoir .....	66
5.1	Calculation of each river flow .....	66
5.2	Preparation of geometric data using Civil 3D modeling.....	68
5.2.1	Description.....	68
5.2.2	Geometric data .....	69
5.2.3	Creation of cross sections .....	70
5.3	Theoretical background of HEC-RAS .....	73
5.3.1	General.....	73
5.3.2	Steady flow .....	74
5.3.3	Unsteady flow .....	82
5.3.4	Quasi-unsteady flow .....	84
5.4	Application of HEC-RAS .....	85
5.4.1	General.....	85
5.4.2	Input data .....	86
5.4.3	Sediment transport simulation .....	95
6	Results and Conclusions.....	97
6.1	Sediment deposition .....	97
6.2	Comparison with other studies.....	100
6.3	Hydrodynamic characteristics .....	103
6.4	Final Conclusions.....	106
6.5	Proposals for further research .....	107
	References.....	108
	Appendix.....	111



# 1 Introduction

## 1.1 General

Floods are defined as the physical phenomenon, during which an initially dry land area is covered by water. Floods are normally caused by extremely high precipitation events or inadequate flood control system. Their evolution mainly depends on geomorphological factors such as soil stability and permeability, vegetation cover, as well as the geometrical characteristics of the river basin. Roughly the same factors can affect the soil loss of a watershed. There are several strategies -described thoroughly below in the present study- to prevent or to diminish the risk of a serious soil loss event.

Generally extreme floods cause a critical soil loss inside a river basin. This accounts for an important sediment flow which can lead to a problematically high accumulation of sediment discharge inside the reservoir. The quantity of sediment load entering the reservoir mostly depends on the upstream drainage network (density, frequency, slope gradients, watershed area) the hydraulics of the river flow and some climatic, soil and geomorphological parameters. The accumulation of sediment volume inside a reservoir is caused by the gradual reduction of the flow velocities when the river enters the reservoir. As a result, the coarse materials deposit at the upstream parts of the reservoir forming the well-known deltaic deposits, while the fine sediments can transfer to downstream parts and deposit near the dam.

There is a plethora of detrimental aspects that comes with the extensive accumulation of dead volume inside a reservoir and is usually a critical issue regarding the design and operation of dams and hydroelectric stations. Firstly, there is an important decrease in the storage capability of the reservoir, while the entrance of sediment inside the water abstraction could be catastrophic for a hydroelectric station. Moreover, the degradation of the water quality is a common phenomenon and the sediment deposits might have some negative geomorphological effects on the river deltas.

A high percentage of the sediment yield in rivers in Greece is transferred during a few intense flood events and is well-known as wash load. However, during dry time periods when there is only transfer of bed load, the total bed load is only a small percentage of the wash load (Zarris et al., 2001). The materials that constitute the wash load, come from the surface of the watershed, and are transferred entirely as suspended load.

Thus, the water level during intense rain episodes is of great importance and can highly influence the location of sediment deposition inside the reservoir. For instance, high water level will cause a deposition of sediment on the upstream parts of the reservoir, whereas low water level facilitates the sediment transport to the downstream levels, near the dam. It is critical to point out that during the design of reservoirs worldwide, the prediction of the long-term dead volume and the simulation of reservoir sediment transport are sometimes omitted. Consequently, the estimation of dead volume as a main design figure is critical and should be treated with caution because it can lead to a wrong estimation of the net storage volume of a reservoir (Zarris et al., 2002).

## 1.2 Objectives of the present study

The **case study** of the developed methodology is the watershed of Kremasta containing the reservoir of Kremasta which is located between the counties of Evritania and Aitoloakarnania in Western Greece. The reservoir covers an area of 80.6 (km<sup>2</sup>) (biggest in Greece) and was formed in 1965 when the dam of Kremasta was built. The inflows of the reservoir are attributed to the rivers of Acheloos, Agrafiotis and Tavropos (Megdovas).

The **scope** of the present undergraduate thesis, entitled as: “Modeling Hydrodynamics and Sediment Transport in Kremasta Reservoir” is to estimate the annual sediment yield that enters Kremasta reservoir pool and to perform a sediment transport analysis in it. Moreover, the aim is to observe how the reservoir bed changes throughout the years due to sediment deposition, extract meaningful conclusions for the design and operation of the reservoir and develop proposals for further academic research.

The study was accomplished using HEC-RAS, the software developed by the Hydrologic Engineering Center of the U.S. Army corps of Engineers. Specifically, HEC-RAS simulates open channel flow (river systems) and sediment transport in rivers and reservoirs.

## 1.3 Outline of the present study

The current thesis is structured in six chapters. A brief description of these chapters follows below:

- **Chapter 1:** Introduction. Subject of the current thesis and case study. Scope and structure of the current thesis.
- **Chapter 2:** Description of the study area, the characteristics of the dam and the hydroelectric station, some geological and geomorphological features. Presentation of the main methodologies to estimate the soil loss and the sediment yield.
- **Chapter 3:** Application of RUSLE equation, GIS modelling, Koutsoyiannis and Tarla method. Usage of Vanoni equation to calculate the annual and long-term sediment yield that ends up into the reservoir.
- **Chapter 4:** Estimation of annual sediment yield using Flow-Sediment Load rating curves. Rating curves are created by deploying sediment data from field measurements and an equation between flow and sediment load is created. Timeseries of inflow data are available.
- **Chapter 5:** Calculation of the three different river flows and processing of the geometric data of the reservoir in Civil 3D 2019 to create cross sections. Input of geometric, flow and sediment data in HEC-RAS and execution of a 1D sediment transport analysis.
- **Chapter 6:** Observation of the effect that deposition has on the bed of the reservoir (part of Acheloos river) and of the hydrodynamic characteristics and conclusions on how the cross sections change throughout a period of 42 years from 1966 to 2008. Proposals for further projects or research.

## 2 Literature review

### 2.1 Study area

#### 2.1.1 General

Kremasta artificial reservoir and dam are located at the region of Western Greece and especially at the aquatic department of Western-Central Greece. It is one of the oldest in Greece as it started to operate in 1966. This time is enough to create a large volume of sediment inside the reservoir and add more fidelity to the research study (Zarris, 2019). The reservoir also includes a hydroelectric station with four units of electricity production and a diversion tunnel for the extra water and the outlet flow.

The three main rivers flowing into the reservoir are Acheloos, Agrafiotis, Tavropos/Megdovas and other smaller tributaries such as Trikeriotis. The area of Kremasta reservoir (80.6 km<sup>2</sup>) and its storage volume (4495 hm<sup>3</sup>) are so big that is reasonable to assume that its capability to withhold sediment has a value close to 1. Moreover, the rivers, which flow into the reservoir, have remarkably high sediment discharge due to the erosive flysch soil of the watershed. The Figure 2.1-1 is a satellite image displaying the reservoir and the surrounding area which contains the basin of Kremasta.



**Figure 2.1-1:** Satellite image of Kremasta reservoir and the surrounding area (Obtained by Zarris, 2019)

### 2.1.2 Technical characteristics

The reservoir and hydroelectric station of Kremasta are the biggest in Greece. The area of the reservoir at the overflow level is approximately 80,6 (km<sup>2</sup>), while the corresponding total storage volume at the higher operation level of water equals to 4.495 (hm<sup>3</sup>). The area of the watershed of Kremasta and its four main rivers, including the marshes and water collections, is 3.570 (km<sup>2</sup>), while the average annual inflow for the hydrological years of 1966-67 to 2000-01 for the reservoir is 117,9 (m<sup>3</sup>/s) (Zarris et al., 2001). The net area of the watershed, used below to calculate the soil loss, is 3.292 (km<sup>2</sup>). All these technical characteristics of the dam and the hydroelectric station are displayed at Table 2.2-1.

**Table 2.2-1:** Technical characteristics of the dam, the reservoir and the hydroelectric station (Obtained by Zarris, 2019)

<b><i>Kremasta Reservoir characteristics</i></b>	
Higher water level	+282 m
Lower water level	+227 m
Total storage volume at higher water level	4.495 hm <sup>3</sup>
Net storage volume	3.300 hm <sup>3</sup>
Maximum area	80,6 km <sup>2</sup>
Mean area	60,9 km <sup>2</sup>
Altitude of dam's ridge	+287 m
<b><i>Hydroelectric Station characteristics</i></b>	
Installed hydropower	437 MW
Gross head	136 m

The diversion tunnel has a diameter of 12,5 (m) and length of 808 (m). The height of Kremasta dam is 153 (m) and its width is 500 (m), being the tallest earthen dam in Europe and having an impermeable clay core, two shells of sand and gravel and a cobble layer (Figure 2.1-3). Furthermore, the mean annual precipitation at Kremasta watershed is 1.433 (mm) and the altitudes of the watershed range from +284 (m) to +2.433 (m), while the mean depth of the reservoir is 60 (m) (Zarris, 2019). The hydroelectric station (Figure 2.1-2), which is controlled by the National Energy Center in Athens, functions with 4 pipes leading the water to 4 turbines of 109 (MW) power each and it produces the highest proportion of hydroelectric energy among all the hydroelectric station in Greece (limnikremaston.gr).

Lots of studies were held in order to build the dam. The first research was carried out by Sehn and Dubois between 1918 and 1921 on behalf of the "Ministry of Public Works". After that, preliminary studies were held by the American company "Cooper" and the "Public Power Corporation S.A." of Greece. Lastly, the American company "Kaizer" performed a construction study and the supervision of the project in 1960 (limnikremaston.gr).

The Figure 2.1-2 below illustrates the several significant constructions of Kremasta reservoir such as the dam, the spillway and the hydroelectric station. Moreover, it shows the outlet flow that leaves the dam (either by the spillway or by the diversion tunnel), whose purpose is not only to maintain the ecosystem of the region but also to release the extra water of the reservoir. The mean value of the outlet flow of Kremasta dam is approximately 21,3 (m<sup>3</sup>/s).

This specific flow is defined as the next part of Acheloos river which continues downstream of Kremasta to fill the reservoir of Kastraki. The dam of Kastraki was also built on Acheloos riverbed and is 95 (m) tall and 530 (m) long, while it contains roughly 1 (hm<sup>3</sup>) of water. After Kastraki the flow continues to flush into Stratos dam (60-70 hm<sup>3</sup> net volume) which is the last one in the sequence of Acheloos dams. This whole drainage network of Western Greece while be described more thoroughly in next chapters.



**Figure 2.1-2:** Kremasta dam, spillway and hydroelectric station  
(Obtained by: agriniopress.gr)

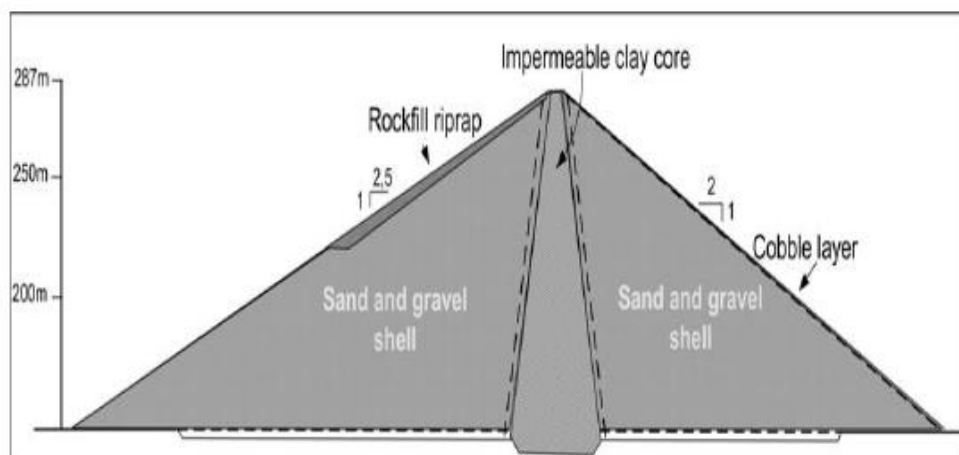


**Figure 2.1-3:** Cross section of Kremasta dam in the max width  
(Obtained by P.P.C. of Greece)

### 2.1.3 Geomorphological and geological characteristics

Watersheds are considered as an “open natural system” with inputs and outputs being high proportions of mass and energy (precipitation, river flows, sediments, and evapotranspiration). This specific approach gives us the chance to correlate the type of terrain a watershed has, with the erosion, sediment transport and deposition procedures. These, of course, are dependent on several other factors (Zarris, 2019). The area of the dam and the reservoir is structured by sedimentary formations of the Gavrovo flysch. The location of the dam is a narrow aisle which has been opened into shingle layers that alternate with several layers of siltstones (Kalfountzos, 2013).

To begin with, the area of the watershed of Kremasta close to Acheloos river is mountainous and is divided into two sections. The first one is northern and upstream of Sykia and the other one is southern and downstream of Sykia. In the upstream part of Sykia, steep slopes are formed mainly in areas where the geological background consists of hard formations of the Pindos zone and the soil layers are multifaceted with slopes almost vertical. At the same time, deep and meandering gorges are created such as that of Fagos which is located between Myrofyllou and Mesounta of Arta. The steep slopes, which are either bare or with dense vegetation, are fragmented by cracks, creating smaller ridges and ravines, rendering the area extremely inaccessible and dangerous. In the area between Gardiki and Mesochora, intense landslides are observed.

In the lower part, that is, from Sykia and to the south, the terrain changes dramatically, as the mountainous features decrease, and the morphology becomes smooth with milder slopes. The riverbed widens and is mainly filled with limestone material, the size of which varies from gravel to rock. This material creates elongated islets resulting in the branching of the main riverbed into two or more riverbeds and the appearance of a complicated flow (Figure 2.1-4). These islets are created due to the large sediment load of the upstream part of the river basin and the inability of the river flow in this section to completely transport this material downstream. The decrease in the transport capability of the flow is mainly due to the widened riverbed but also to the reduced slope. The watersheds of Agrafiotis and Tavropos have approximately the same geomorphological characteristics as those of the eastern part Acheloos river basin since the geological structure is the same (Kalfountzos, 2013).

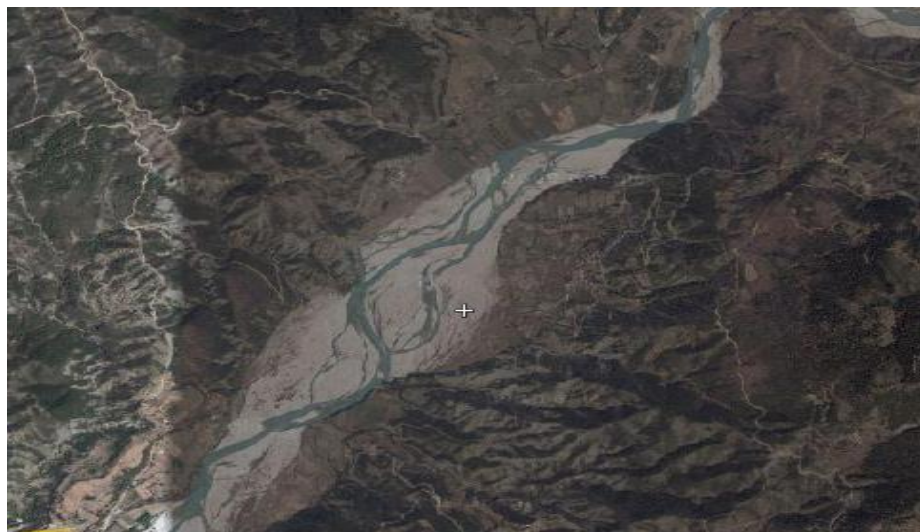


**Figure 2.1-4:** Islets and complicated flow of Acheloos river (Obtained by Zarris, 2019)

The study of the characteristics of the geological formations that exist in the basin of the Kremasta reservoir and in particular at the location of Avlaki, helps significantly in the initial assessment regarding the erosion of soil and geological formations. The area occupied by the basin of Kremasta reservoir is structured by the formations of the “Ionian”, “Gavrovo”, “Pindos” and “Hyperpindiki” zones, as well as by newer formations. Thus, geological base of Kremasta basin mainly consists of flysch of Pindos and Gavrovo, limestone of the same regions and alluvial deposits, as observed in Figure 2.1-5 below (Vachaviolos, 2014):

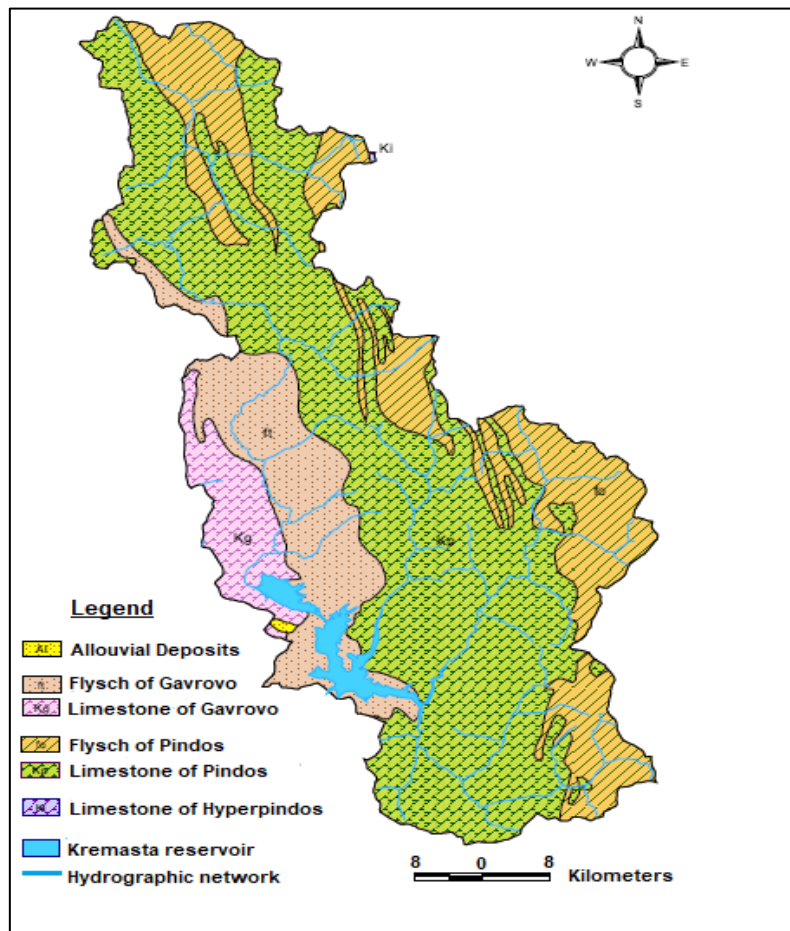


**Figure 2.1-5:** Geological formations of the watershed of Kremasta reservoir  
(Obtained by Zarris et al., 2001)

The geotectonic zones, in which the Greek mountain ranges are subdivided, consist of specific stratigraphic sequence and tectonic behavior of their geological formations, elements that mainly depend on their geotectonic position, geodynamic movements, and tectonics deformation, but also their ancient geographical location.

Due to the intense tectonic processes, the Greek area is characterized by highly fragmented hydrographic networks. More specifically, it is drained by many small and medium mountain streams that cross steep, narrow valleys, with strong flow and sediment load figures, flowing ashore with a significant slope. However, there are some larger low-slope rivers that cross these zones, mainly in western Greece, forming extensive floodplains and deltaic plains, presenting significantly higher sediment yields than the rest of the available data set (Zarris, 2019).

A series of fractures have been found near the dam during the initial geological study before the construction (1963-1966). They are in an order parallel to the axis of the dam. They are symbolized with letters from A to F and their locations are evident in Figure 2.1-6:

- Fracture A: in the upstream boundary of the dam,
- Fracture B: upstream of the axis of the dam, close to the water abstraction,
- Fracture C: upstream of the axis of the dam,
- Fracture D: downstream of the axis of the dam,
- Fracture E: in the middle of the distance between the axis and the downstream basis of the dam,
- Fracture F: downstream of the dam.

The results of the permeability tests showed that the fractures are impermeable in places with mudstones, while they are permeable in locations where pebbles exist (ECI, 1974· Kalfountzos, 2013).

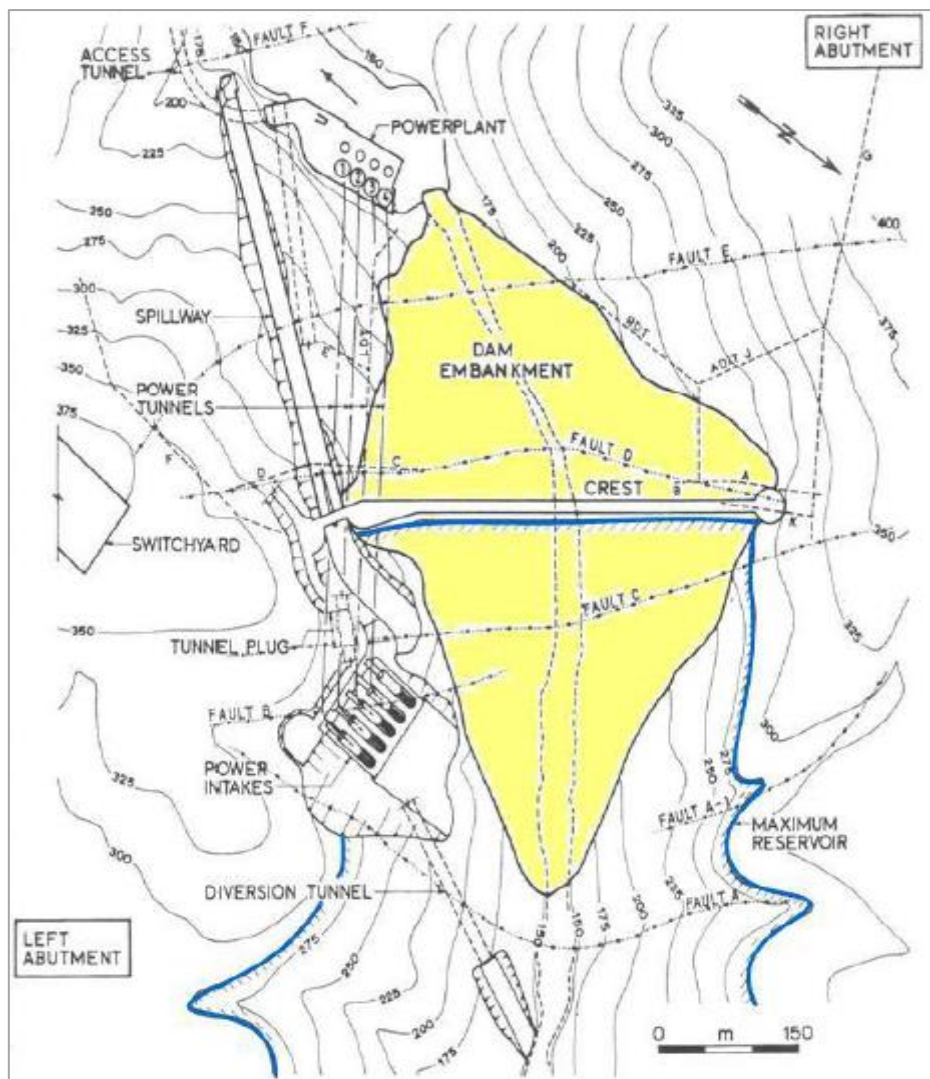


**Figure 2.1-6:** Ruptured zones near the dam of Kremasta (Obtained by ECI, 1974)

#### 2.1.4 Hydrogeological characteristics

From the above it is obvious that the watershed is mainly constituted of flysch and limestone. Regarding the hydrogeological side of this issue these formations have the following natural and hydrological characteristics, derived from the hydrogeological map of the Water Department of Western Central Greece (Ministry of Development and Investments, 2005).

The flysch is generally a geological formation with significant erosion, while on the contrary limestone is a low erodible material regarding the production of suspended sediment. More specifically, Koutsoyiannis and Tarla (1987) classified the soil formations according to their erosion rate using an empirical factor named erosion factor,  $\kappa$ . This coefficient for flysch was set at the value  $\kappa_1 = 1$  while for limestones it was set at  $\kappa_3 = 0.1$  (Zarris, 2019).

Classification of geological formations into three categories according to their erodibility by water, using the  $\kappa$  coefficient as an empirical measure of the erodibility (Koutsoyiannis and Tarla, 1987):

- |   |                  |
|---|------------------|
| 1. Category of high erodibility:<br>alluvial deposits, flysch                             | $\kappa_1 = 1$   |
| 2. Category of medium erodibility:<br>sandstones, marls, slates                           | $\kappa_2 = 0,5$ |
| 3. Category of low erodibility:<br>limestones, dolomite, metamorphic rocks, igneous rocks | $\kappa_3 = 0,1$ |

By using this method, it is easy to estimate a mean indicator of the erodibility of a watershed and will be used below in the present study to estimate the sediment yield.

The flysch of Gavrovo usually has high values of strength and permeability, especially its hard rocks, which due to the existence of cracks. The flysch of Pindos has some obvious signs of tectonic deformations (cracks, inversions etc.), whereas it is often characterized as unstable because of the frequent contacts among the layers in combination with the intense terrain and the steep slopes (Zarris, 2019). Limestone is more often found in the basins of Agrafiotis and Tavropos and is generally characterized by moderate mechanical erosion. The limestone of Gavrovo has moderate to high water permeability and shows intense karstification, due to its significant chemical erosion. Their large surface growth, their intense tectonic stress, their lithological composition, and their stratigraphic structure contribute to the development of porous cracks and discontinuities (secondary porous). As a result, their water permeability ranges from moderate to high (Zarris, 2019).

The water permeability of a formation has velocity dimensions (m/s) and is measured by using the permeability coefficient ( $K$ ) which expresses the distance the rocks can be classified into categories of permeability according to Zarris (2019):

- High permeability ( $K = 10^{-1} - 10^{-3} \text{ m/s}$ ): limestones
- Medium permeability ( $K = 10^{-3} - 10^{-5} \text{ m/s}$ ): alluvial deposits, sandstones, shingles
- Low permeability ( $K = 10^{-5} - 10^{-7} \text{ m/s}$ ): marls, clay, flysch, volcanic rocks

### 2.1.5 Natural characteristics and surrounding area

Figure 2.1-7 shows the drainage network of this specific area in Western Greece which includes a system of 6 different dams connecting with each other and the diversion tunnels of Acheloos river. The whole system takes advantage of Acheloos river which derives from mountain range of Pindos and more specifically the mount Lakmos and after 225 (km) of distance it empties into the Ionian Sea. Acheloos is the 2<sup>nd</sup> longest river in Greece and 4 hydroelectric stations (Kremasta, Kastraki, Tavropos, Stratos) deploy its water to produce energy (limnikremaston.gr).

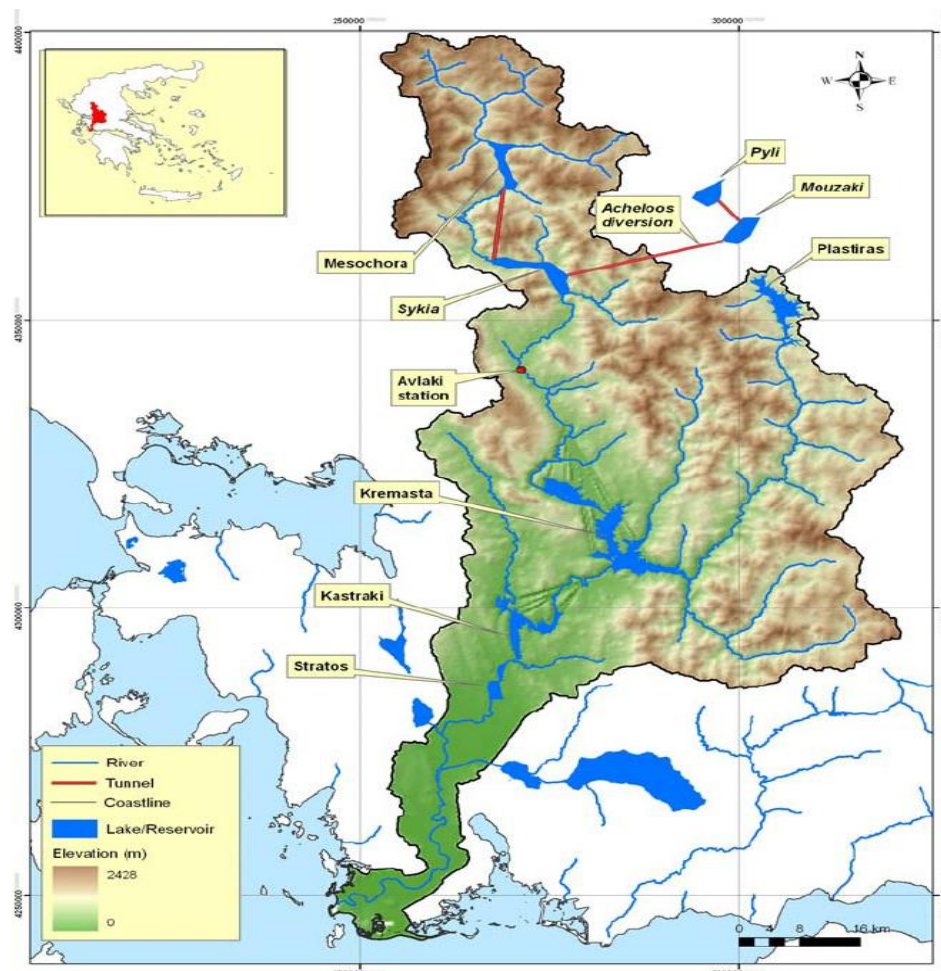


**Figure 2.1-7:** Hydrographic network of the surrounding area (Obtained by Zarris, 2019)

Lots of villages such as Episkopi village “disappeared” below water level when the reservoir was full. Along with the old Tatarna bridge and some other historical bridges and monuments, the monastery of Episkopi also sank (limnikremaston.gr). Figure 2.1-8 below shows the bridge of Episkopi -near the old village- which connects the two counties of Evritania and Aitolokarnania. Another bridge near the homonymous monastery is the new bridge of Tatarna displayed in Figure 2.1-9. The surrounding area and the reservoir of Kremasta are included in the protection program Natura 2000. Moreover, the reservoir is used for recreational activities such as Canoe-Kayak and Rafting. The reservoir of Kremasta is 57 (km) away from the city of Kremasta and 60 (km) away from the city of Agrinio, while the dam is very close to the village Kremasta Sykias from which it took its name (lakesnetwork.org).



**Figure 2.1-8:** Bridge of Episkopi (Obtained by: wikipedia.gr)



**Figure 2.1-9:** Bridge of Tatarna (Obtained by: iaitoloakarnania.gr)

The dam was built on a narrowing of the bed of Acheloos river, at the point where an old myth says that the hero Katsantwnis jumped from the one riverbank to the other, so that he escapes from the Turkish forces. Hence, this place was named “The jump of Katsantwnis” (naturagraeca.com).

Near the reservoir lots of wildlife refuges (such as Kanala, Velouxi, Megdovas, Agios Nikolaos) do exist. The flora and fauna of the region consist of a wide range of plants, trees and animals, mainly because of the big length of coastline of the reservoir and the habitats it contains. Around the lake there is mackerel vegetation with species such as yew, arbutus and big trees such as oak, chestnut and plane trees. The area also has a broad variety of reptile fauna and birdlife. Furthermore, the lake is the habitat of lots of fish species like eels (*Anguilla anguilla*), the Cyprinus (*Cyprinus carpio*), the Peloponnesian bream (*Barbus peloponnesius*), the cobras (*Coregonus lavaretus*), the herbivorous cypress (*Ctenopharyngodon idella*) etc. (naturagraeca.com).

The incomparable beauty of the lake with its turquoise water, fjords created, and the numerous small islands creates an impressive environment reminding us of some exotic destinations (lakesnetwork.org). It also offers a great habitat for animals to live in and for tourists to admire (Figures 2.1-10 and 2.1-11).



**Figure 2.1-10:** Acheloos islets and exotic nature (Obtained by: greekreporter.gr)



**Figure 2.1-11:** Kremasta reservoir (Obtained by: greenfromgreece.gr)

## 2.2 Soil loss and sediment transport

### 2.2.1 Definitions and basic meanings

- *Sediment yield*,  $S_Y$ , is the figure that correlates three major natural processes: soil loss, sediment transport, sediment deposition. It represents the total mass of sediment that drains from a cross-section of a river in the unit of time divided by the area of the upstream watershed (mass / time / area) (Vanoni, 1977).
- *Sediment discharge*,  $Q_S$ , represents the total mass of sediment that drains from a cross-section of a river in the unit of time, without including the area of the watershed (mass / time).
- *Gross erosion* describes the quantity of soil that detaches from the ground surface of the basin due to the action of the rainfall and runoff in the unit of time and area (mass / time / area). *Net erosion* is the figure that expresses the percentage of sediment that detaches from the ground surface and does not deposit inside the same unit of area (Zarris, 2019).
- *Sediment Delivery Ratio*, *SDR*, is the ratio of sediment yield divided by the total soil loss and expresses the percentage of detached sediment that is transported as surface runoff to a specific location such as the reservoir. It is a dimensionless figure, always lower than 1.

The three rivers with the highest mean annual sediment discharge in the world are river Huanghe (China), river Ganga (India) and river Amazon (Brazil). Huanghe, although its basin is 1/8 of Amazon's basin and its mean annual runoff much less than the runoff of Amazon, had a mean annual sediment discharge  $1,1 \cdot 10^9$  (t) for the period 1950-1980. This value is close to these of Amazon and Ganga (Figure 2.2-1). This happens due to the significant soil erosion of the loose soils of China and the intense storms that result in extremely high runoffs from August to October. Another interesting case is that of Taiwan, where the mean annual value of sediment load of the island was measured  $300 \cdot 10^6$  (t) (sediment yield  $10000 \text{ t/km}^2$ ), a figure that is slightly lower than the total sediment discharge of U.S.A. (Zarris, 2019).

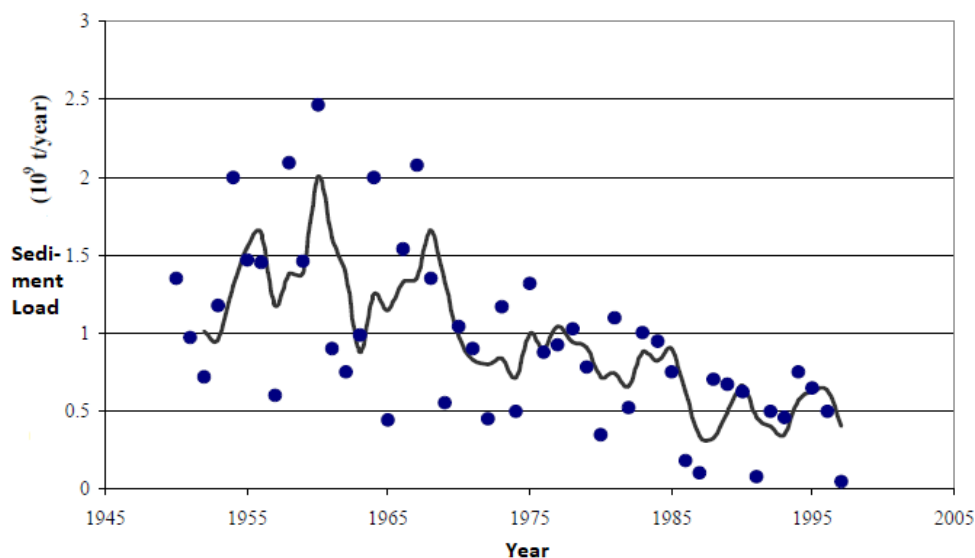


**Figure 2.2-1:** Annual sediment load of river Huanghe (Obtained by Zarris, 2019)

### 2.2.2 Water erosion and soil loss

Soil Erosion is a natural process of detachment, transport and deposition of soil or rock material due to water or wind. Hydrology is mainly engaged with water erosion which is caused by precipitation or surface runoff. The main factors that contribute to water erosion are the climatic, hydrological, geological, geomorphological, vegetation and the cover management situation of the examined region.

There are several different types of water erosion, but they can generally be grouped into four main types. These are inter-rill erosion, rill erosion, gully erosion, and streambank erosion. Inter-rill erosion, also known as raindrop erosion, is the movement of soil by rainfall and its resulting surface flow. Erosion also tends to remove the lighter, smaller soil particles first (such as clay and silt), leaving fine and coarse sand behind. Transported materials are often high in nutrients and fine particles (Renard et al., 1991).

#### A. Four main types of water erosion (gld.gov.au)

*Inter-rill erosion* also known as raindrop erosion, is the movement of soil by rainfall and its resulting surface flow. It is primarily caused by rainfall, but other factors such as climate, elevation, topography, and vegetative cover also contribute to this type of erosion.

*Rill-Sheet erosion:* Rill erosion occurs when runoff water forms small channels as it concentrates down a slope. These rills can be up to 0.3m deep. If they become any deeper than 0.3m they are referred to as gully erosion. Sheet erosion occurs when a thin layer of topsoil is removed over a whole hillside paddock and may not be readily noticed

*Gully erosion:* refers to the movement of soil by larger streams of water. This type of erosion scours channels in the soil that are at least one foot deep and cannot be smoothed over completely by normal agricultural operations.

*Streambank erosion:* it is caused by fast-running rivers and streams cutting into the banks. This type of erosion can be found at the lower end of stream tributaries and in streams that have relatively flat gradients. This type of erosion can cause large masses of soil to slip down slopes and damage surrounding fields.

#### B. Categorization of some rocks based on resistance to erosion (Efstratiadis et al., 2015)

*High resistance to erosion:* fine-grained granites, strongly compacted sandstones, limestones (generally), gabbro, quartzites

*Low resistance to erosion:* crystalline granites, slightly compacted sandstones, basalt (generally), dolomites, marbles, soft sediments, slate, flysch

Soil erosion as a term is sometimes confused with soil loss. However, soil loss comprises the first part of the erosion process -the detachment of soil materials- which happens before the transport and deposition of sediment. It is expressed in mass units divided by the area of the basin and most of the existing formulas and methods calculate the soil loss in the first place and afterwards the transport and deposition (Vachaviolos, 2014).

### 2.2.3 Types of sediment transport

The distinction of sediment into categories can be held in terms of two factors: (a) the way they are transported and (b) their origins. The transported material can be divided in suspended load, when sediments are transferred by the turbulence with exceedingly rare contact to the riverbed and the bed load, when sediment are totally in contact with the riverbed during transportation. This distinction is not totally trustworthy because sometimes sediment of the same size and same mineralogical composition can be transported either as bed or as suspended load, depending on the hydraulics of the flow (flow velocities, turbulence). Generally, there a notion that bed load sediment are those with a size bigger than 0,85 (mm), a distinction that is based on the criterion of equality between the subsidence velocity and the traction velocity (Koutsoyiannis and Tarla, 1987· Zarris et al., 2001).

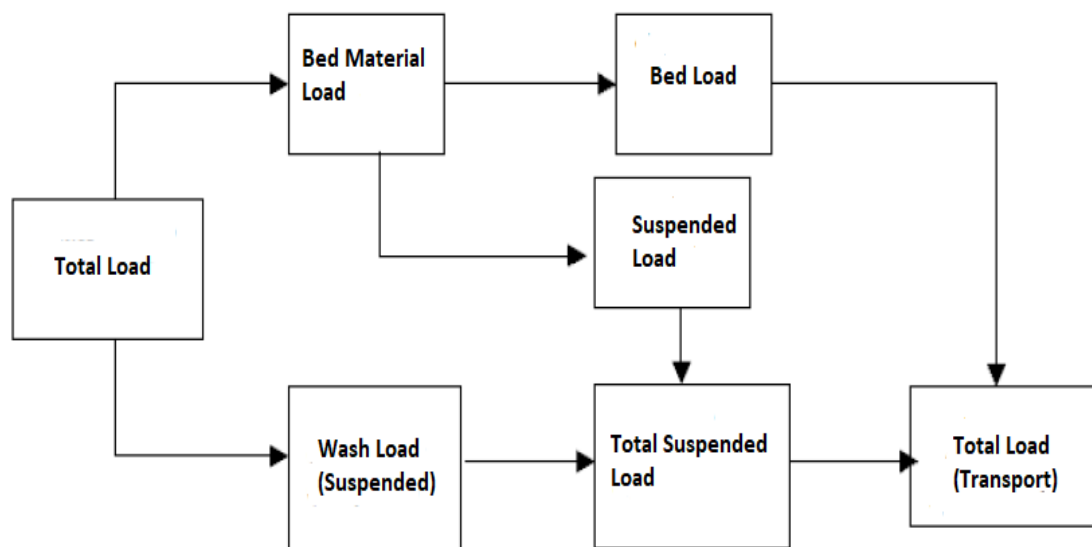


**Figure 2.2-2:** Types of sediment transport (Obtained by Zarris et al., 2001)

In terms of their origins, they can be separated in bed material load and wash load. The bed material load, which can be transported either as bed load or suspended, refers to sediment that already exists at the riverbed of the drainage network and is the only source of sediment during dry time periods. On the other hand, wash load is only produced during intense flood events, comes from the soil erosion of the watershed, and finally ends up inside the river by small channels or streams. Wash load is transferred along with the flooding and is usually finer (such as clay); hence it is most of the time suspended (Koutsoyiannis and Tarla, 1987). It is also easily measurable because it is evenly distributed across the cross-section of the riverbed. All these types of load and divisions are presented in Figure 2.2-2.

The sediment discharge of the wash load inside a stream or a channel mostly depends on the existence of sediment available to erode and move, rather than the hydraulic capability of the flow to transport them. Especially in the Mediterranean countries, wash load comprises a remarkably high percentage of the total sediment yield of a basin (Zarris et al., 2001). The time and space scale play an important role in the development

of the erosion and the parameters that define it (Vachaviolos, 2014). Figure 2.2-3 below illustrates the different stages of this process and when and where they take place.

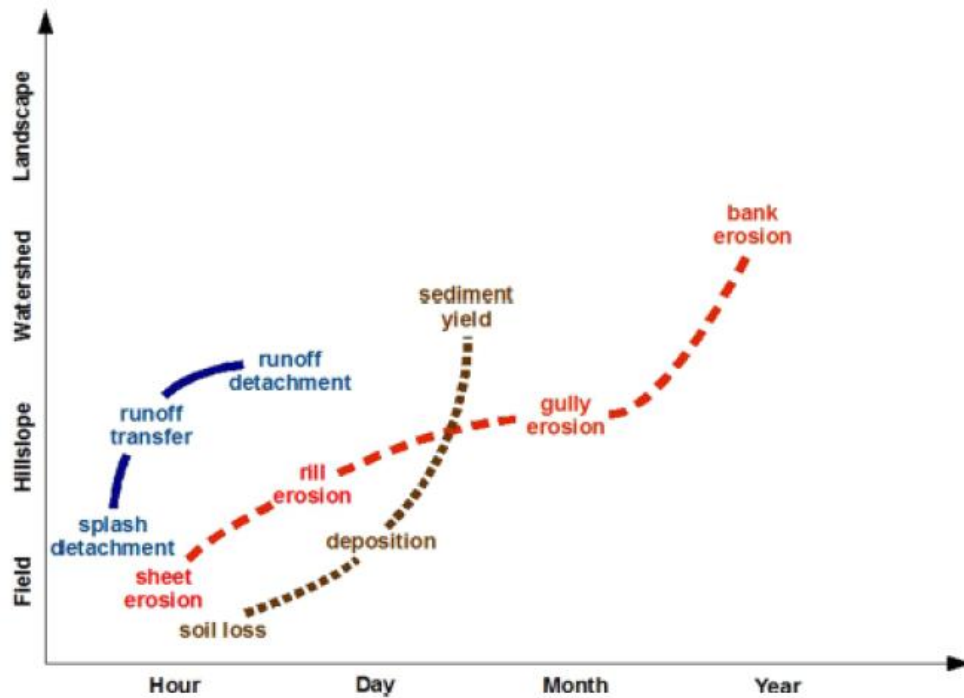


**Figure 2.2-3:** Process of erosion (blue line), types of erosion (red line), significant sediment procedures (brown line) in space-time scale (Obtained by Vachaviolos, 2014)

#### 2.2.4 Reservoir sediment deposition

The final deposits of sediment could take place, depending on the circumstances, either in natural sources -river deltas, sea, lakes- or inside artificial ones such as reservoirs. The deposition of sediment inside a reservoir is a matter of great academic interest and will be examined further during the present thesis.

The validity and reliability of the estimation of the sediment deposits -usually for a 100-year-period- is critical for the proper design of the dead volume of the reservoir and generally for the sustainability of the project. During the design of the reservoir and dam, the choice of dead volume and the corresponding water level, affect the stage of the water abstraction which of course defines the potential to generate electric energy at the downstream hydroelectric station (depends on gross head). Moreover, an underestimation in the prediction of the dead volume could result in lower water supplies.

Another case, and probably the most common, is for a study to overestimate the sediment deposits and the dead volume which usually leads to an extreme increase of the technical and economic figures of the project. Nevertheless, there are also cases in which an underestimation takes place such as Louros dam in Epirus, where due to wrong calculations, the net storage volume (0,37 hm<sup>3</sup>) filled with sediment within a few years (Vachaviolos, 2014).

Regarding the distribution of sediment inside a reservoir the first studies supported that sediment is transported up to the dam and depositing there. After several hydrographic surveys of reservoirs mainly in the U.S.A. and South Africa this theory proved wrong. What is now believed is that sediment is evenly distributed across the reservoir bed, gradually reducing the storage volume in almost every location. However, a significant part of the total sediment yield deposits at the river deltas (mouth) -the location where the river enters the reservoir and flow velocities decrease- forming the well-known delta/deltaic deposits. Worth mentioning is also that finer sediment is usually transferred to locations near the dam, through density currents, while coarse materials most of the times settle at the river deltas (mouth) (Vachaviolos, 2014). Figure 2.2-4 below indicates the sediment deposit locations inside a reservoir.

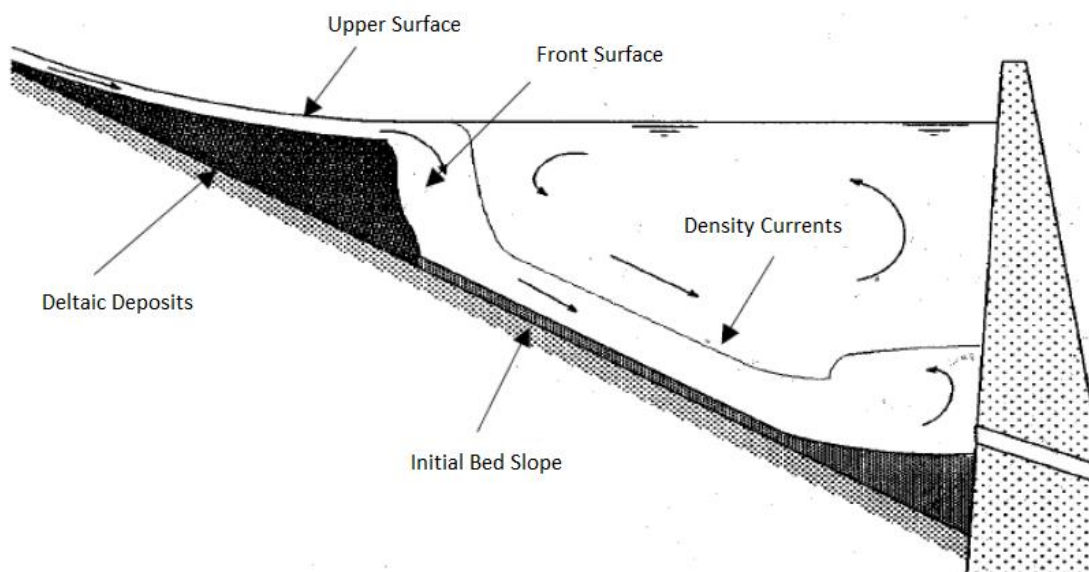


**Figure 2.2-4:** Sediment deposits inside reservoir (Obtained by Zarris et al., 2001)

The initial design study for Kremasta dam before the construction and operation predicted that for a design period of 50 years of operation, 8,8 % of the total storage capacity of the reservoir would have been filled up by the deposits volume (Table 2.2-1). However, Zarris et al. (2002) based on a hydrographic survey calculated that in 35 years only 66 (hm<sup>3</sup>) of sediment volume deposited (of which 41,3 hm<sup>3</sup> were at Acheloos section). This value reveals that the initial study overestimated the deposits which could lead to an overdesigning of the storage volume of the reservoir, although sediment transport and its specific sizes are exceedingly difficult to be predicted.

**Table 2.2-1:** Initial prediction of the dead sediment volume (Obtained by Zarris et al., 2002)

Years of operation of Kremasta dam	Predicted sediment volume (hm <sup>3</sup> )	Percentage of the total reservoir storage (%)
1	8.1	0.2
50	394.0	8.8
100	782.0	17.4

## 2.3 Methods to estimate soil loss and sediment yield

### 2.3.1 General

The estimation of soil loss and sediment yield is a challenging and complex issue to deal with, because beyond the stochastic parameters of the erosion process, it is difficult to measure or approach satisfyingly the quantities of suspended load and especially bed load. The measurement of suspended load is a standard process of collecting samples of sediment from the river and analyzing these in labs to find the concentration of suspended load. Today, these measurements can also be held using sensors. On the contrary, bed load is much more difficult to be measured, although there are some techniques to trap and weigh the sediment that osculates the riverbed. However, this process is expensive and time consuming considering that it depends on the frequency of intense precipitation or flood phenomena (Vachaviolos, 2014). Thus, the two main categories of methods to estimate soil loss and sediment yield are the empirical formulas and the analytical models which also include some empirical correlations. Below these methods are thoroughly presented and applied.

### 2.3.2 RUSLE method

As an empirical equation derived from experimental data, the USLE/RUSLE adequately represents the first-order effects of the factors that affect sheet and rill erosion. In the meantime, the RUSLE remains the most powerful, widely used, and practical tool for estimating sheet and rill erosion. Below is presented the Revised Universal soil loss equation (Renard et al., 1991):

$$A = R \cdot K \cdot L \cdot S \cdot C \cdot P \quad (2.3-1)$$

where

A is computed soil loss per unit area (t/ha),  
R is the rainfall- runoff erosivity factor (MJ·mm/ha·h),  
K is a soil erodibility factor (t·h/MJ·mm),  
L is the slope length factor,  
S is the slope steepness factor,  
C is a cover management factor,  
P is a supporting practices factor.

This empirically based equation, derived from a large mass of field data, computes sheet and rill erosion using values representing the four major factors affecting erosion. These factors are (Renard et al., 1991):

- Climate erosivity represented by R
- Soil erodibility represented by K
- Topography represented by LS
- Land use and management represented by C and P

### 2.3.2.1 Rainfall Erosivity (R-factor)

Rainfall erosivity is a factor that represents in what rate rainfall can provoke soil erosion. It derives from the intensity and kinetic energy of the rain. It is the factor that drives sheet and rill erosion processes, and extreme storms can lead to massive soil erosion.

#### Theoretical characteristics

R-Factor is thought to have the most significant effect on the soil erosion calculation process (Renard and Freimund, 1994). A notable characteristic is its spatial variability, due to differences in weather conditions. For example, in southern Illinois nearly twice as much erosion is expected than in northeast, because of differences in climatic erosivity between the two locations (Renard et al., 1991).

Rainfall erosivity is not distributed uniformly throughout the year. It is an extremely sensitive and volatile figure, on an annual, seasonal, and monthly basis, even at the level of individual rain events (Papapetrou, 2017). Some of the most erosive rain events happen in the spring while in summer, rainfall erosivity is usually insignificant. However, spring is a season when land is ready for planting and vulnerable to erosion. Thus, the magnitude of this figure must be addressed in relation to the cropping system and seasonal variability (Renard et al., 1991).

What is more, there are several ways to estimate the erosivity of rain. Being able to gather rainfall data gives us the chance to use analytical methods. Otherwise empirical methods can provide us with reliable approaches of the R-factor.

#### Methods to estimate R-factor

Concerning the calculation of rainfall erosivity it's remarkable that it is hard to find precipitation data from a rain gauge station inside or near the watershed of the study, in order to estimate the kinetic energy and the intensity of the rain. Thus, empirical methods are usually rendered as the only solution to approach the R-factor. More specific, simple linear regression formulas compute the R-factor as a function of mean rainfall (mm) of the year (P). However, there is not a formula, connecting R-factor with mean yearly rainfall (P) for the Greek climate and weather conditions, so formulas developed for other countries are used in this case. Below, both empirical and analytical method.

#### Empirical Methods

Below, several equations developed in Europe, are mentioned.

1) Van der Knijff et al., Tuscany Italy:

$$R = a \cdot P \quad (2.3-2)$$

where

$a$  is a determination parameter, usually from 1 to 1,5,

$P$  is the average annual rainfall (mm).

2) Torri et al. (2006), Italy:

$$R = -944 + 3,08 \cdot P \quad (2.3-3)$$

where

P is the average annual rainfall (mm).

Greece has similar climate to Italy and proximity, so it can be applied to Kremasta.

3) Renard and Freimund (1994), Europe:

$$R = 0,0483 \cdot P^{1,61} \quad (2.3-4)$$

where

P is the average annual rainfall (mm).

4) Schwertmann et al. (1990), Germany:

$$R = 0,83 \cdot P - 17,7 \quad (2.3-5)$$

where

P is the average annual rainfall (mm).

#### **Wischmeier and Smith (1978) and Renard et al. (1997) analytical method**

The methodology used to compute the rainfall erosivity is based on the analysis of USLE and RUSLE, as described by Wischmeier and Smith (1978) and Renard et al. (1997). Is one of the most common-used and precise analytical ways to calculate the rainfall erosivity. Other methods, like the one developed by Koutsoyiannis and Tarla (1987), can also be utilized to estimate the erosivity of the rain.

It would be useful to collect and have available for use, long-term rainfall timeseries (20 years or more), in order to extract more reliable and accurate results, concerning the average annual rainfall erosivity.

The annual rainfall erosivity factor occurs as the sum of all the R-factors of the rainfall events of the year. The erosivity value of each episode is the product of the kinetic energy E (MJ/ha) and maximum 30-minute intensity of the rain  $I_{30}$  (mm/h), during the episode. The timescale usually used is 5,10 or 30 minutes. In the present study only data with 30-minute time step were available.

The three following formulas conclude on the calculation of rainfall erosivity:

$$R = \frac{1}{n} \cdot \sum_{j=1}^n [(\sum_{k=1}^m (E) \cdot (I_{30}) \cdot k)] \cdot j \quad (2.3-6)$$

$$\bullet E = \sum_{r=1}^m (e_r \cdot \Delta V_r) \quad (2.3-7)$$

$$\bullet e_r = 0,29 \cdot [1 - 0,72 \cdot \exp(-0,05 \cdot I_r)] \quad (2.3-8)$$

where

n are years of data collection,

m is the number of rainfall events per year,

I<sub>30</sub> is the maximum 30-minute intensity of the rainfall event (mm/h),

E is the total kinetic energy of the rainfall event (MJ/ha),

e<sub>r</sub> is the specific rainfall kinetic energy of each timespan of the rainfall event (MJ/ha·mm),

ΔV<sub>r</sub> is the rainfall height of each timespan of the rainfall event (mm),

I<sub>r</sub> is the intensity of the rainfall event (mm/h).

The kinetic energy is computed for each rainfall event of the year. It is usually related to the rainfall intensity by formulas extracted from field measurements. Moreover, there are many different formulas -developed in European countries by Wischmeier and Smith (1978) and Diodato and Bellocchi (2007)- that calculate the kinetic energy of the rain:

$$\bullet KE \text{ time} = I_r \cdot (11,87 + 8,73 \cdot \log(I_r)) \quad (2.3-9)$$

$$\bullet E = 1,213 + 0,89 \cdot \log(I_{30}) \quad (2.3-10)$$

$$\bullet KE \text{ time} = -1195,7 + 483,181 \cdot \ln(I_r) \quad (2.3-11)$$

where:  $R^2 = 0.81$ , the fitted logarithmic equation

$$\bullet E = \sum_{r=1}^m (e_r \cdot \Delta V_r) \quad (2.3-12)$$

$$\text{where } e_r = 0,29 \cdot [1 - 0,72 \cdot \exp(-0,05 \cdot I_r)] \quad (2.3-13)$$

- **where I<sub>r</sub> is the rainfall intensity (mm/h) and I<sub>30</sub> is the maximum 30-minute intensity of the rain (mm/h).**

### 2.3.2.2 Soil Erodibility (K-factor)

The K-factor is a measure of the inherent erodibility of a given soil under the standard condition of plot maintained in continuous fallow. Values for K typically range from about 0.01 to 0.45, with high-sand and high-clay content soils having the lower values and high-silt content soils having the higher values (Renard et al., 1991). K-factor accounts for the influence of soil properties on soil loss during storm events (Renard et al., 1997).

#### Theoretical characteristics

The best way to evaluate K-factor in any study area is to collect soil samples from every geological structure of the watershed and specify the ground characteristics via laboratory analysis (Papapetrou, 2017). Though in case of inability to collect and process soil samples values of K for the concerned soil and geological formations can be extracted by bibliography and previous studies. Although this practice might not be the most appropriate, it is used since the first decades of application of USLE equation as at the manual of (Wischmeier and Smith, 1978) method there are values of K attached for different types of soils (Vachaviolos, 2014). While these equations are suitable for large parts of the USA (for which the USLE was originally developed), they produce unreliable results when applied to soils with textural extremes as well as well-aggregated soils. Therefore, they are not ideally suited for use under European

conditions. Otherwise K-factor is sometimes estimated using erodibility nomographs, but they do not apply to some soils (Van der Knijff et al. 2000a&b).

The RUSLE also varies K seasonally. Experimental data show that K is not constant but varies with season, being highest in the spring with soil fluffing from freeze-thaw actions and lowest in mid-fall and winter following rainfall compaction or a frozen soil. The seasonal variability is addressed by weighting the instantaneous estimate of K in proportion to the EI (the percent of annual R) for 15-day intervals. Instantaneous estimates of K are made from equations relating K to the frost-free period and the annual R-factor (Renard et al., 1991).

### Methods to estimate K-factor

According to USLE and RUSLE literature the soil erodibility factor (t·h/MJ·mm) is determined by nomographs or in case of content in clay <70%, by using Wischmeier and Smith (1978) relationship (Vachaviolos, 2014). The best and most precise method is to collect soil samples of the study area and every soil formation and carry out experimental research to approach the soil characteristics. Otherwise it is possible to extract the value of K for every type of soil, by already existing tables of Greek or foreign bibliography or use several formulas:

#### A. Wischmeier and Smith (1978) and soil erodibility nomographs

The following equation was developed by Wischmeier and Smith in 1978:

$$K = \frac{[2,1 \cdot 10^{-4} \cdot (12 - OM) \cdot M^{1,14} + 3,25 \cdot (s - 2) + 2,5 \cdot (p - 3)]}{100} \quad (2.3-14)$$

where

M is the product of the primary particle size fractions: (% modified silt or the 0,002-0,1 mm size fraction) · (% silt + % sand),

OM is the percentage of organic matter,

s are the classes for structure,

p is the permeability.

This equation is appropriate for soils with percentage of organic matter lower than 4%. This limit exists in order to avoid an underestimation of K-factor for this type of soils. In case that the content of clay is lower than 70%, erodibility nomographs are used (Figure 2.3-1) (Panagos et al., 2014c).

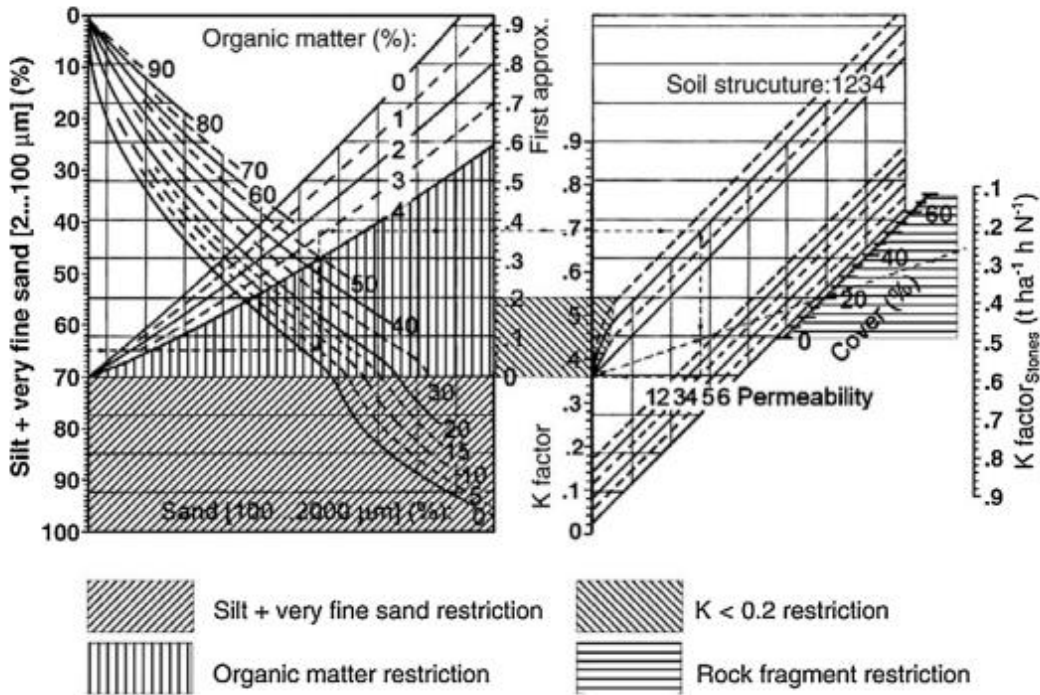


**Figure 2.3-1:** Soil erodibility nomograph (Obtained by Wischmeier and Smith, 1978)

While these equations are suitable for large parts of the USA (for which the USLE was originally developed), they produce unreliable results when applied to soils with textural extremes as well as well-aggregated soils (Römken et al., 1986). Therefore, they are not ideally suited for use under European conditions (Van der Knijff et al., 2000a&b).

### B. Römken et al., 1986

Later research concluded on the following formula which can describe better the variety of geological formations in Europe and other continents apart from America (Van der Knijff et al., 2000a&b):

$$K = 0,0034 + 0,0405 \cdot \exp \left[ -0,5 \cdot \left( \frac{\log Dg + 1,659}{0,7101} \right)^2 \right] \quad (2.3-15)$$

Where  $Dg$  is the geometric mean weight diameter of the primary soil particles and is calculated by the following equation:

$$Dg = \exp \left( \sum f_i \cdot \ln \left( \frac{d_i + d_{i-1}}{2} \right) \right) \quad (2.3-16)$$

Where for every particle's category (clay, sand etc.):

- $d_i$  is the maximum particle's dimension (mm),
- $d_{i-1}$  is the minimum particle's dimension (mm),
- $f_i$  is the corresponding mass fraction.

### C. European databases of soil erodibility values

Different research projects across Europe have contributed to the effort of creating European grids with values for soil erodibility. For example, Van der Knijff et al. (2000a&b) research displays the classification and corresponding K-values for a range of soils as shown at the Table 2.3-1 and Figure 2.3-2 below:

**Table 2.3-1:** Representative texture parameters for each texture class  
(Obtained by Zarris et al., 2001)

TEXT	Dominant surface textural class. (Present in: STU)	% clay	% silt	% sand	K
0	No information	-	-	-	
9	No texture (histosols, ...)	-	-	-	
1	Coarse (clay < 18 % and sand > 65 %)	9	8	83	0.0115
2	Medium (18% < clay < 35% and sand > 15%, or clay < 18% and 15% < sand < 65%)	27	15	58	0.0311
3	Medium fine (clay < 35 % and sand < 15 %)	18	74	8	0.0438
4	Fine (35 % < clay < 60 %)	48	48	4	0.0339
5	Very fine (clay > 60 %)	80	20	0	0.0170

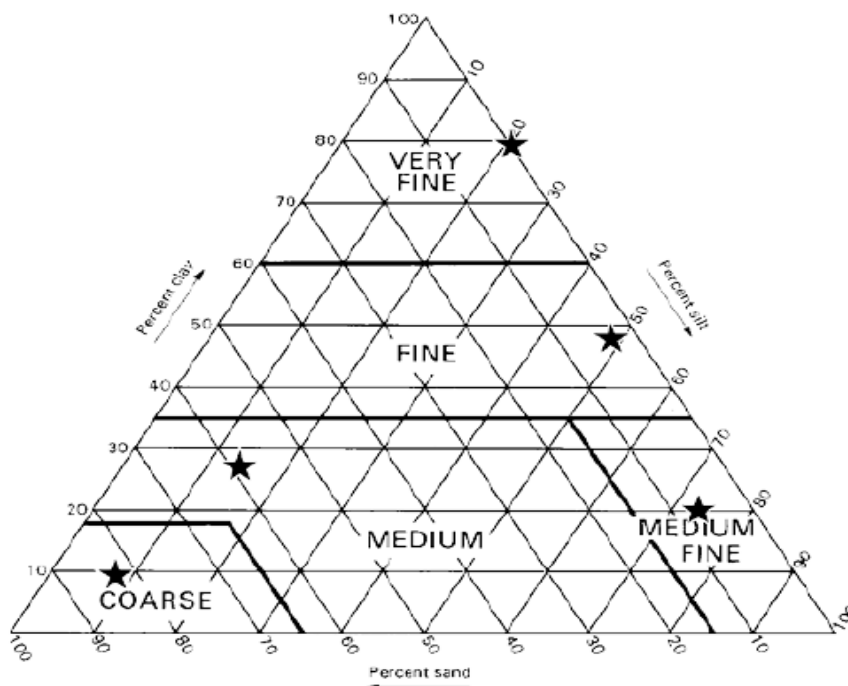


**Figure 2.3-2:** Position of the above representative values of K within the texture triangle  
(Obtained by Panagos et al., 2015)

An evolution in the effort of calculation of K-factor was the published research of Panagos et al. (2014) which, apart from the very big soil data collection, includes a map that exhibits the several values of soil erodibility all across Europe with the remarkable resolution of 500 x 500 (m) cell size at grid form. This map was created with the aid of LUCAS - Land Use/Cover Area frame Survey database, a collection of 20.000 European soil samples. It also includes for the first time the effect of rocky geological formations on K-values. These rocky areas are usually ignored during the computation of K which leads to its overestimation especially in countries with stony terrain like

Greece. Such soils reduce the production of soil erosion, up to 40% in some cases in areas of Greek territory.

Thus, Panagos et al. (2014) in cooperation with the European Soil Data Center (ESDAC) of Joint Research Centre (JRC) of European Union created some high-resolution soil erodibility maps for the countries of the European Union. Figure 2.3-3 displays the Panagos et al. (2014) soil erodibility map for Europe:

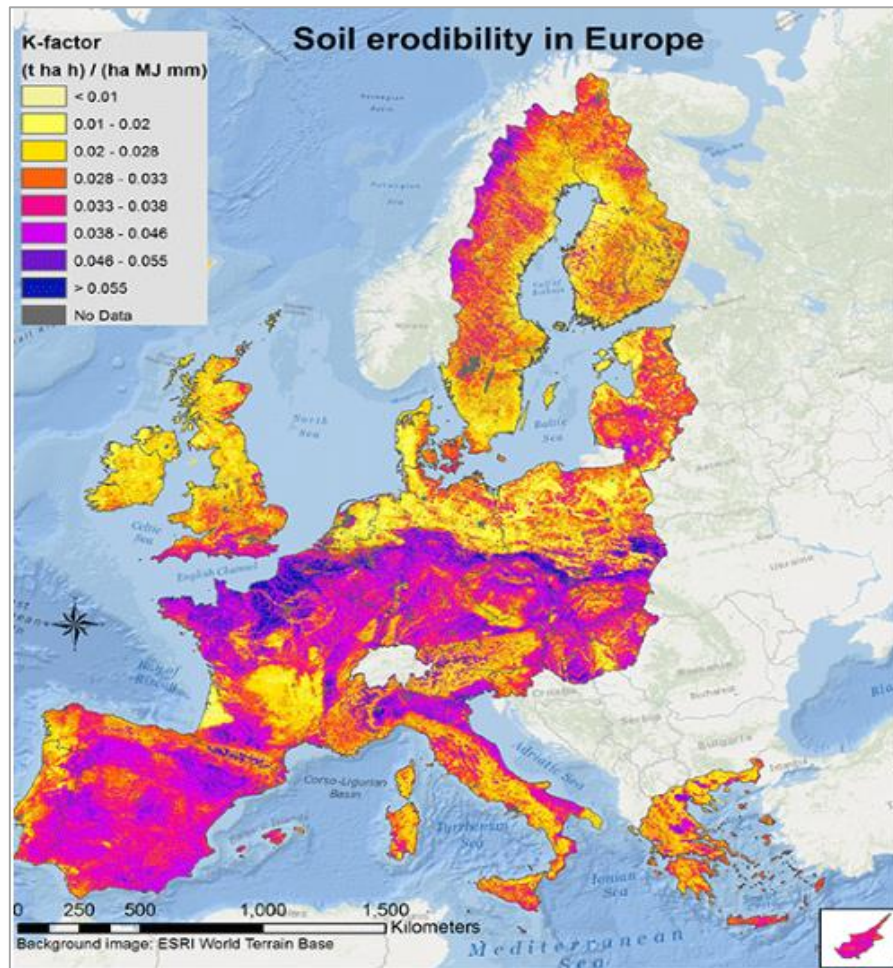


**Figure 2.3-3:** High-resolution (500 m grid cell size) map of Soil Erodibility estimated as K-factor in the European Union (Obtained by Panagos et al., 2014)

Van der Knijff et al. (2000a&b) in cooperation with Soil Geographical Database of Europe (ESGDB) also developed a soil erodibility map (K-factor) ( $t \cdot h / MJ \cdot mm$ ). Efthimiou (2020) is another recent study that describes the development of the new soil erodibility map of Greece. The calculation of the K-factor was based on field samples deriving from the pan-European LUCAS database and the Greek NAGREF, utilizing the K-factor nomograph by Wischmeier and Smith (1978) (Efthimiou, 2020).

### 2.3.2.3 Slope length and steepness factor (LS-factor)

The Slope Length & Steepness factor (LS-factor) determines the effect of topography and terrain on the process of soil erosion, and that is why some use the term topographic factor or terrain factor to describe it. Thus, it can be estimated from a digital elevation model (DEM).

An increase in the value of L and S, can cause significant augmentation of the soil erosion, because the steepest slopes (S) give higher water-flow velocities and the longest slopes (L) accumulate surface runoff which leads again to the increase of flow velocities (Papapetrou, 2017). Soil loss is more sensitive to changes in steepness than in slope length (McCool et al., 1987). According to the USLE (Wischmeier and Smith, 1978), LS-factor is defined as:

$$LS = \left(\frac{\lambda}{22.13}\right)^n \cdot (0.065 + 0.045 \cdot S + 0.0065 \cdot S^2) \quad (2.3-17)$$

where

L is the slope length factor,

S is the slope steepness factor,

$\lambda$  is the steepness length (m),

S is the steepness (%),

n is 0,2 for  $S < 1\%$ , 0,3 for  $1\% \leq S \leq 3,5\%$ , 0,4 for  $3,5\% \leq S \leq 5\%$  and 0,5 for  $S > 5\%$ .

Another commonly known formula is the one used by RUSLE in which L is calculated as above while for S is computed from McCool et al. (1987) relationship:

$$LS = \left(\frac{\lambda}{22.13}\right)^n \cdot (10.8 \cdot \sin\beta + 0.03) \quad S < 9\% \quad (2.3-18)$$

$$LS = \left(\frac{\lambda}{22.13}\right)^n \cdot (16.8 \cdot \sin\beta - 0.50) \quad S \geq 9\% \quad (2.3-19)$$

Where  $\beta$  which is the steepness angle ( $^\circ$ ) is defined as:

$$\beta = \tan^{-1} \cdot \left(\frac{S}{100}\right) \quad (2.3-20)$$

A number of researchers (Moore and Burch, 1986· Mitasova et al.,1996), taking advantage of the possibility of spatial distribution of physical processes such as erosion, through the use of Geographic Information Systems, have suggested replacing the steepness length ( $\lambda$ ) with the upstream area that contributes to erosion ( $A_s$ ).

All these modern and revised formulas improve the estimation of LS-factor (Panagos et al., 2012), because with the above replacement and the integrated calculation of sloping through the curvature, more realistic estimations occur. This is an advantage especially in cases of geomorphologically complex terrains such as Kremasta area. The relationship proposed by Moore and Burch (1986) is applicable to slopes with  $\lambda < 100$  m and  $\beta < 14^\circ$  (Di Stefano et al., 2000):

$$LS = \left(\frac{A_s}{22.13}\right)^m \left(\frac{\sin\beta}{0.0896}\right)^n \quad (2.3-21)$$

where

As is the upstream area that contributes to erosion (m<sup>2</sup>),  
β is the steepness angle (°),  
m, n are factors that according to Panagos et al. (2012) are 0,4 and 1,3 respectively.

Mitasova and Mitas (2001a), further developed the research on exporting a more representative relationship for LS-factor, resulting in the following equation:

$$LS = (m+1) \left( \frac{As}{22.13} \right)^m \left( \frac{\sin\beta}{0.09} \right)^n \quad (2.3-22)$$

where

As is the upstream area that contributes to erosion (m<sup>2</sup>),  
β is the steepness angle (°),  
m, n are factors that range from 0,4≤m≤0,6 και 1,0≤n≤1,3, depending on the type of erosion.

All the above formulas are applicable to areas inside the watershed that there is not deposition of transferred sediment. Thus, the usage of these equations usually leads to an overestimation of the LS-factor. Nevertheless, in most cases, rainfall erosivity is underestimated, so researchers sometimes keep this overestimation of LS to achieve a level of balance at RUSLE equation.

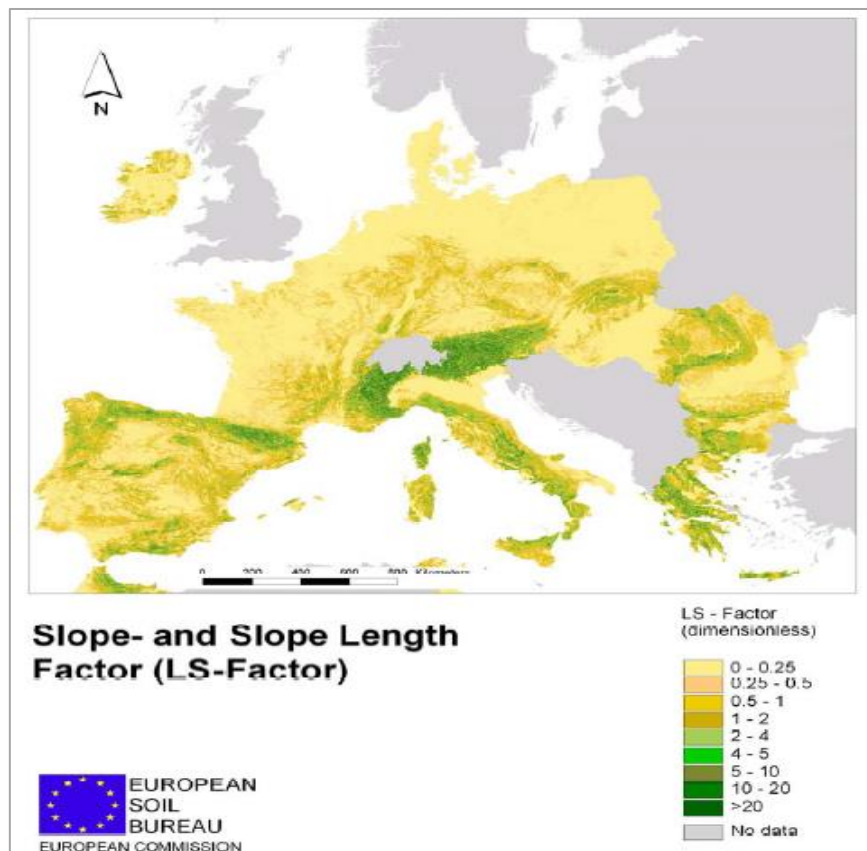


**Figure 2.3-4:** Slope / Slope length factor map (LS)  
(Obtained by Van der Knijff et al., 2000a&b)

Other methods such as Panagos et al. (2014) and Van der Knijff et al. (2000a&b) use maps in grid form, in cooperation with the European Soil Data Center (ESDAC) and LUCAS European database (2009), in order to extract the LS-factor. More specifically, they make use of European digital elevation models (EU-DEM) and some algorithms to extract the raster maps displayed in Figures 2.3-4 and 2.3-5:

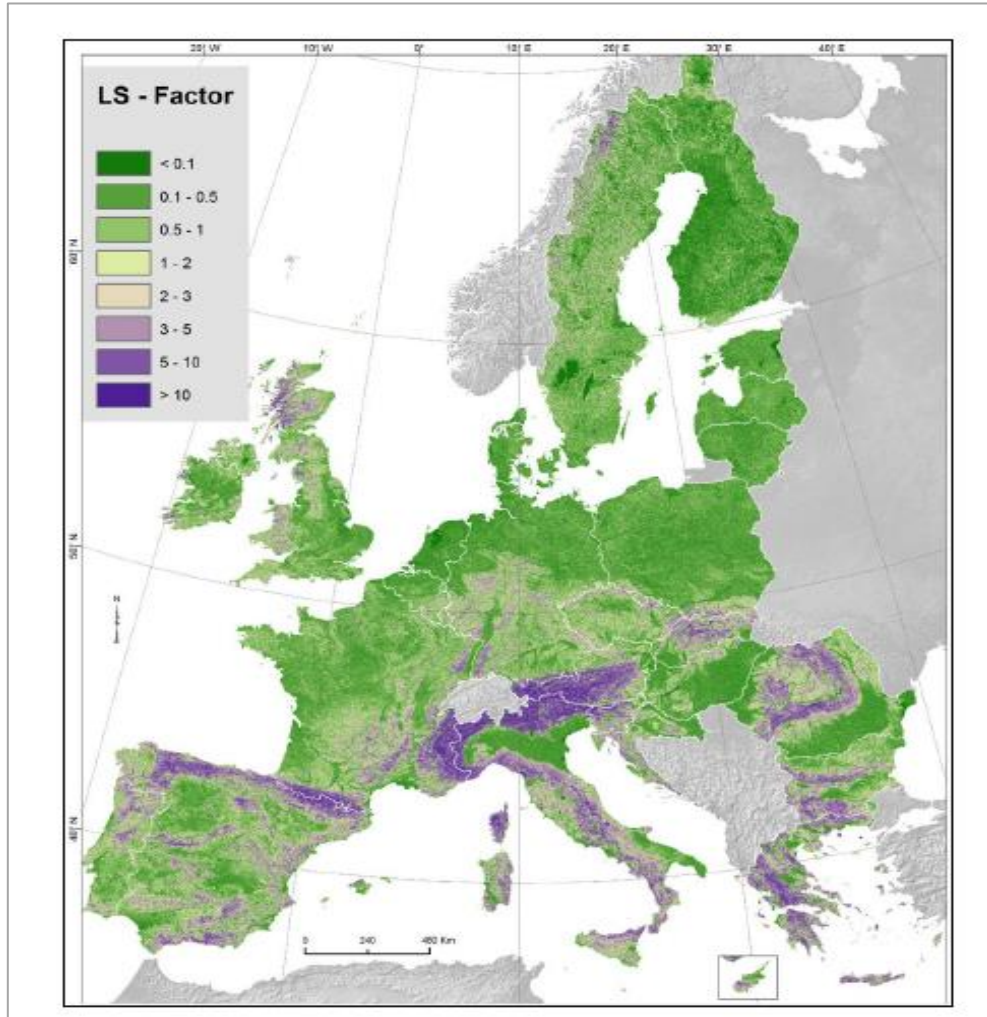


**Figure 2.3-5:** Slope / Slope length factor map (LS)  
(Obtained by Panagos et al., 2015)

#### 2.3.2.4 Cover Management factor (C-factor)

The Cover Management factor or Cropping Management factor determines the effect of land use on the rate of soil loss. C-factor depends on vegetation type, stage of growth and cover percentage. Values for C can vary from near zero for a very well-protected soil to 1.5 for a finely tilled, ridged surface that produces much runoff and leaves the soil highly susceptible to rill erosion (Renard et al., 1991).

Vegetation cover is – after topography – the second most important land factor that controls soil erosion risk. In the Revised Universal Soil Loss Equation (Renard et al., 1997), the effect of vegetation cover is incorporated in the cover management factor (hereafter called C-factor). It is defined as the ratio of soil loss from land cropped under specific conditions to the corresponding loss from clean-tilled, continuous fallow (Wischmeier and Smith, 1978). The effect of mulch cover, crop residues and tillage operations should also be accounted for in the C-factor. In RUSLE, the C-factor is subdivided into 5 separate sub-factors that account for the effects of prior land use, canopy cover, surface cover, surface roughness and soil moisture, respectively. Below are exhibited several methods to estimate the cover management factor:

- In RUSLE, the C-factor is subdivided into 5 separate sub-factors that account for the effects of prior land use, canopy cover, surface cover, surface roughness and soil moisture, respectively. So, the values of C in RUSLE occur from the following equation:

$$C = PLU \cdot CC \cdot SC \cdot SR \cdot SM \quad (2.3-23)$$

where

*PLU*: Prior Land Use – range 0~1,  
*CC*: Canopy Cover – range 0~1,  
*SC*: Surface Cover – range 0~1,  
*SR*: Surface Roughness – range 0~1,  
*SM*: Soil Moisture – range 0~1.

The above factors of the equation can be calculated with several formulas created by Renard et al. (1997).

- In European scale it would be problematic to assign monthly or annual C-values to classes in the CORINE land cover database by means of a lookup-table. That is because Europe encompasses a wide variety of climatic conditions which results in large spatial and temporal variations in growing season (Van der Knijff et al., 2000a&b). However, up to the regional scale the assignment of C-values to each land use, would be a fine method. Afterwards, having available the CORINE land cover map for the area of study, a mean value for C-factor could be extracted.
- An alternative way to determine the cropping management factor is with the use of remote sensing methods, by sorting satellite images and using vegetation indicators (Vegetation Indexes/VI's) (Vachaviolos, 2014).

### 2.3.2.5 Support Practices factor (P-factor)

The Control factor or Support Practices factor represents the effect of several cultivation techniques (Figure 2.3-6) on the reduction of soil erosion, namely the effect of soil texture conditions in water flow. Such techniques are the cultivation parallel to contours, with alternate crop strips (or grass margins) and with the use of terraces (or stone walls).



**Figure 2.3-6:** Strips and stone walls as measures to prevent soil loss  
(Obtained by Panagos et al., 2015)

Of all the RUSLE coefficients it is the most unreliable. For example, in contouring cultivation the rainfall and runoff water, is directed at the perimeter of the slope and therefore with much smaller slopes. However, as field measurements show, the effect of contour farming on soil erosion can range from 0 to 90%. As a result, there is a lack of stability in P-factor (Renard et al., 1997).

The values of support practice factor can, notably, reduce the soil erosion, while it usually receives values from 0-1. According to Panagoulia and Dimou (2002) for cultivation parallel to contours it ranges from 0,6-0,9, for alternate crop strips from 0,3-0,45, and when terraces exist it varies from 0,12 to 0,18 (Vachaviolos, 2014). Several methods to estimate K-factor exist. The most reliable and widespread is the one below.

At European level, the effect of support practices (compulsory for farmers to receive incentives under the CAP-GAEC) on soil loss were assessed by P-factor estimation taking into account: (a) contour farming, (b) maintenance of stone walls, and (c) grass

margins. *P*-factor was proposed as a product of those 3 sub-factors by [Blanco and Lal \(2008\)](#); applied by [Lopez-Vicente and Navas \(2009\)](#) (Panagos et al., 2015):

$$P = P_c \cdot P_{sw} \cdot P_{gm} \quad (2.3-24)$$

where:

- $P_c$  is the contouring sub-factor for a given slope of a field,
- $P_{sw}$  is the stone walls sub-factor (known as terrace sub-factor),
- $P_{gm}$  is grass margins sub-factor (known as strip cropping sub-factor and buffer strips).

Using the Digital elevation model with 25 (m) resolution, the arable lands of 8 European countries have been attributed a *P*-factor based on their topographic feature (slope %) (Panagos et al., 2015). These three sub-factors (Table 2.3-2) are usually determined by field measurements.

**Table 2.3-2:** Support practice (P-factor) and sub-factors per country  
(Obtained by Panagos et al., 2015)

Country	$P_c$ (contouring)	$P_{sw}$ (stone walls)	$P_{gm}$ (grass margins)	<i>P</i> -factor
AT	1	0.9996	0.9887	0.9883
BE	1	0.9998	0.9467	0.9465
BG	1	0.9999	0.9912	0.9911
CY	0.9909	0.9828	0.9991	0.9730
CZ	1	0.9999	0.9983	0.9982
DE	1	0.9998	0.9784	0.9782
DK	1	0.9999	0.9844	0.9843
EE	0.9995	0.9998	0.9996	0.9989
ES	0.9926	0.9580	0.9778	0.9293
FI	1	0.9998	0.9943	0.9942
FR	1	0.9935	0.9691	0.9627
GR	0.9939	0.9676	0.9883	0.9502
HR	1	0.9999	0.9995	0.9994

### 2.3.3 Other methods to estimate soil loss and sediment yield

The performance of a hydrographic survey or measurements of flow - sediment load are probably the most valid methods to estimate the sediment yield that enters the reservoir every year. However, they require plenty of technical and economic means to be completed with accuracy and they also consider only the suspended sediment load. Following this notion some other empirical and analytical methods to calculate soil loss or sediment yield were developed. Apart from RUSLE equation, Koutsoyiannis and Tarla (1987) introduced the following equation based on mean sediment yield measurements in several locations of North-western Greece. Thus, the mean annual sediment yield ( $G$  in  $t/km^2$ ) is calculated as follows:

$$G = 15 \cdot \gamma \cdot e^{3P} \quad (2.3-25)$$

where,  $P$  is the mean annual precipitation in the watershed (m) and  $\gamma$  is the geological factor given from the following formula:

$$\gamma = k1 \cdot p1 + k2 \cdot p2 + k3 \cdot p3 \quad (2.3-26)$$

where,  $k1$ ,  $k2$ ,  $k3$  are factors describing the erodibility of each group of geological formations that the watershed consists of and in particular:

- High erodibility:  $k1 = 1$
- Medium erodibility:  $k2 = 0,5$
- Low erodibility:  $k3 = 0,1$

and  $p1$ ,  $p2$ ,  $p3$  the equivalent ratios of area where each category of formations appears divided by the total area of the watershed and are estimated using geological maps.

The empirical models result from a regression analysis. The stability of the factors during each time scale considers the soil situation to be stable and permanent which is not always true. In every change of the soil situation empirical models are not considered to be appropriate for this process, and a new collection of data and building of the parameters is required (Zarris, 2019).

Nowadays, the comfort and technological development to create a Digital Elevation Model, makes the area the only geomorphological parameter that is included in the empirical equations. Before having the capability to create a DEM without so much effort, the collection of geomorphological data was an extremely hard and complex procedure which required the extraction of these parameters from old topographic plans. Moreover, today there are plenty of software options and tools to calculate the geomorphological parameters of every watershed (such as Surfer, RiverTools etc.) (Zarris, 2019).

The estimation of sediment yield using rating curves is a method that uses data from field flow ( $Q$ ) - sediment discharge ( $Q_s$ ) measurements from hydrographic stations on a river inside or near the watershed. The main concept is to build a relationship between  $Q$  and  $Q_s$  and by having a timeseries of flows (daily flows for example) to extract the equivalent values for sediment discharge. Then, it is easy to estimate a mean annual value for sediment yield that enters the reservoir, if having a dataset big enough to be valid and a variety of measurement locations to include all the inflows in the model.

### 3 Estimation of soil loss and sediment yield

#### 3.1 First method: RUSLE equation

##### 3.1.1 R-factor

As mentioned already R-factor can be calculated by many analytical methods, though sometimes due to lack of small timescale rainfall data, empirical equations are the only solution.

##### *3.1.1.1 Empirical Methods*

Let us begin with the empirical ways to calculate R-factor. Initially, precipitation data are gathered from the Hellenic Ministry of Environment and Energy, the Public Power Corporation and the Hellenic National Meteorological Service, associations that manage the rain gauge stations near Kremasta. Seventy-seven rain gauge stations were used for the extraction of the mean annual rainfall height (mm). Some of the stations are close but not inside the watershed of Kremasta, however all of them are used in the present study, so that the results are more precise. Table 3.1-1 reveals the altitude and the mean annual rainfall height of each rain gauge station.

**Table 3.1-1:** Mean annual precipitation at Kremasta basin (Obtained by Zarris, 2019)

	Station	Service	Altitude (m)	Watershed	Mean Annual Rainfall (mm)
1	ΑΓΙΟΣ ΒΛΑΣΙΟΣ	ΥΠΔΕ	850	Αχελώου	1046.8
2	ΑΓΡΙΝΙΟ	ΕΜΥ	24	Αχελώου	890.7
3	ΑΝΑΤΟΛΙΚΗ ΦΡΑΓΚΙΣΤΑ	ΔΕΗ	680	Αχελώου	1198.7
4	ΑΝΘΗΡΟ	ΔΕΗ	779	Αχελώου	1969.4
5	ΑΝΙΑΔΑ	ΔΕΗ	1060	Αχελώου	1324.9
6	ΑΡΑΧΩΒΑ	ΔΕΗ	960	Εύηνου	1142.7
7	ΑΡΓΙΘΕΑ	ΔΕΗ	992	Αχελώου	1594.1
8	ΑΡΔΑΝΟΒΟ	ΔΕΗ	315	Αχελώου	1190.6
9	ΑΣΤΡΟΧΩΡΙ	ΔΕΗ	560	Αχελώου	1772.8
10	ΒΑΘΥΡΡΕΜΜΑ	ΔΕΗ	920	Αχελώου	1879.9
11	ΒΑΚΑΡΙΟ	ΔΕΗ	1150	Αχελώου	1533.0
12	ΒΕΛΑΟΡΑ	ΔΕΗ	560	Αχελώου	1354.8
13	ΒΙΝΙΑΝΗ	ΥΠΔΕ	620	Αχελώου	1015.9
14	ΒΟΥΛΠΗ	ΔΕΗ	660	Αχελώου	1283.0
15	ΒΡΑΓΚΙΑΝΑ ΜΙΚΡΑ	ΔΕΗ	580	Αχελώου	1248.3
16	ΒΡΟΝΤΕΡΟ	ΔΕΗ	853	Πηνειού	1475.0
17	ΓΑΒΑΛΟΥ	ΥΠΔΕ	50	Αχελώου	1044.4
18	ΓΕΦ. ΕΠΙΣΚΟΠΗΣ	ΔΕΗ	277	Αχελώου	1028.1
19	ΓΡΑΝΙΤΣΑ	ΥΠΔΕ	850	Αχελώου	1100.5
20	ΓΡΕΒΙΑ	ΔΕΗ	800	Αχελώου	1108.1
21	ΔΟΜΝΙΣΤΑ	ΔΕΗ	1016	Αχελώου	1529.9
22	ΕΛΑΤΗ	ΥΠΔΕ	900	Πηνειού	1633.0

	Station	Service	Altitude (m)	Watershed	Mean Annual Rainfall (mm)
23	ΔΡΥΜΩΝΑΣ	ΔΕΗ	992	Εύηνου	1263.9
24	ΕΠΙΝΙΑΝΑ	ΔΕΗ	1050	Αγελώου	1653.8
25	ΘΕΟΔΩΡΙΑΝΑ	ΥΠΔΕ	950	Αγελώου	2272.5
26	ΚΑΡΙΤΣΑ	ΥΠΔΕ	1130	Αγελώου	1439.6
27	ΚΑΡΟΠΛΕΣΙ	ΔΕΗ	910	Αγελώου	1462.9
28	ΚΑΡΠΕΝΗΣΙ	ΥΠΔΕ	960	Αγελώου	1101.0
29	ΚΑΤΑΦΥΛΛΙΟ	ΥΠΔΕ	980	Αγελώου	1677.0
30	ΚΑΤΑΦΥΤΟ	ΥΠΔΕ	1000	Αγελώου	1283.0
31	ΚΑΨΑΛΑ	ΔΕΗ	840	Αγελώου	2192.1
32	ΚΛΕΙΣΤΟ	ΔΕΗ	780	Αγελώου	1166.8
33	ΚΡΙΘΑΡΙΑ	ΔΕΗ	2000	Αραχθού	1950.3
34	ΚΡΙΚΕΛΛΟ	ΔΕΗ	1120	Αγελώου	1280.4
35	ΛΕΟΝΤΙΟ	ΔΕΗ	950	Αγελώου	1623.5
36	ΛΕΠΕΝΟΥ	ΥΠΔΕ	190	Αγελώου	1024.8
37	ΛΕΣΙΝΙ	ΥΠΔΕ	1	Αγελώου	761.1
38	ΜΑΛΕΣΙΑΔΑ	ΔΕΗ	380	Αγελώου	1096.4
39	ΜΑΤΣΟΥΚΙ	ΔΕΗ	50	Αγελώου	982.3
40	ΜΑΥΡΟΜΑΤΑ	ΔΕΗ	900	Αγελώου	1748.5
41	ΜΕΣΟΠΥΡΓΟΣ	ΔΕΗ	420	Αγελώου	1398.6
42	ΜΕΣΟΧΩΡΑ	ΔΕΗ	850	Αγελώου	1683.9
43	ΜΙΚΡΟ ΠΕΡΙΣΤΕΡΙ	ΔΕΗ	1040	Λώου	1238.4
44	ΜΟΛΟΧΑ	ΔΕΗ	790	Αγελώου	1348.3
45	ΜΟΝΑΣΤΗΡΑΚΙ	ΔΕΗ	660	Αγελώου	1661.0
46	ΜΟΥΧΑ	ΔΕΗ	870	Αγελώου	1453.5
47	ΜΠΕΖΟΥΛΑ	ΥΠΔΕ	901	Αγελώου	1332.2
48	ΜΥΡΙΝΗ	ΔΕΗ	1100	Αγελώου	1258.6
49	ΝΙΚΟΥΛΙΤΣΑ	ΔΕΗ	2000	Αραχθού	1688.4

50	ΠΑΛΑΙΟΧΩΡΙ	ΔΕΗ	581	Πηνειού	1278.2
51	ΠΑΠΠΑΡΟΥΖΙ	ΔΕΗ	660	Αγελώου	1063.5
52	ΠΑΤΙΟΠΟΥΛΟ	ΔΕΗ	525	Αγελώου	1392.5
53	ΠΑΥΛΟΠΟΥΛΟ	ΔΕΗ	880	Αγελώου	1094.9
54	ΠΑΧΤΟΥΡΙ	ΔΕΗ	950	Αγελώου	1959.4
55	ΠΕΡΔΙΚΑΚΙ	ΥΠΔΕ	680	Αγελώου	1515.1
56	ΠΕΡΤΟΥΛΙ	ΥΠΔΕ	1160	Αγελώου	1441.8
57	ΠΕΤΡΑΛΩΝΑ	ΔΕΗ	880	Αγελώου	1185.3
58	ΠΟΛΥΝΕΡΙ	ΔΕΗ	802	Αγελώου	1981.4
59	ΠΡΟΥΣΟΣ	ΔΕΗ	920	Αγελώου	1686.2
60	ΡΕΝΤΙΝΑ	ΥΠΔΕ	903	Πηνειού	1112.0
61	ΣΑΡΓΙΑΔΑ	ΔΕΗ	433	Αγελώου	1061.0
62	ΣΚΟΥΛΙΚΑΡΙΑ	ΔΕΗ	827	Αραχθού	1375.0
63	ΣΤΑΜΝΑ	ΥΠΔΕ	142	Αγελώου	942.1
64	ΣΤΑΝΟΣ	ΥΠΔΕ	150	Υπόλοιπα	1018.5
65	ΣΤΟΥΡΝΑΡΑΙΚΑ	ΔΕΗ	860	Πηνειού	1646.0
66	ΤΕΜΠΛΑ	ΔΕΗ	306	Αγελώου	1143.4

	Station	Service	Altitude (m)	Watershed	Mean Annual Rainfall (mm)
67	ΤΟΠΟΛΙΑΝΑ	ΥΠΔΕ	408	Αγελώου	1194.3
68	ΤΡΙΚΛΙΝΟ	ΔΕΗ	620	Αγελώου	1446.3
69	ΤΡΙΠΟΤΑΜΟΣ	ΔΕΗ	650	Αγελώου	1108.5
70	ΤΡΟΒΑΤΟ	ΔΕΗ	1060	Αγελώου	1782.0
71	ΥΗΣ ΚΑΣΤΡΑΚΙΟΥ	ΔΕΗ	75	Αγελώου	1034.0
72	ΥΗΣ ΚΡΕΜΑΣΤΩΝ	ΔΕΗ	390	Αγελώου	1084.3
73	ΥΗΣ ΠΛΑΣΤΗΡΑ - ΥΔΡΟΛΗΨΙΑ	ΔΕΗ	800	Αγελώου	986.4
74	ΥΗΣ ΠΛΑΣΤΗΡΑ - ΦΡΑΓΜΑ	ΔΕΗ	801	Αγελώου	1171.4
75	ΦΟΥΣΙΑΝΑ	ΔΕΗ	950	Αγελώου	1243.6
76	ΦΡΑΞΟΣ	ΔΕΗ	700	Αραχθού	1459.4
77	ΧΕΛΙΔΟΝΑ	ΥΠΔΕ	630	Αγελώου	1195.7

As occurs, the resulting mean annual rainfall height is **1.433 (mm)** which is particularly high due to the location of the reservoir at the west part of Western Greece, a region with an unstable and intense climate. This is also obvious in the study of Hydroscope research program (Figure 3.1-1) which collected data from 80 Greek stations.

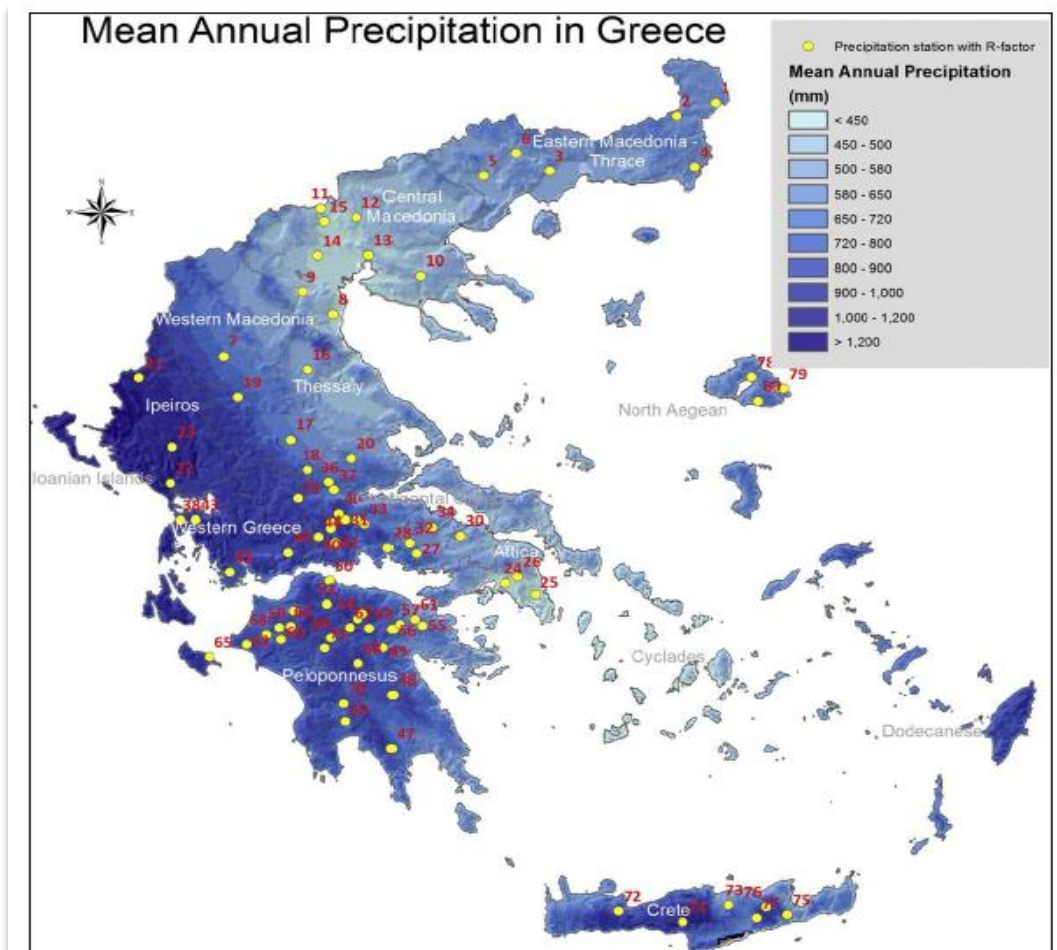


**Figure 3.1-1:** Spatial distribution of the mean annual precipitation and the rain gauge stations used in Hydroscope research program (Obtained by Panagos et al., 2015)

Thirty years of data collection with a 30-minute timestep and spatial distribution with mean density of one station per 40 x 40 (km) pixel size, led to the extraction of the above map. It shows that in Western Greece, due to the abnormal terrain and climate, there is high mean annual precipitation, generally higher than 1.200 (mm) (Panagos et al., 2015).

The value of mean annual rainfall height is used to estimate R-factor by the following European empirical formulas. Since there are no formulas for Greece, Italy, which has a similar Mediterranean climate, could be a decent approach for the calculation of R-factor.

**Table 3.1-2:** Calculation of R-factor by European empirical equations.

Method	Area of application	Formula	Mean Annual Rainfall (mm)	R-factor (MJ·mm/ha·h)
Van der Knijff et al.	Tuscany, Italy	$R = a \cdot P$	1.433	<b>2.149,5</b>
Torri et al.	Italy	$R = -944 + 3,08 \cdot P$	1.433	<b>3.470</b>
Renard and Freimund	Europe	$R = 0,0483 \cdot P^{1,61}$	1.433	<b>5.827,8</b>
Schwertmann et al.	Germany	$R = 0,83 \cdot P - 17,7$	1.433	<b>1.171,7</b>

The cause of the remarkable variance between the values of R-factor (Table 3.1-2) is its spatial sensitivity and changeability. It is also due to the lack of precision of these empirical methods (Vachaviolos, 2014). Thus, analytical methods (one of them is used in this study) can provide us with more pertinent and proper conclusions.

### 3.1.1.2 Analytical Method

For the analytical calculation of R-factor, formulas described by Renard and Freimund (1994) and presented previously in this study, are chosen. The rainfall erosivity factor at Kremasta watershed is calculated based on a thirty-minute rainfall time step. R-factor is usually estimated using mean monthly or even mean annual rainfall data. However, the use of rainfall intensity in small timescales, allows for safer conclusions. In this study, data were available for a span of 20 hydrological years (08/1975-12/1995) with minor gaps. Thirty-minute rainfall heights are processed for all the significant rainfall events of each year (80-120 events). Data are collected from [hydroscope.gr](http://hydroscope.gr), and particularly from Monastiraki rain gauge station (Figure 3.1-2) which is the closest station to the reservoir of Kremasta. This station is managed by the Hellenic Public Power Corporation.

Below the analytical calculations of R-factor are displayed, by counting the values of kinetic energy, rainfall intensity and maximum 30-minute intensity of each episode of the year. Due to enormously big number of episodes and years of precipitation data, only some of the episodes of the first year are exhibited in Table 3.1-3 as a sample.

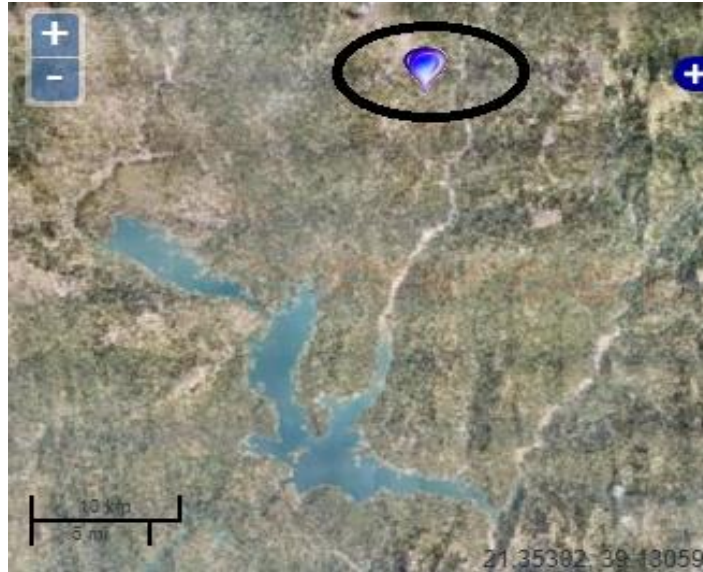


**Figure 3.1-2:** Monastiraki rain gauge station near Kremasta reservoir  
(Obtained by: Hydroscope.gr)

**Table 3.1-3:** Calculations for 1<sup>st</sup> and 18<sup>th</sup> Rain Episode of the year 1975

Year	Month	Day	Rainfall Recorder			Rain Event			Energy	
			Hour	Rain height	Cumulative Height	Time Step	Rain height	Intensity	Specific Kinetic Energy	Kinetic Energy
			tr (h)	Vr (mm)	Vr 2 (mm)	$\Delta T$ (min)	$\Delta Vr$ (mm)	Ir (mm/h)	er (MJ/ha·mm)	E (MJ/ha)
1975	8	4	12:00	0,000	0					
1975	8	4	12:30	0,262	0,262	30	0,262	0,524	0,087	0,023
1975	8	4	13:00	0,252	0,514	30	0,252	0,504	0,086	0,022
1975	8	4	13:30	0,152	0,666	30	0,152	0,304	0,084	0,013
1975	8	4	14:00	0,148	0,814	30	0,148	0,296	0,084	0,012
1975	8	4	14:30	0,012	0,826	30	0,012	0,024	0,081	0,001
1975	8	4	19:00	0,005	0,831	270	0,005	0,001	0,081	0,000
1975	8	4	19:30	0,073	0,904	30	0,073	0,146	0,083	0,006
1975	8	4	20:00	0,157	1,061	30	0,157	0,314	0,084	0,013
1975	8	4	20:30	0,192	1,253	30	0,192	0,384	0,085	0,016
1975	8	4	21:00	0,115	1,368	30	0,115	0,230	0,084	0,010
1975	11	19	20:00	0,026	0,026	30	0,026	0,052	0,082	0,002
1975	11	19	20:30	12,174	12,2	30	12,174	24,348	0,228	2,778
1975	11	19	21:00	9,057	21,257	30	9,057	18,114	0,206	1,862
1975	11	19	21:30	0,521	21,778	30	0,521	1,042	0,092	0,048
1975	11	19	22:00	2,867	24,645	30	2,867	5,734	0,133	0,382
1975	11	19	22:30	0,046	24,691	30	0,046	0,092	0,082	0,004
1975	11	19	23:00	0,024	24,715	30	0,024	0,048	0,082	0,002
1975	11	19	23:30	0,007	24,722	30	0,007	0,014	0,081	0,001
1975	11	20	2:30	0,040	24,762	180	0,040	0,013	0,081	0,003
1975	11	20	3:00	0,208	24,97	30	0,208	0,416	0,085	0,018
1975	11	20	3:30	0,434	25,404	30	0,434	0,868	0,090	0,039

As shown in Table 3.1-3 above the rainfall recorder measures the rainfall height ( $V_r$  or  $\Delta V_r$ ) in millimeters, during a time step of thirty minutes. The calculations for each time span of the episode involve the cumulative rainfall height ( $V_r$  2), the intensity of the rain ( $I_r$ ), the specific kinetic energy ( $er$ ) and the kinetic energy ( $E$ ) computed as:

$$\text{➤ } I_r = V_r / \Delta T \quad (\text{mm/hr}) \quad (3.1-1)$$

$$\text{➤ } er = 0,29 \cdot [1 - 0,72 \cdot \exp(-0,05 \cdot I_r)] \quad (\text{MJ/ha} \cdot \text{mm}) \quad (3.1-2)$$

$$\text{➤ } E = \Delta V_r \cdot er \quad (\text{MJ/ha}) \quad (3.1-3)$$

Lastly, the value of the maximum 30-minute rainfall intensity, the total kinetic energy and the rainfall erosivity is counted for each episode as:

- $\text{Max}I_{30}$  (mm/hr) is the maximum of all the rainfall intensities of the episode,
- Total kinetic energy of the episode is the sum of all the kinetic energies calculated for each span,
- Rainfall erosivity ( $\text{MJ} \cdot \text{mm/ha} \cdot \text{hr}$ ) of each episode is the product of the total kinetic energy and the  $\text{Max}I_{30}$ .

Subsequently, the results of these two episodes of the first year taken as an example are presented below:

<b>Max I30=</b>	<b>0,524</b>
<b>Total E=</b>	<b>0,116</b>
<b>Rainfall</b>	
<b>Erosivity =</b>	<b>0,061</b>

→ **1<sup>st</sup> Rain Episode**

<b>Max I30=</b>	<b>24,348</b>
<b>Total E=</b>	<b>5,138</b>
<b>Rainfall</b>	
<b>Erosivity =</b>	<b>125,112</b>

→ **18<sup>th</sup> Rain Episode**

It is evident that in the 1<sup>st</sup> episode, the fact that all the values of rainfall heights are low ( $< 1$  mm), leads to an insignificant rainfall erosivity value. At the same time, in the 18<sup>th</sup> episode there are extremely high rainfall heights such as 12 or 9 (mm) in 30-minute timespan which shows a big amount of kinetic energy ( $E$ ) and a very intense rain ( $I_r$ ). Thus, occurs a rainfall erosivity of 125 ( $\text{MJ} \cdot \text{mm/ha} \cdot \text{hr}$ ) for just one rain event. This value contributes to a high soil erosion due to rainfall erosivity. The same technique is followed for all the rain episodes of the 20 years of data. Eventually, the mean annual rainfall erosivity for Kremasta region, during a 20-year period of available precipitation data is:

<b>R total (<math>\text{MJ} \cdot \text{mm/ha} \cdot \text{hr}</math>) =</b>	<b>1.297,813</b>
--	------------------

### 3.1.2 K-factor

It was not possible to gather and analyze soil samples from the study area, neither to use the nomograph or the Wischmeier and Smith (1978) formula due to lack of data. Thus, in order to determine the value of K-factor for Kremasta basin, where the soil formations consist of flysch, limestone and alluvial deposits, the following references are used:

- Research projects of Van der Knijff et al. (2000a&b) and the results occur from them and presented in Figure 3.1-4
- Research projects of Panagos et al. (2012&2014) and their conclusions for European values of K-factor
- New soil erodibility map of Greece by Efthimiou (2020)

As mentioned earlier, concerning the geological conditions, the area of Kremasta consists mostly of sedimentary rock formations such as flysch and limestone. So, for the estimation of K-factor, soils are classified into different types of flysch, limestone and alluvial deposits, and the area of each category is measured. Subsequently, typical values of K-factor are extracted from international literature (Van der Knijff et al., 2000) and adjusted to Kremasta study area. As shown in Figure 3.1-3, the geological map of Kremasta watershed was available (Zarris, 2019) and used for the computation of areas in AutoCAD environment:

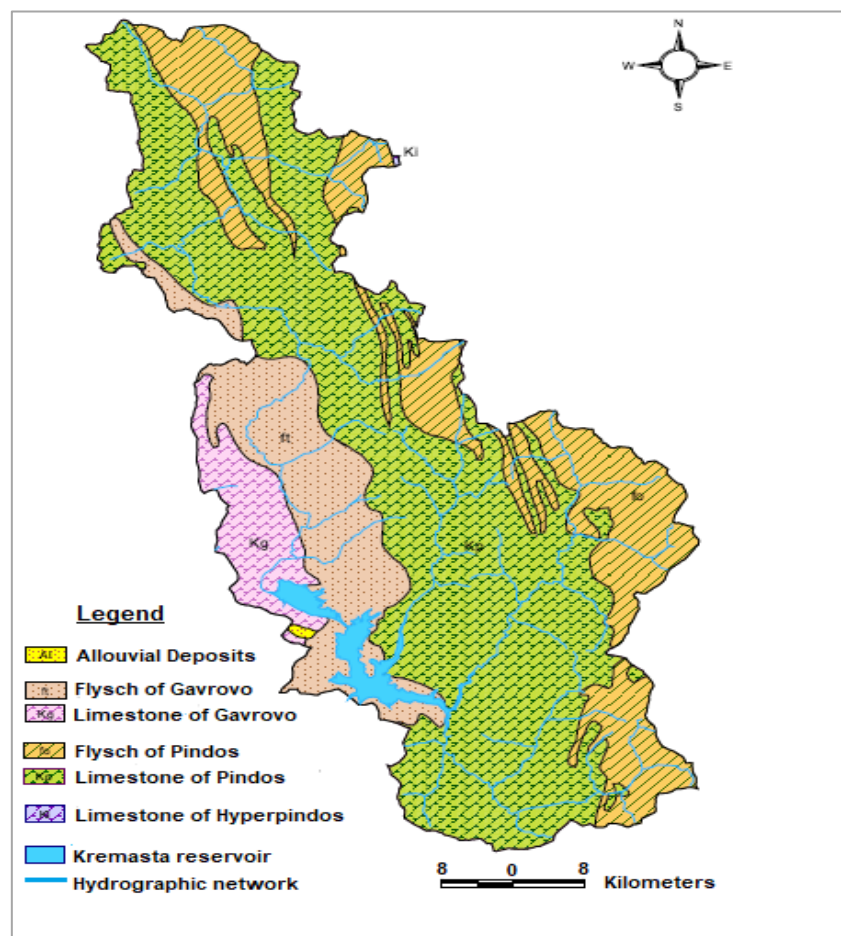


**Figure 3.1-3:** Geological formations of the watershed of Kremasta reservoir  
(Obtained by Zarris et al., 2001)

**Table 3.1-4:** Individual and mean values of K-factor for the formations of Kremasta

Geological Formation	Ai (km <sup>2</sup> )	Ki (t·h/MJ·mm)	pi (Ai/A)	Ki · pi
Flysch of Gavrovo	510,26	0,02	0,155	0,003099
Flysch of Pindos	737,41	0,035	0,224	0,007838
Allouval deposits	3,29	0,1	0,001	0,000100
Limestone of Pindos	1.850,1	0,004	0,562	0,002247
Limestone of Gavrovo	190,94	0,003	0,058	0,000174
Hyperpindos Limestone	0,99	0,008	0,0003	0,000002
<b>Total</b>	<b>3.292</b>	-	<b>1</b>	-
			<b>K (t·h/MJ·mm)</b>	<b>0,0135</b>

Based on the above-mentioned soil and petrographic conditions of Kremasta watershed and bearing in mind the percentage of clay, sand and silt from Panagos et al. (2014), the soils of this region are ranked in medium class (composition). From Table 2.3-1 it is obvious that K-factor for these soils is roughly 0,0311 (t·h/MJ·mm).

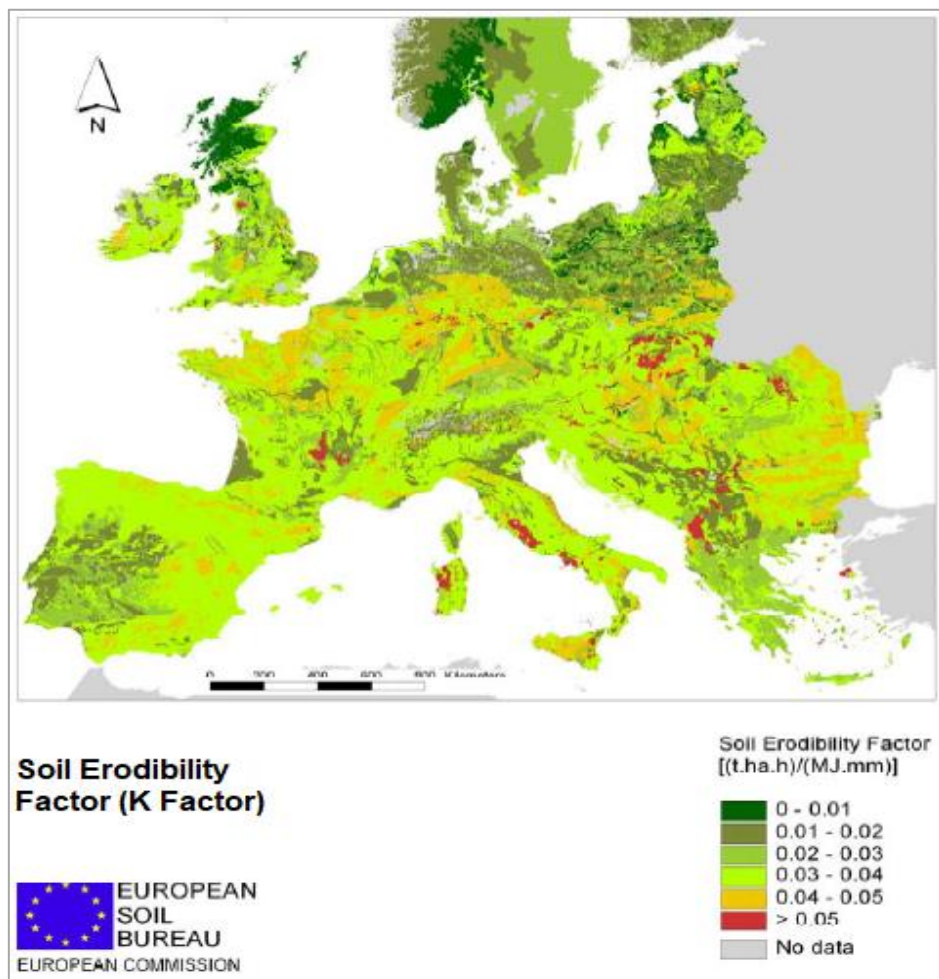


**Figure 3.1-4:** Calculation of K-factor (Obtained by Van der Knijff et al., 2000)

Efthimiou (2020) is another recent study that describes the development of the new soil erodibility map of Greece (Figure 3.1-5). The calculation of the K-factor was based on field samples deriving from the pan-European LUCAS database and the Greek NAGREF, utilizing the K-factor nomograph by Wischmeier and Smith (1978).

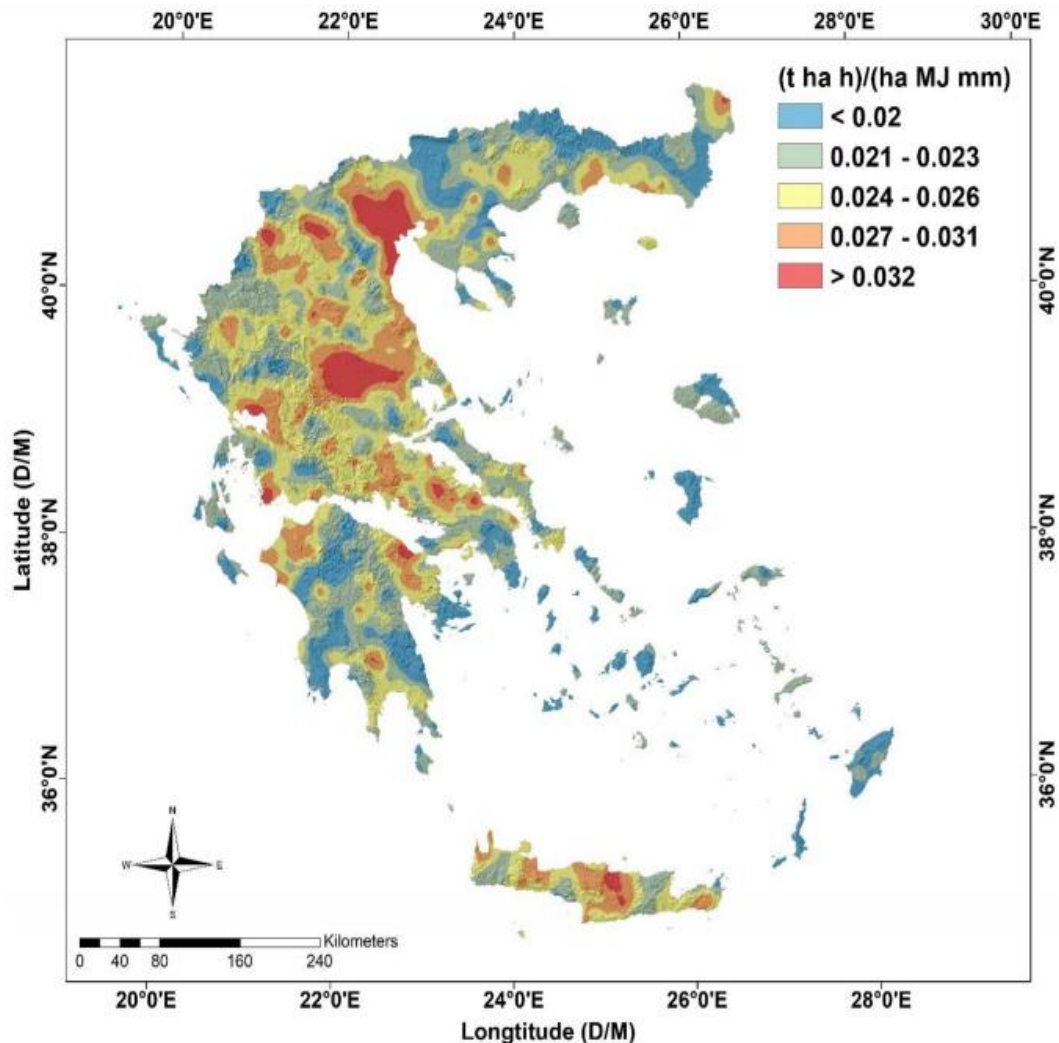


**Figure 3.1-5:** New soil erodibility map (K-factor) (Obtained by Efthimiou, 2020)

According to the results of the work of Panagos et al. (2012&2014), soil erodibility factor for Western Greece ranges from 0,02-0,028 ( $t \cdot h / MJ \cdot mm$ ). Van der Knijff's map (Figure 3.1-4) considers the K-factor for Western Greece to be 0,02-0,03 ( $t \cdot h / MJ \cdot mm$ ) (LUCAS European database). However, this value has a high probability of error because it is applicable to a large variety of soils and is also not so close to the value of K occurred from the analytical method. Moreover, Efthimiou (2020) map -more recent study- shows that K-factor for Kremasta is less than 0,02 ( $t \cdot h / MJ \cdot mm$ ). Thus, the chosen value for K-factor in the frame of this project is the one which is calculated analytically (Table 3.1-4): **0,0135**.

### 3.1.3 LS-factor

The calculation of LS-factor is held in Geographic Information System (GIS) environment; namely, QGIS program is used. The European Soil Data Centre (ESDAC) having as input a 1-km resolution digital elevation model (DEM) of Europe, estimated the steepness angle ( $\beta$ ) and the upstream area contributing to erosion ( $A_s$ ). Subsequently, the slope and slope length factors were estimated using the equation of Mitasova and Mitas (2001a). Eventually, the output of the GIS modelling is a map in grid form and resolution of 25 x 25 m (pixel size) showing the variation of LS values in the watershed of Kremasta. It displays values of LS-factor from 0,109 (minimum value) to 89.45 (maximum value), while the statistics mean extracted from the map is **8,124**, with as standard deviation of 5,11. As perceived, the mean value is high and this occurs mainly because of the abnormal terrain of Kremasta region which is evident at the DEM where the altitudes range from +240 (m) to +2500 (m). Figure 3.1-6 shows the resulting LS-map in GIS.

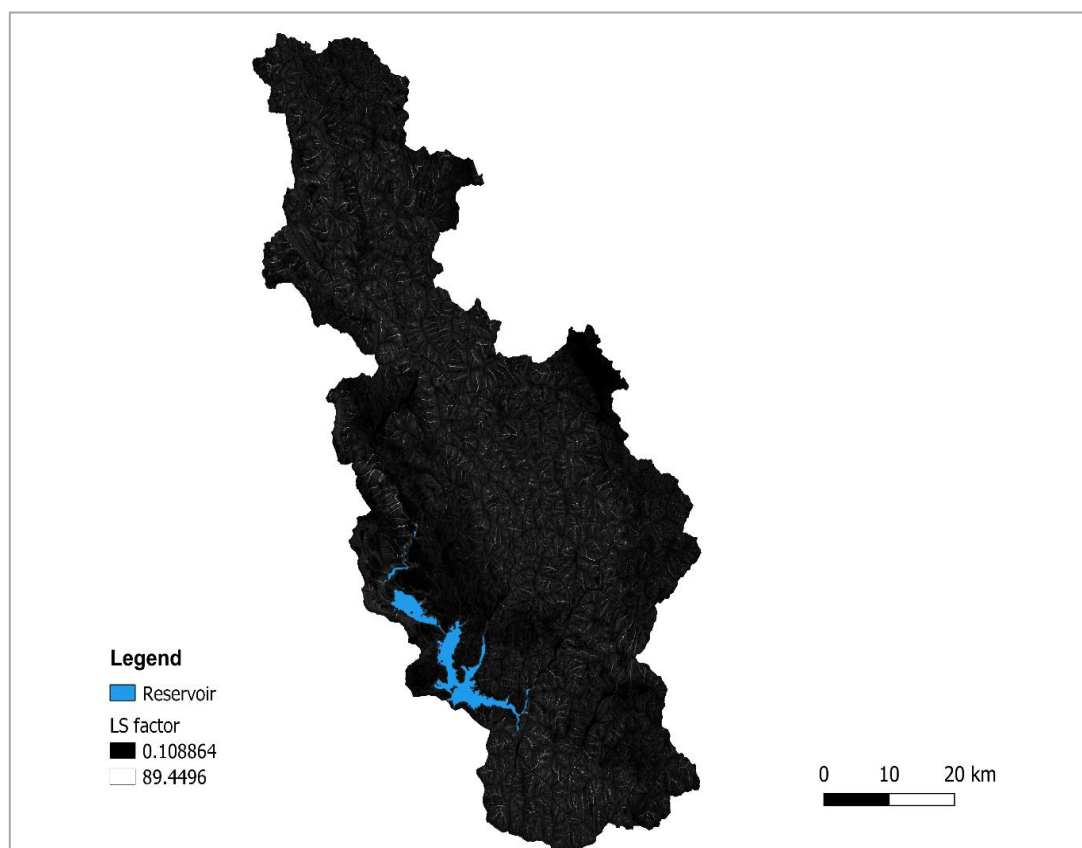


**Figure 3.1-6:** LS-factor map in GIS environment (QGIS 3.6.1)

From international literature such as Van der Knijff et al. (2000) and Panagos et al. (2014), it is obvious that for the surrounding area of Kremasta watershed, slope length and steepness (LS-factor) ranges from **5-10**. Therefore, the calculated value of **8,124** seems to be a decent approximation, regarding the size of this research study.

### 3.1.4 C-factor

The values of C-factor for every land use at Kremasta watershed, occur from international bibliographic research such as Wischmeier and Smith (1978), Lambrakis et al. (2011), Van Der knijff et al. (2000) and Zarris (2019). Based on variations that appear in the literature at values of C, it usually ranges from 0,001-0,6. In the frame of this study is chosen to keep the lower values of C, in order to balance the overestimation of R-factor.

The different land uses of Kremasta area are determined according to the digital maps of Corine Land Cover (2000) with scale of 1:100.000 and ΕΘΙΑΓΕ (a Greek research institute) with scale of 1:20.000. Accordingly, a value of C-factor is assigned to each one coded land use (Ci):

**Table 3.1-5:** Calculation of C-factor

Land Use	Ai (km <sup>2</sup> )	Ci	pi (Ai/A)·100%	Ci·pi
Continuous urban fabric	2,7	<b>0,001</b>	0,1	0,000001
Complex cultivation patterns	20,9	<b>0,18</b>	0,6	0,0011
Agriculture with natural vegetation	209,6	<b>0,07</b>	5,9	0,0041
Broad-leaved forest	131,5	<b>0,003</b>	3,7	0,0001
Coniferous forest	822,8	<b>0,001</b>	23,0	0,0002
Mixed forest	356,3	<b>0,002</b>	10,0	0,0002
Natural pastures	183,7	<b>0,3</b>	5,1	0,0154
Sclerophyllous vegetation	629,1	<b>0,02</b>	17,6	0,0035
Transitional woodland-shrub	649,4	<b>0,02</b>	18,2	0,0036
Beaches, dunes, sands	23,7	<b>0,6</b>	0,7	0,0040
Bare rocks	23,7	<b>0,02</b>	0,7	0,0001
Sparsely vegetated areas	434,9	<b>0,45</b>	12,2	0,0548
Inland marshes	81,7	<b>0,0001</b>	2,3	0,000002
<b>Total:</b>	<b>3.570</b>	-	<b>100</b>	<b>0,08724</b>

Table 3.1-5 above indicates that the lower values of cover management factor are observed in areas with high vegetation cover (e.g. forests) which declares the natural and significant protection that vegetation offers against the phenomenon of soil erosion. On the contrary, sparsely vegetated areas, sandy areas and pastures are highly exposed to erosion, so they are represented by a high cover management factor. The mean value of C occurred is **0,08724**.

According to Van der Knijff et al. (2000) cover management factor map for European Union, the figure attributed to C-factor for the Western Greece is between 0,05 and 0,2. Therefore, the value of **0,08724** which occurred from the calculations of the current thesis project and lies between those boundaries, is a decent approximation of the cover management situation of the area and certainly close to values suggested in international literature.

### 3.1.5 P-factor

The support practices factor, as occurs from international literature, usually receives the value of 1, without further research on the effect of alternative cultivation techniques to prevent the phenomenon of soil loss (Vachaviolos, 2014). Though, Kremasta watershed, which is a highly erodible area, is expected to have a low value of P because of these techniques. Therefore, P-factor should be thoroughly considered during the soil loss estimation because it can significantly reduce the soil loss.

The land cover for Kremasta basin is defined by Corine Land Cover (2000), the same way as with C-factor. Values of P-factor for each land use are extracted from international literature and projects such as Zarris (2019) and Vachaviolos (2014). The coefficients of the P-values for the different land uses in the Kremasta watershed are presented in Table 3.1-6.

**Table 3.1-6:** P-values for the different land uses of Kremasta watershed

Land Use	Ai (km <sup>2</sup> )	Pi	pi (Ai/A)-100%	Pi·pi
Continuous urban fabric	2,7	1	0,1	0,0008
Complex cultivation patterns	20,9	0,75	0,6	0,0044
Agricultural with natural vegetation	209,6	0,85	5,9	0,0499
Broad-leaved forest	131,5	1	3,7	0,0368
Coniferous forest	822,8	1	23,0	0,2305
Mixed forest	356,3	1	10,0	0,0998
Natural pastures	183,7	1	5,1	0,0515
Sclerophyllous vegetation	629,1	1	17,6	0,1762
Transitional woodland-shrub	649,4	1	18,2	0,1819
Beaches, dunes, sands	23,7	0,8	0,7	0,0053
Bare rocks	23,7	0,8	0,7	0,0053
Sparsely vegetated areas	434,9	1	12,2	0,1218
Inland marshes	81,7	1	2,3	0,0229
<b>Total:</b>	<b>3.570</b>	<b>-</b>	<b>100</b>	<b>0,9871</b>

As observed, the final mean value of P-factor for Kremasta watershed is **0,9871**. According to Panagos et al. (2015), the most erosive areas (R-factor > 900 MJ·mm/ha·h·yr) such as Kremasta mainly located in the Mediterranean basin have mean P-factor equal to 0,9574. On the contrary, in the less erosive areas (R-factor < 410 MJ·mm/ha·h·yr) the mean P-factor is 0,9845. The support practices are mainly focusing in erosive prone areas (Panagos et al., 2015). However, in Kremasta basin, which is a highly erodible area, P-factor has a high value because it is mainly composed of forests and sparse vegetation without special cultivation methods to prevent soil loss.

According to Panagos et al. (2015) (Figure 3.1-7) for the study area, which is located in Western Greece, P-factor ranges from **0,9-0,99**, so the value of **0,9871** is considered as a good approximation very close to values from international literature.

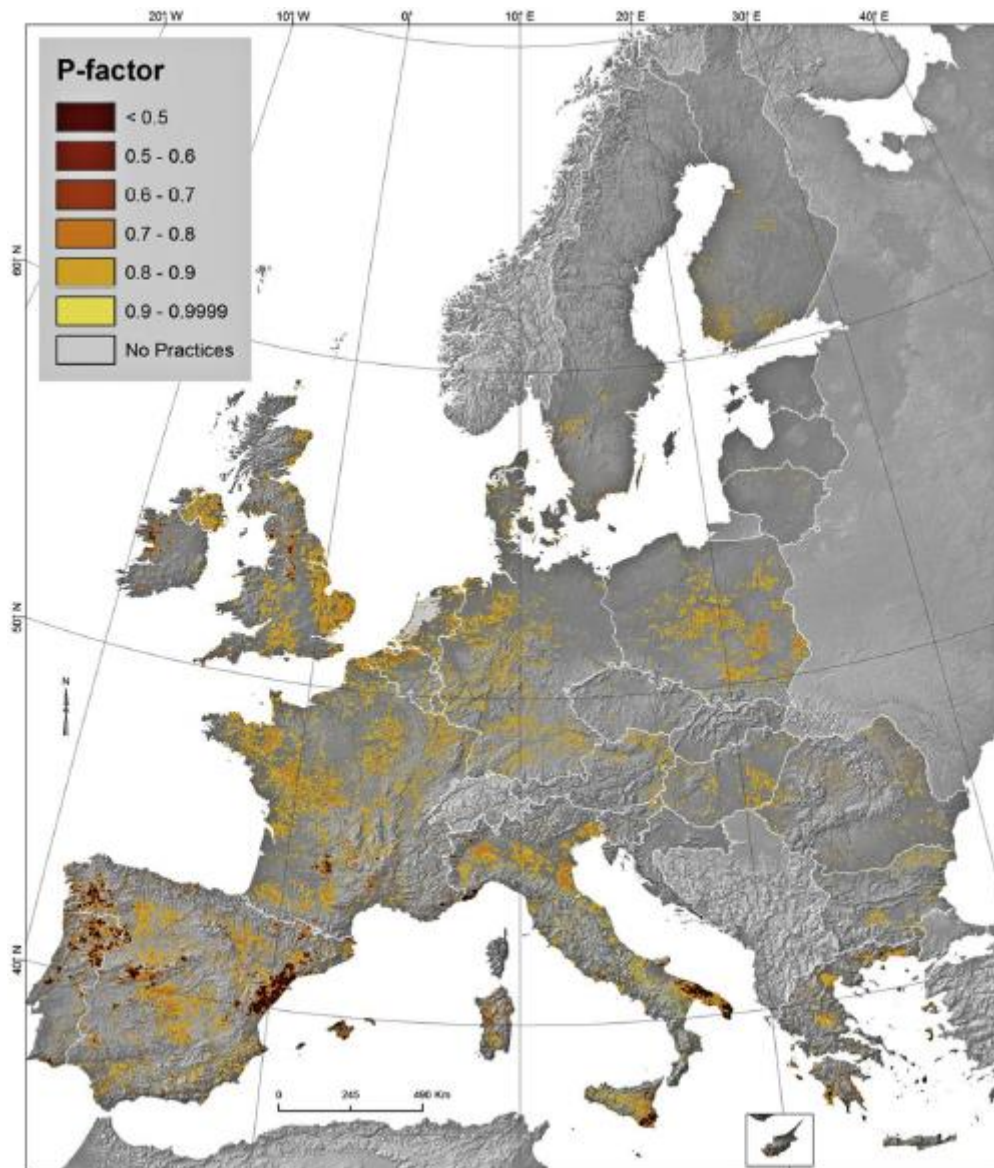


**Figure 3.1-7:** Support conservation practices factor in European-regional level  
(Obtained by Panagos et al., 2015)

All the aforementioned calculations contribute to the estimation of a value for the soil loss (t/ha) using the RUSLE equation:

$$A = R \cdot K \cdot LS \cdot C \cdot P = 1297,8 \cdot 0,0135 \cdot 8,124 \cdot 0,0872 \cdot 0,987 = 12,257 \text{ (t/ha)}$$

### 3.2 Second method: GIS modeling

The second methodology to estimate the soil loss in Kremasta watershed includes the use of GIS modelling and the RUSLE equation. The program used is QGIS which has a simple and friendly interface presented in Figure 3.2-1. Moreover, the European Soil Data Centre (ESDAC) provided us with high resolution maps in grid form, for every single factor of RUSLE formula for all the European countries. Thus, the first step is to define the area and geometry of Kremasta watershed and specify its boundaries and afterwards to extract each factor map and the information that contains (Figure 3.2-2).

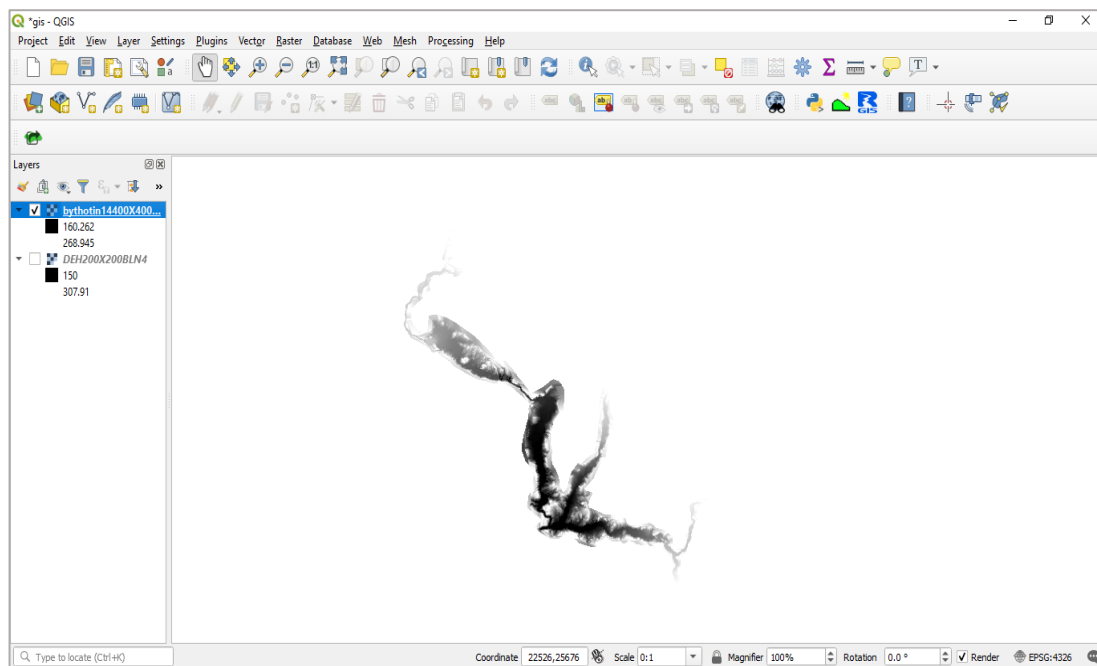


Figure 3.2-1: QGIS Interface (QGIS 3.6.1)

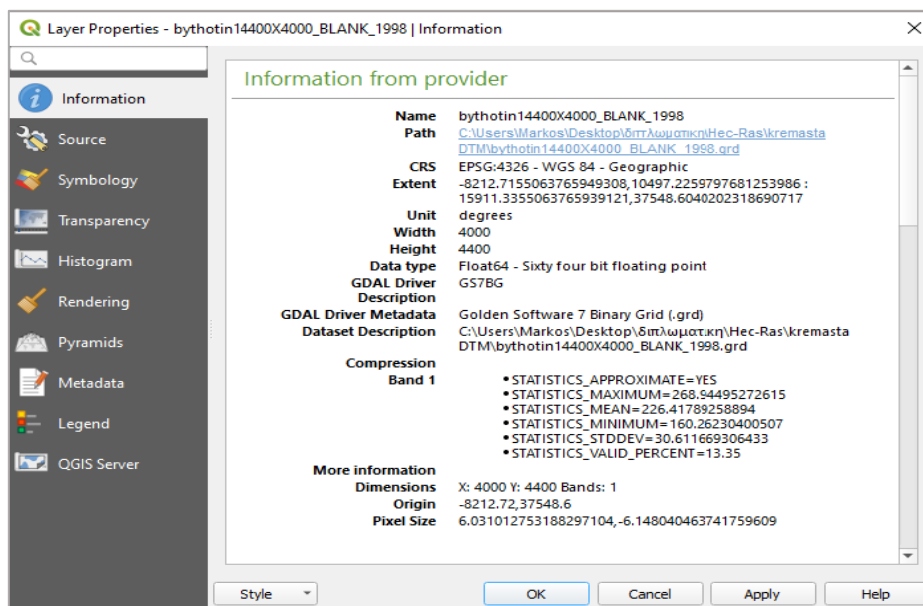
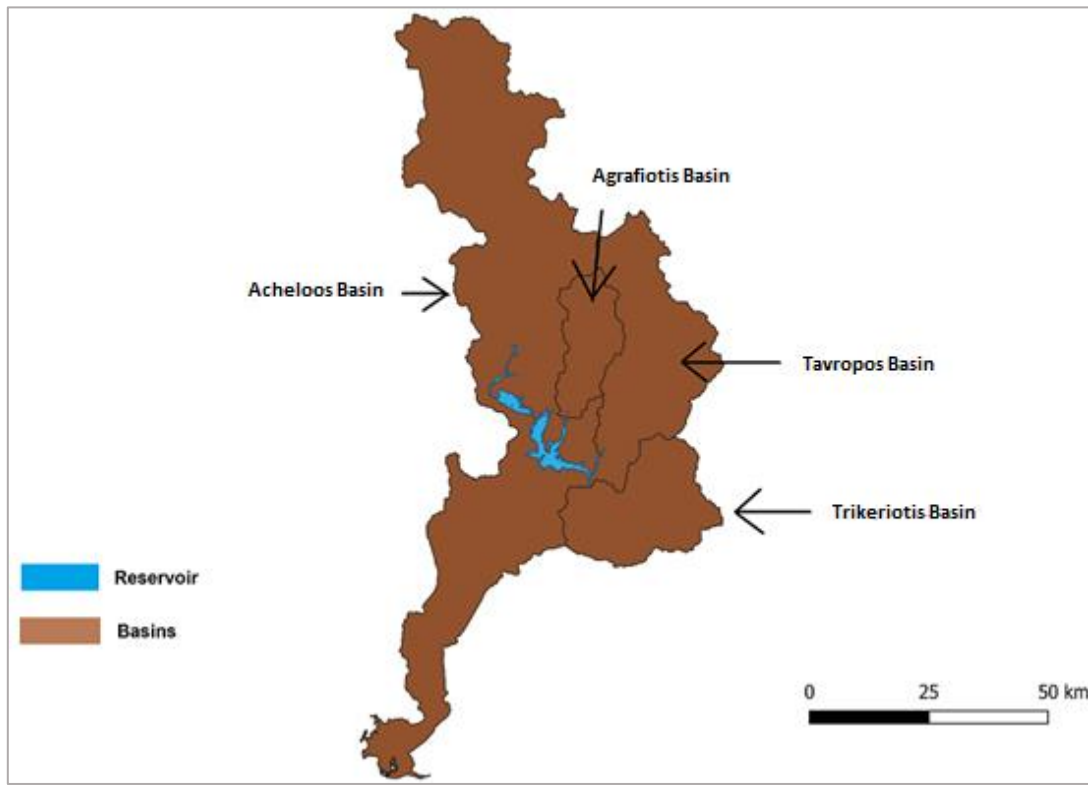


Figure 3.2-2: Layer properties window (QGIS 3.6.1)

### 3.2.1 Geometry of the surrounding area

Initially, the four basins of the main rivers of the surrounding area are presented in vector form in QGIS environment in Figure 3.2-3:



**Figure 3.2-3:** Four main basins of the surrounding area of Kremasta in vector form (QGIS 3.6.1)

Data concerning the reservoir and the sub-basins is gathered from [geodata.gov](http://geodata.gov). Subsequently, the watershed of Kremasta reservoir is determined in Figure 3.2-4:

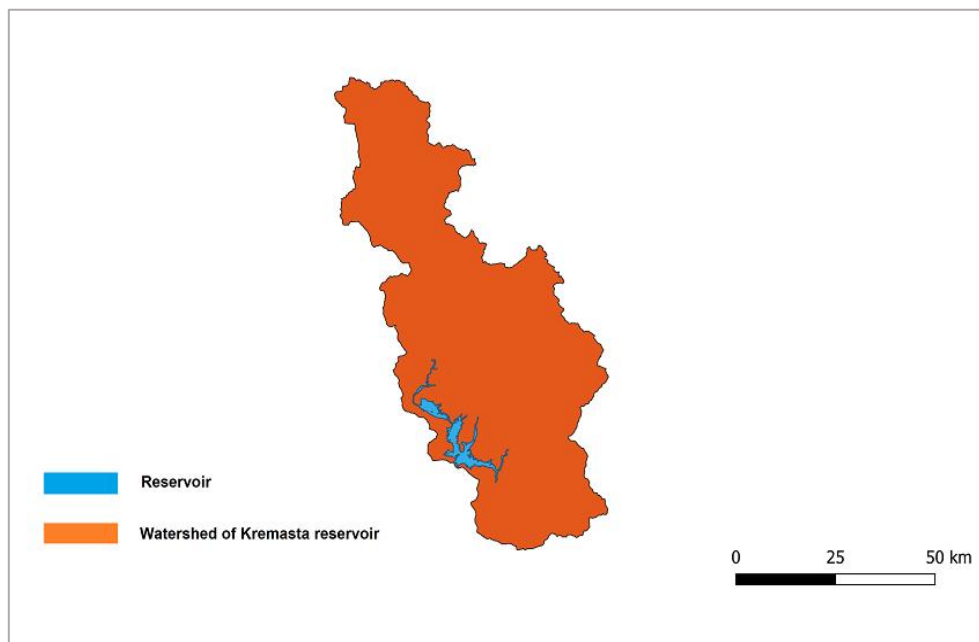


**Figure 3.2-4:** Watershed of Kremasta reservoir in vector form (QGIS 3.6.1)

### 3.2.2 Grids of RUSLE factors

In QGIS it is easy to import layers (“Vector”, “Raster” and “Mesh” are the most common types) which include information usually regarding soil or ground properties (such as Digital Elevation/Terrain Models) as Figure 3.2-5 indicates.

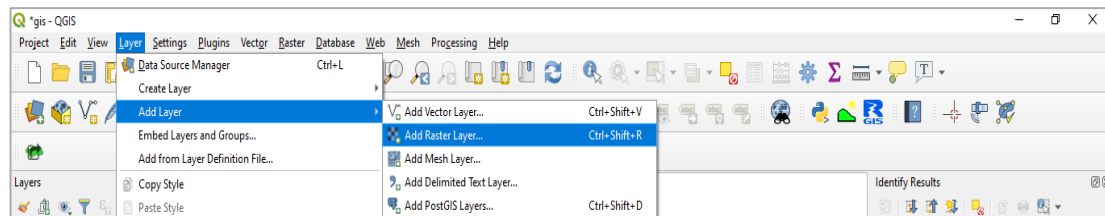


**Figure 3.2-5:** Process needed to add a layer in QGIS (QGIS 3.6.1)

All the grids below are extracted from European Soil Data Centre (ESDAC) site and contain information concerning the RUSLE equation factors.

#### 3.2.2.1 *R-factor:*

The Figure 3.2-6 indicates how the values of R-factor (rainfall erosivity) range across the watershed of Kremasta:

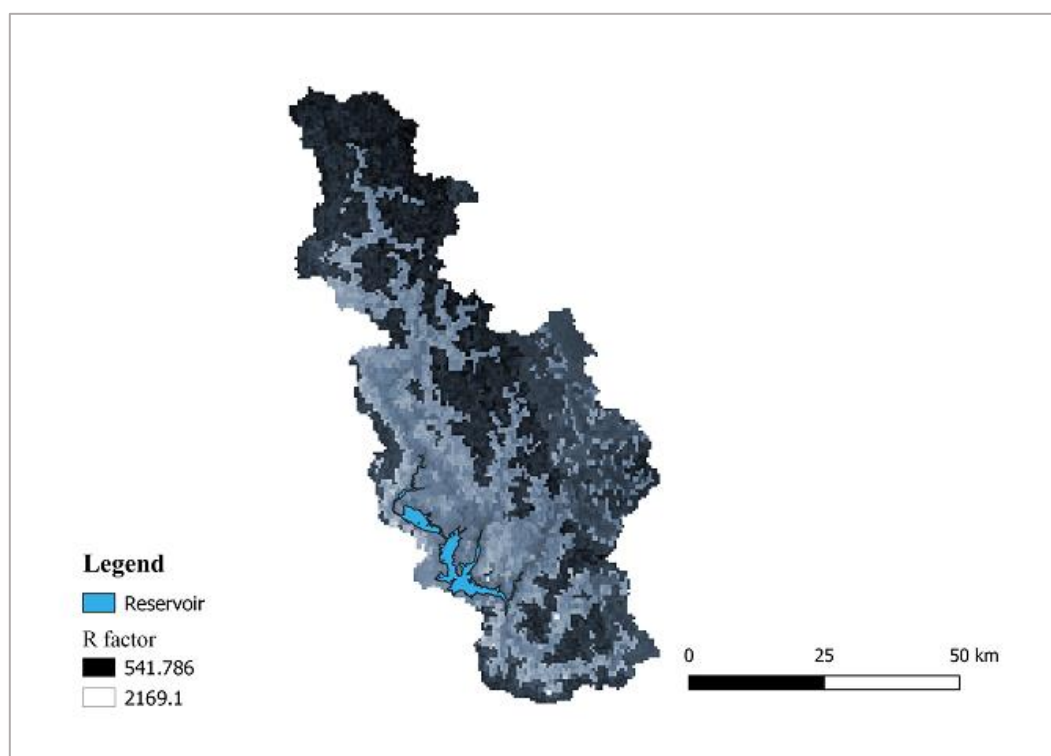


**Figure 3.2-6:** Grid revealing the R-factor values of the watershed (QGIS 3.6.1)

The resolution (pixel size) of the above grid is 500 x 500 (m) and it displays values of rainfall erosivity factor from 541,8 (minimum value) to 2.169,1 (maximum value), while the statistics mean extracted from the map is **1.100,3** (MJ·mm / ha·h), with a standard deviation of 306,2.

### 3.2.2.2 *K and LS factors:*

The Figure 3.2-7 below is in grid form and resolution (pixel size) of 500 x 500 (m) and displays values of soil erodibility factor from 0,0075 (minimum value) to 0,0434 (maximum value), while the statistics mean extracted from the map is **0,0204** ( $t \cdot h / MJ \cdot mm$ ), with a standard deviation of 0,00397.

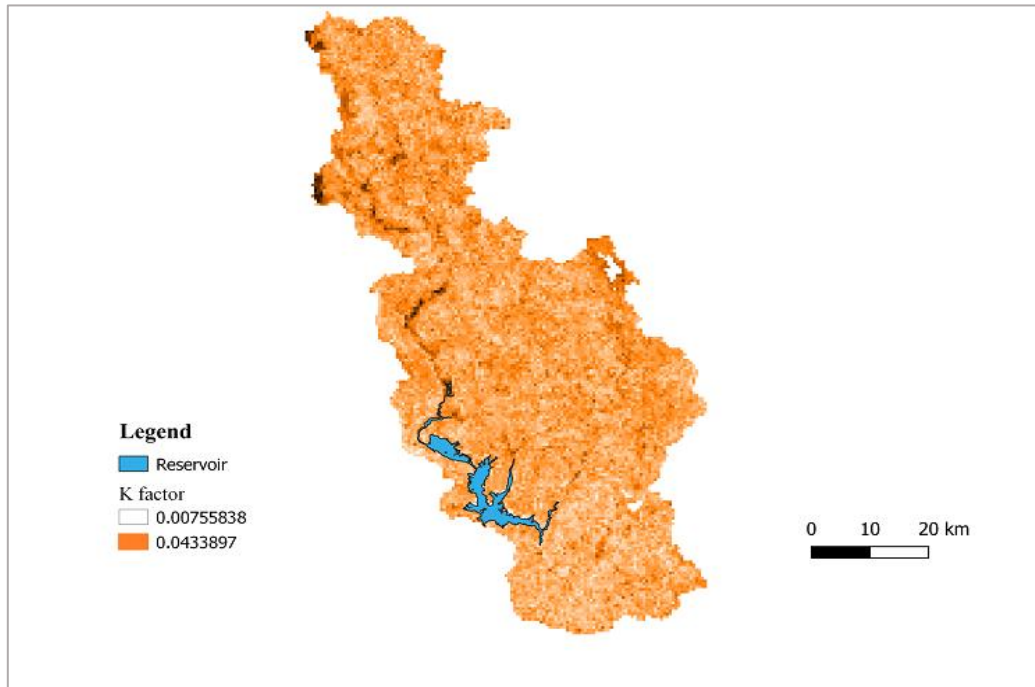


**Figure 3.2-7:** Grid revealing the K-factor values of the watershed (QGIS 3.6.1)

The Figure 3.2-8 below is in grid form and resolution (pixel size) of 25 x 25 (m) and shows the variation of LS-values in the watershed of Kremasta:

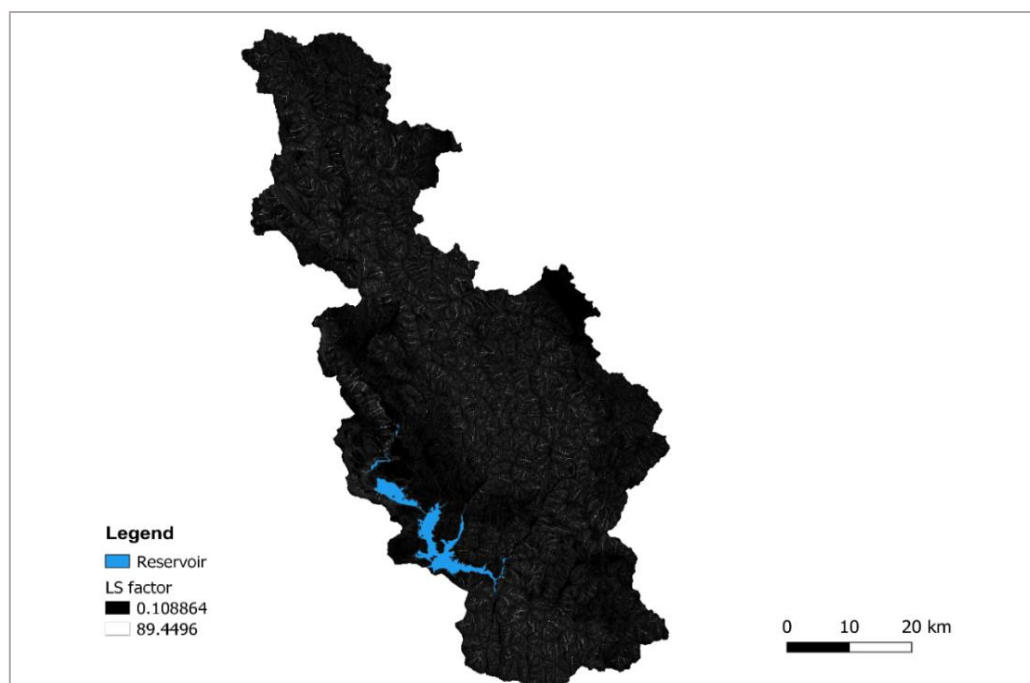


**Figure 3.2-8:** Grid revealing the LS-factor values of the watershed (QGIS 3.6.1)

It displays values of LS-factor from 0,109 (minimum value) to 89,45 (maximum value), while the statistics mean extracted from the map is **8,124**, with a standard deviation of 5,11. The maximum values of LS-factor (the white ones) appear at the ridges of the mountains and in areas of rough terrain.

### 3.2.2.3 C-factor:

The Figure 3.2-9 below is in grid form and resolution of 100 x 100 (m) and shows the variation of C-values in the watershed of Kremasta:

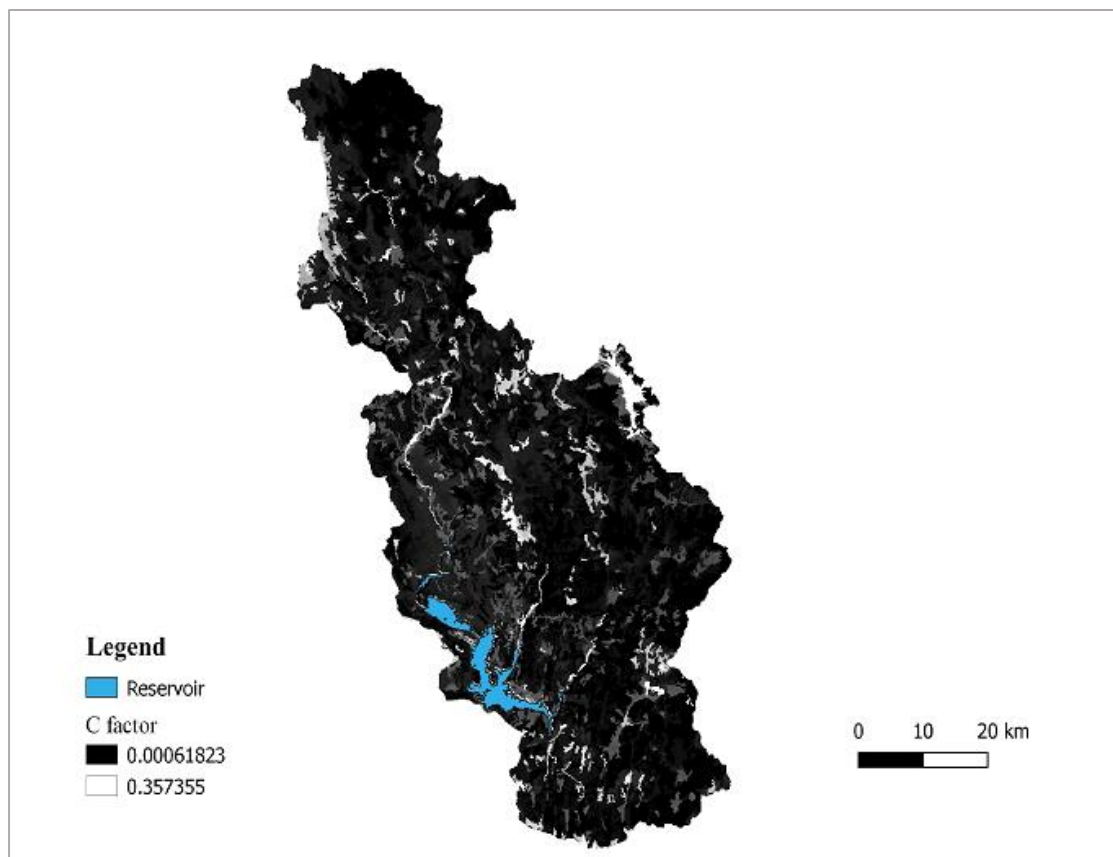


**Figure 3.2-9:** Grid revealing the C-factor values of the watershed (QGIS 3.6.1)

It displays values of C-factor from 0,0006 (minimum value) to 0,3573 (maximum value), while the statistics mean extracted from the map is **0,0406** with a standard deviation of 0,0634. The maximum values of C-factor (the white ones) appear in sparsely vegetated areas, natural pastures etc. On the opposite side, the minimum values are displayed in low erodibility areas such as forests and urban fabrics.

### 3.2.2.4 P-factor:

The Figure 3.2-10 below is in grid form and resolution of 100 x 100 (m) and shows the variation of P-values in the watershed of Kremasta.

It displays values of P-factor from 0,6 (minimum value) to 1 (maximum value), while the statistics mean extracted from the map is **0,9975** with a standard deviation of 0,0271. The maximum values of P-factor (the black ones) appear in areas with no special cultivation technique to prevent erosion such as forests and other natural vegetated regions. On the contrary, the minimum values are displayed in complex cultivation patterns and areas with contouring methods.

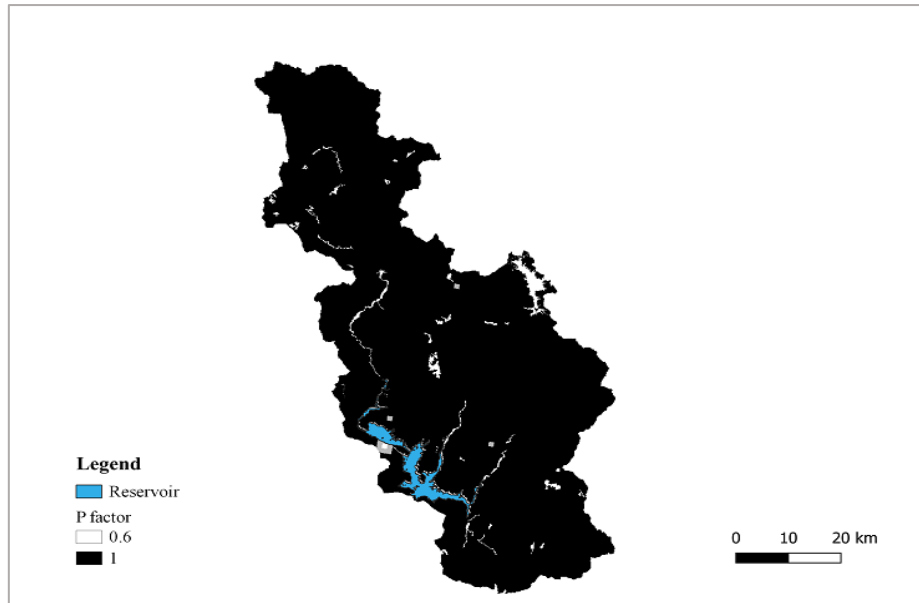


**Figure 3.2-10:** Grid revealing the P-factor values of the watershed (QGIS 3.6.1)

### 3.2.3 Soil loss

After extracting all the maps in grid form, the next step is to calculate the soil loss by multiplying the rasters, using the RUSLE equation. This is feasible due to the raster calculator tool of QGIS and a boundary raster of the basin. The white-colored areas are the ones for which data are not available. In the Figure 3.2-11 below, the resulting map of soil loss in grid form, is presented. The result is a raster of soil loss (25 x 25 m resolution) for Kremasta basin, with a minimum value (black) of 0,000874 (t/ha), a maximum value (yellow-green) of 300,38 (t/ha) and a **mean annual** soil loss value of **7,385** (t/ha).

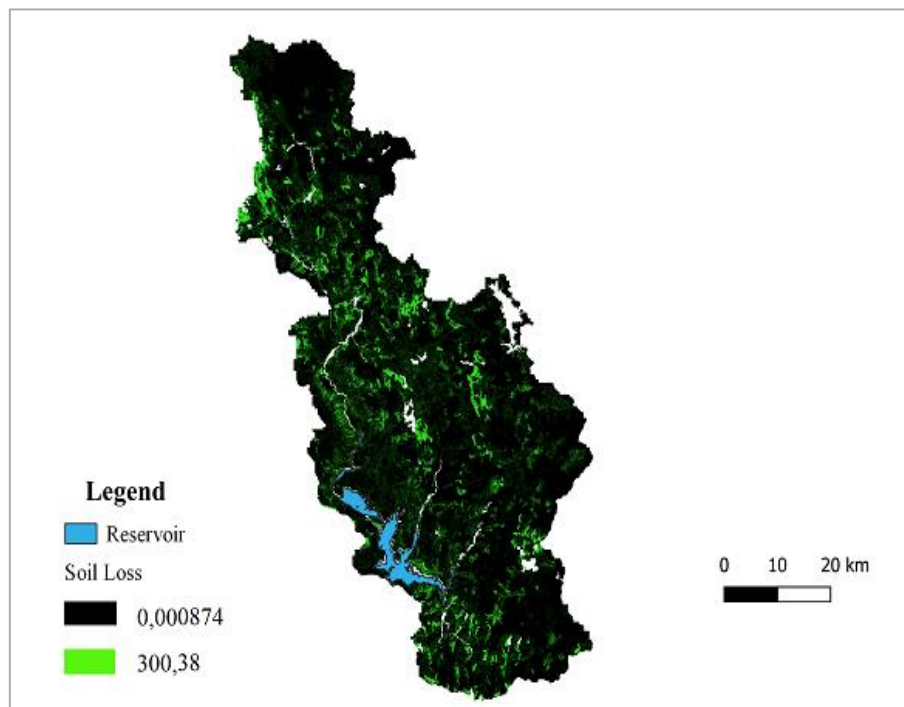


**Figure 3.2-11:** Grid of soil loss (QGIS 3.6.1)

### 3.3 Aggregated results of the two methods and further calculations

#### 3.3.1 Comparison of the two methods

The first method to calculate the soil loss is the application of RUSLE equation and analytical formulas for its factors, ending up in a mean value for each RUSLE factor. The second methodology is the extraction of grids for every factor of RUSLE, in GIS environment and the multiplication of grids to extract a final soil loss grid.

The results that occurred from these two methodologies are presented and compared at Table 3.3-1 below:

**Table 3.3-1:** Comparison of the two methodologies

	Analytical use of RUSLE	GIS and RUSLE
R-factor (MJ·mm/ha·h):	1.297,8	1.100,3
K-factor (t·h/MJ·mm):	0,0135	0,0204
LS-factor	8,124	8,124
C-factor	0,0872	0,0406
P-factor	0,987	0,9975
<b>Soil Loss (t/ha):</b>	<b>12,257</b>	<b>7,385</b>

As observed at Table 3.3-1, the average **annual** soil loss occurred from the analytical RUSLE application is much higher than the one from GIS modelling. This happens due to the wide variety of the values attributed to C-factor for every land use and also the overestimation of R-factor in the analytical application of RUSLE, due to lack of long-term precipitation data. According to Panagos et al. (2015), the soil loss of the area of Kremasta ranges from 5-10 (t/ha), so both approximations seem to be more satisfying.

#### 3.3.2 Estimation of sediment yield

The issue of the transition from soil loss ( $A_s$ ) to sediment yield ( $S_y$ ), has been a field of intensive research efforts from the 1960s to today (Vachaviolos, 2014). Sediment yield is defined as the quantity of sediment that ends up in the reservoir. The following equation connects the sediment yield with the soil loss through a delivery ratio:

$$SDR = \frac{S_y}{A_s} \quad (3.3-1)$$

where

SDR is the Sediment delivery ratio (0~1),

$S_y$  is the sediment yield (t/ha),

$A_s$  is the soil loss (t/ha).

The sediment delivery ratio is the part of soil loss that is converted into sediment yield through the hydrographic network. From a natural point of view, the sediment yield is the difference between the produced soil loss and the quantity of sediment that is repositioned somewhere in the watershed, but not inside the reservoir.

There are several morphological, geological, climatic and hydrological factors that play a significant role in the “transformation” of soil loss into sediment yield. For the estimation of SDR, empirical equations are used and they correlation the factor either with the Area (mi<sup>2</sup>), or with other characteristics of the watershed. The first formulas are usually preferred due to their good statistic correlation and their simple application. The most common formulas are:

- $\text{Log}(SDR) = 1,7935 - 0,14191 \cdot \log(A)$ , **Renfro (1975)** (3.3-2)

- $SDR = 0,51 \cdot A^{-0,11}$ , **USDA-SCS (1971)** (3.3-3)

- $SDR = 0,42 \cdot A^{-0,125}$ , **Vanoni (1975)** (3.3-4)

Where A is the Area in (mi<sup>2</sup>). In the frame of this study Vanoni (1975) equation is used, with the area of Kremasta basin being approximately 3292 (km<sup>2</sup>) = 1271 (mi<sup>2</sup>). Thus, the results of sediment delivery ratio by Vanoni (1975) equation and sediment yield by the equation 3.3-1 above are as presented in Table 3.3-2 below:

**Table 3.3-2:** Estimation of sediment yield by empirical equations

	Analytical use of RUSLE	GIS and RUSLE
Soil Loss (t/ha)	12,252	7,385
A (mi <sup>2</sup> )	1.271	1.271
SDR	0,172	0,172
Sediment Yield (t/ha):	2,107	1,270
<b>Sediment Yield (t/km<sup>2</sup>):</b>	<b>210,7</b>	<b>127</b>

### 3.4 Koutsoyiannis & Tarla (1987) method

Apart from RUSLE equation, Koutsoyiannis and Tarla (1987) introduced the following equation based on measurements on the mean sediment yield in several locations of North-western Greece. This method ignores the fact that sometimes the same percentages of geological formations may have vastly different properties in terms of erodibility, because totally different areas are examined. It considers that every geological formation has a mean group of standard properties and hence it can give a quantitative estimation of the sediment yield based on that (Koutsoyiannis and Tarla, 1987). Thus, the mean annual sediment yield (G in t/km<sup>2</sup>) is calculated as follows:

$$G = 15 \cdot \gamma \cdot e^{3P} \quad (3.4-1)$$

where P is the mean annual precipitation in the watershed (m) and γ is the geological factor given from the following formula:

$$\gamma = k1 \cdot p1 + k2 \cdot p2 + k3 \cdot p3 \quad (3.4-2)$$

where k1, k2, k3 are factors describing the erodibility of each group of geological formations that the watershed consists of and in particular:

- High erodibility:  $k_1 = 1$  for alluvial deposits, flysch
- Medium erodibility:  $k_2 = 0,5$  for sandstones, marls, slates
- Low erodibility:  $k_3 = 0,1$  for limestones, dolomite, metamorphic rocks, igneous rocks

and  $p_1, p_2, p_3$  the equivalent ratios of area where each category of formations appears divided by the total area of the watershed and are estimated using geological maps.

For the case of Kremasta reservoir the  $p_1, p_2, p_3$  percentages are measured from geological maps (obtained by Zarris et al., 2001) in AutoCAD 2D environment using a simple “Area” command. The results indicate that alluvial deposits and flysch account for 38% of the area of the basin, while sandstone, marls and slates have 1% and limestones account for 61%. Thus,  $p_1$  is 38%,  $p_2$  is 1% and  $p_3$  is 61%. Moreover, the mean annual precipitation of Kremasta watershed is 1,433 (m). As so from equations 3.4-1 and 3.4-2:

$$\gamma = 0,38 \cdot 1 + 0,01 \cdot 0,5 + 0,61 \cdot 0,1 = 0,446$$

$$G = 15 \cdot 0,446 \cdot e^{3 \cdot 1,433} = 492,6 \text{ (t/km}^2\text{)}$$

As observed, the sediment yield that occurs from Koutsoyiannis and Tarla (1987) method is 492,6 (t/km<sup>2</sup>), while the RUSLE equation and GIS method resulted in 210,7 (t/km<sup>2</sup>) and 127 (t/km<sup>2</sup>) accordingly. It is evident that these methods differ in terms of the parameters they examine and the empirical features they contain, so the disparity among the results is anticipated at a certain level. Moreover, the unpredictability of sediment erosion and transport as natural stochastic processes contributes to this discrepancy.

Apart from the precipitation and the geological factor, this method does not consider other factors such as land cover management, the slopes of the terrain of the watershed and “anti-erosion” techniques that might exist. All these could play an important role and decrease the erosion dramatically. For example, vegetation cover can sometimes inhibit the erosion rate up to 1% in comparison with a “naked” surface (Koutsoyiannis and Tarla, 1987). This method takes into account the current soil situation and the precipitation of the examined area. However, it only considers the case of suspended sediment transport.

Koutsoyiannis and Tarla (1987) found that by comparing different watersheds, there is a positive correlation between the sediment yield and the appearance ratio of flysch inside the basin, whereas for limestone this correlation is negative. This conclusion is reasonable because flysch is highly erodible, while limestone is not. In addition, the material produced from limestone erosion is more often carried as bed load, rather than in suspension, thus not resulting in high sediment yield values (Koutsoyiannis and Tarla, 1987).

## 4 Estimation of sediment yield using rating curves

### 4.1 Collection of data

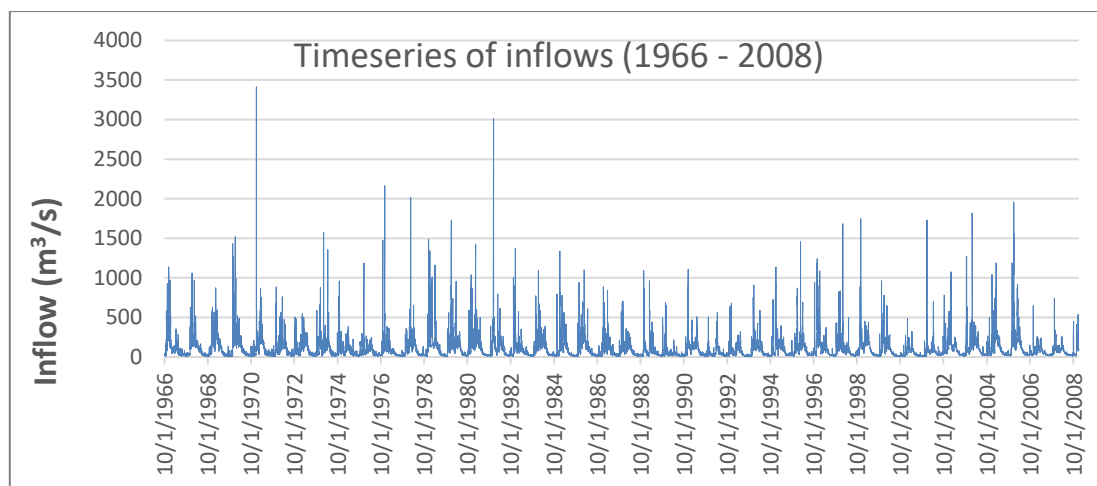
Another way to estimate the sediment yield ending up inside the Kremasta reservoir is to build a relationship between the flow and the sediment load, by using data occurred from field measurements. The gathering and editing of flow data for Acheloos river and its tributaries (flow of the rivers that end up into Kremasta reservoir) was not an easy process. Years of continuous measurements, work and research from a team of scientists at National Technical University of Athens and other institutions, led to the collection of nearly 42 years of inflow data from 1/10/1966 (before the beginning of the dam's operation) to 31/12/2008, as observed below in Table 4.4-1 and Graph 4.4-1. Worth mentioning here is that the inflow data available are daily and cover roughly a 42-year period. Thus, concerning that it was not feasible to present all the flow series in Table format, only a sample of them is presented below along with the plot (Graph 4.1-1) that shows how the total inflows of the reservoir vary through the aforementioned time period.

**Table 4.1-1:** Inflow data at Kremasta reservoir (1966-2008)

Date	Flow (m3/s)
1/10/1966	32,5
2/10/1966	24,9
3/10/1966	39,6
4/10/1966	43,0
5/10/1966	46,3
6/10/1966	42,2
7/10/1966	38,0
8/10/1966	17,7
9/10/1966	17,7
10/10/1966	38,8
11/10/1966	32,5
12/10/1966	10,8
13/10/1966	18,5
14/10/1966	23,6
15/10/1966	30,4
16/10/1966	30,4
17/10/1966	30,4
18/10/1966	30,4
19/10/1966	163,4
20/10/1966	81,8
21/10/1966	22,8
22/10/1966	23,9
...	...
7/12/2008	142,5
8/12/2008	120,4
9/12/2008	93,8
10/12/2008	90,5
11/12/2008	76,8
12/12/2008	105,5
13/12/2008	182,5
14/12/2008	192,4
15/12/2008	192,3
16/12/2008	175,7
17/12/2008	127,2
18/12/2008	537,7
19/12/2008	510,4
20/12/2008	356,9
21/12/2008	238,1
22/12/2008	175,2
23/12/2008	152,4
24/12/2008	129,0
25/12/2008	113,8
26/12/2008	113,8
27/12/2008	116,2
28/12/2008	94,1
29/12/2008	99,4
30/12/2008	78,9
31/12/2008	73,2

The main soil parameters that affect the routing of the surface runoff are (Zarris, 2019):

- The permeability of the soils,
- The available soil moisture,
- The mean slope, the slope length and manning's roughness factor.



**Graph 4.1-1:** Hydrograph of Kremasta reservoir inflows (1966 - 2008)

Sediment load measurements were held by the Public Power Corporation (PPC S.A.) of Greece between 1967 and 1970 with a different frequency per season and data concerning the sediment discharge of Acheloos river and its tributaries were collected. The areas of sediment load measurements are: Avlaki, Megdovas, Mesochora and Kremasta, all of them included in Kremasta's reservoir watershed. The values of such measurements (only for Kremasta and Mesochora hydrographic station) are illustrated below in Tables 4.1-2 and 4.1-3.

**Table 4.1-2:** Field measurements of flow and sediment flow at Kremasta area (Obtained by Zarris, 2019)

Date	Flow (m <sup>3</sup> /s)	Sediment Flow (kg/s)
22/1/1964	85	7.92
23/1/1964	88	11.75
24/1/1964	85	6.79
25/1/1964	80	6.72
26/1/1964	79	8.45
27/1/1964	76	9.56
29/1/1964	70	6.78
30/1/1964	73	10.37
31/1/1964	86	38.19
1/2/1964	101	25.46
2/2/1964	101	33.80
15/2/1964	800	3460.65
16/2/1964	352	581.02
17/2/1964	205	190.39
28/2/1964	230	274.31
1/3/1964	775	806.71
2/3/1964	1780	12094.91
3/3/1964	1150	6585.65

**Table 4.1-3:** Field measurements of flow and sediment flow at Mesochora area  
(Obtained by Zarris, 2019)

Date	Flow (m <sup>3</sup> /s)	Sediment Flow (kg/s)
12/12/69	50.08	2.82
12/17/69	55.95	2.95
4/10/70	51.3	3.41
4/13/70	79.97	10.17
2/7/72	18.25	0.54
2/14/72	42.52	1.11
2/24/72	42.49	2.94
5/3/72	36.61	2.36
6/7/72	11.88	0.42
6/14/72	9.3	0.28
2/24/73	25.66	0.78
2/26/73	34.55	1.25

The other data extracted from Zarris (2019) research project is presented in the Appendix at the end of the present thesis project. The number of measurements held seems insufficient to calculate accurately the mean annual sediment yield and indeed Wischmeier and Smith (1978) believe that at least 22 years of precipitation measurements are needed to estimate the rainfall erosivity. This means (especially for wide basins) that the time needed for soil loss to “transform” into sediment yield is extremely high. In the frame of the current study it is going to be proved (by comparing the results with Zarris (2019) study) that even short-term flow - sediment load measurements can reveal the real situation of the deposition in the reservoir pool.

## 4.2 Flow - sediment load rating curves

In this unit, two different cases are examined. At the first one, only data measured at Kremasta hydrometric station are used, while at the second case, data are gathered from measurements carried out at 4 hydrometric stations into the watershed (Avlaki, Megdovas, Mesochora, Kremasta). The goal is to compare the outcome of the two different datasets in terms of accuracy and proximity to the hydrographic survey of Zarris et al. (2001). It would also be meaningful to investigate if the methodology that uses rating curves is more representative and closer to the real situation of the reservoir (according to hydrographic surveys), than the other methods. The method used is the simple regression between the logarithmic values of Q and Q<sub>s</sub>.

### 4.2.1 First case

The first area, with data measured in 1964, is the location of Acheloos river at Kremasta region, before the construction and operation of the dam. The goal here is to derive a formula between the river flow and sediment discharge (Q-Q<sub>s</sub>). It usually has an exponential form as below:

$$Q_s = a \cdot Q^\beta \quad (4.2-1)$$

The factors “a” and “b” of the equation are calculated by using the “slope” and “intercept” functions of excel programming and the flow and sediment load data for the year 1964, where:

- $b = slope$  (4.2-2)

- $a = e^{intercept}$  (4.2-3)

Table 4.2-1 presents the flow and sediment discharge data along with their logarithms, while Table 4.2-2 shows the construction of the relationship between them.

**Table 4.2-1:** Flow and sediment load measurements and logarithms

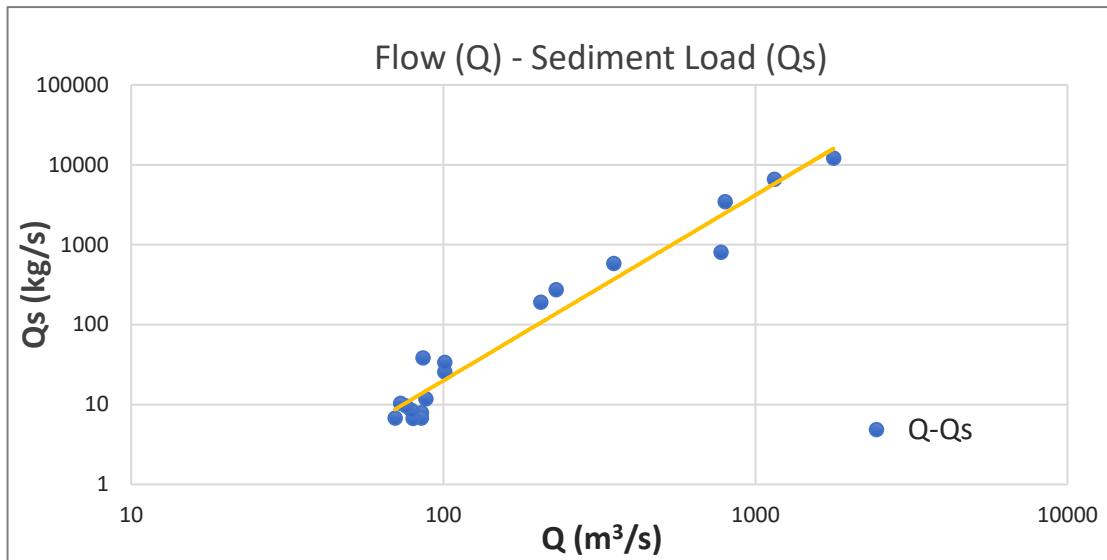
Date	Q (m <sup>3</sup> /s)	Qs (kg/s)	ln (Q)	ln (Qs)
22/1/1964	85	7,92	4,443	2,069
23/1/1964	88	11,75	4,477	2,464
24/1/1964	85	6,79	4,443	1,915
25/1/1964	80	6,72	4,382	1,905
26/1/1964	79	8,45	4,369	2,134
27/1/1964	76	9,56	4,331	2,258
29/1/1964	70	6,78	4,248	1,914
30/1/1964	73	10,37	4,290	2,339
31/1/1964	86	38,19	4,454	3,643
1/2/1964	101	25,46	4,615	3,237
2/2/1964	101	33,8	4,615	3,520
15/2/1964	800	3460,65	6,685	8,149
16/2/1964	352	581,02	5,864	6,365
17/2/1964	205	190,39	5,323	5,249
28/2/1964	230	274,31	5,438	5,614
1/3/1964	775	806,71	6,653	6,693
2/3/1964	1780	12094,91	7,484	9,401
3/3/1964	1150	6585,65	7,048	8,793

**Table 4.2-2:** Values of a, b factors and correlation between Q and Qs

<b>a =</b>	0,00045
<b>Slope (b) =</b>	2,32254
<b>Intercept =</b>	-7,706
<b>Correlation =</b>	0,978

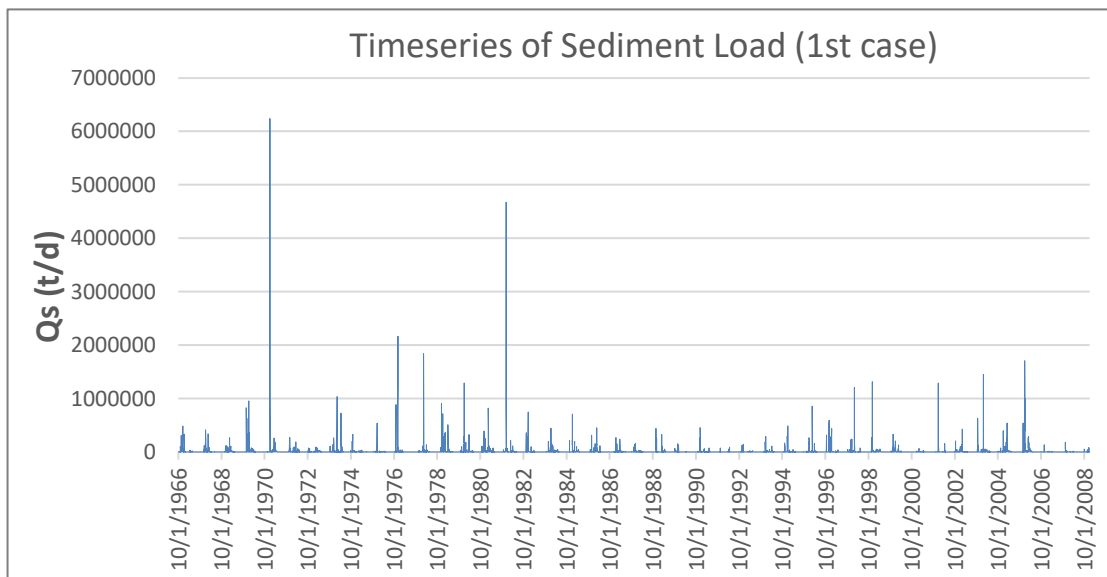
So, the resulting formula and double logarithmic plot of Q-Qs (Graph 4.2-1) for Kremasta area are:

$$Q_s = 0,00045 \cdot Q^{2,323}$$



**Graph 4.2-1:** Double logarithmic plot of: Flow ( $m^3/s$ ) - Sediment Load ( $kg/s$ )

By generalizing and applying this formula to the flow data presented at Table 4.1-1 from 1966 to 2008, the fluctuation of daily values of sediment load  $Q_s$  (t/d) that flows into the reservoir from Acheloos and its tributaries, for this specific time period is revealed in Graph 4.2-2 below:



**Graph 4.2-2:** Timeseries of sediment load flowing into the reservoir (1966-2008)

Table 4.2-3 below displays the mean annual value of sediment yield flowing into Kremasta reservoir in tons and tons per square kilometer of the area of the watershed. The calculated a and b factors are also presented along with the area of the watershed. Sediment yield is calculated by using measurement data only from Kremasta hydrometric station (1<sup>st</sup> case).

**Table 4.2-3:** Mean annual value of sediment yield (Sy)

<b>a=</b>	0,00045
<b>b=</b>	2,32254
<b>A (km<sup>2</sup>) =</b>	3.292
<b>Sy (t) =</b>	1.464.183
<b>Sy (t/km<sup>2</sup>) =</b>	444,8

#### 4.2.2 Second case

In this case a bigger dataset is used, with measurements from the four above-mentioned locations inside the basin of Kremasta reservoir. The goal again is to build a relationship between the river flow and sediment discharge (Q-Qs), by using data from field measurements of the four locations. This formula is exponential such as 4.2-1:

$$Q_s = a \cdot Q^b$$

The methodology followed here is the same as the first case with the difference that in this one, two different formulas (therefore two curves of Q-Qs) are built. The large dataset in this case, led to the figuration of two different patterns between the values. Thus, the construction of two different equations between Q and Qs, is considered as the most effective way to describe this wide range in values. The whole process of constructing the formula is displayed below, in the Table 4.2-4:

**Table 4.2-4:** Flow and sediment load measurements at 4 areas of the watershed and logarithms

Date	Q (m <sup>3</sup> /s)	Qs (kg/s)	ln (Q)	ln (Qs)
22/9/1976	6,2	0,14	1,825	-1,966
14/6/1972	9,3	0,28	2,230	-1,273
7/6/1972	11,88	0,42	2,475	-0,868
7/12/1970	18,05	1,17	2,893	0,157
7/2/1972	18,25	0,54	2,904	-0,616
2/12/1970	24,32	2	3,191	0,693
24/2/1973	25,66	0,78	3,245	-0,248
16/6/1967	26,57	8,86	3,280	2,182
15/6/1968	31,26	3,09	3,442	1,128
26/2/1973	34,55	1,25	3,542	0,223
3/5/1972	36,61	2,36	3,600	0,859
3/6/1967	37,67	1,15	3,629	0,140
8/4/1967	41,34	1,34	3,722	0,293
24/2/1972	42,49	2,94	3,749	1,078
14/2/1972	42,52	1,11	3,750	0,104
24/3/1967	44,79	2,19	3,802	0,784
28/3/1967	46,27	1,56	3,834	0,445
29/5/1968	46,59	2,9	3,841	1,065
13/1/1969	49,35	4,51	3,899	1,506
12/12/1969	50,08	2,82	3,914	1,037

Date	Q (m <sup>3</sup> /s)	Qs (kg/s)	ln (Q)	ln (Qs)
24/1/1969	50,16	5,17	3,915	1,643
10/4/1970	51,3	3,41	3,938	1,227
17/12/1969	55,95	2,95	4,024	1,082
9/5/1968	59,71	1,92	4,089	0,652
27/1/1970	62,42	2,1	4,134	0,742
12/4/1983	65,15	1,28	4,177	0,247
24/5/1967	67,07	6,29	4,206	1,839
26/1/1970	67,83	3,4	4,217	1,224
29/1/1964	70	6,78	4,248	1,914
30/1/1964	73	10,37	4,290	2,339
27/1/1964	76	9,56	4,331	2,258
12/4/1967	78,66	8,08	4,365	2,089
26/1/1964	79	8,45	4,369	2,134
13/4/1970	79,97	10,17	4,382	2,319
13/4/1970	79,97	10,17	4,382	2,319
25/1/1964	80	6,72	4,382	1,905
25/1/1967	80,42	19,32	4,387	2,961
27/3/1968	82,86	5,58	4,417	1,719
22/1/1964	85	7,92	4,443	2,069
24/1/1964	85	6,79	4,443	1,915
31/1/1964	86	38,19	4,454	3,643
20/1/1969	86,13	13,59	4,456	2,609
23/1/1964	88	11,75	4,477	2,464
20/4/1967	88,97	16,41	4,488	2,798
15/4/1970	98,98	95,15	4,595	4,555
1/2/1964	101	25,46	4,615	3,237
2/2/1964	101	33,8	4,615	3,520
29/4/1969	108,43	21,39	4,686	3,063
4/4/1968	109,34	14,83	4,694	2,697
7/11/1966	110,9	88,09	4,709	4,478
17/4/1967	113,05	31,53	4,728	3,451
4/6/1968	117,32	82,83	4,765	4,417
24/4/1969	141,27	71,8	4,951	4,274
13/4/1970	147,43	46,26	4,993	3,834
17/1/1969	162,18	72,09	5,089	4,278
17/12/1969	196,24	93,23	5,279	4,535
17/2/1964	205	190,39	5,323	5,249
28/2/1964	230	274,31	5,438	5,614
16/2/1964	352	581,02	5,864	6,365
1/3/1964	775	806,71	6,653	6,693
15/2/1964	800	3460,65	6,685	8,149
3/3/1964	1150	6585,65	7,048	8,793
2/3/1964	1780	12094,91	7,484	9,401

Values of flow from 6,2-85 (m<sup>3</sup>/s) belong to the first branch of the curve, whereas values from 86-1.780 (m<sup>3</sup>/s) belong to its second branch. This is done in order to separate low from high values and thus have a more accurate approach. What follows next is the construction of the formula that connects Q and Q<sub>s</sub>. Thus, next step is the calculation of the parameters of the 2 equations by using functions in Microsoft Excel environment:

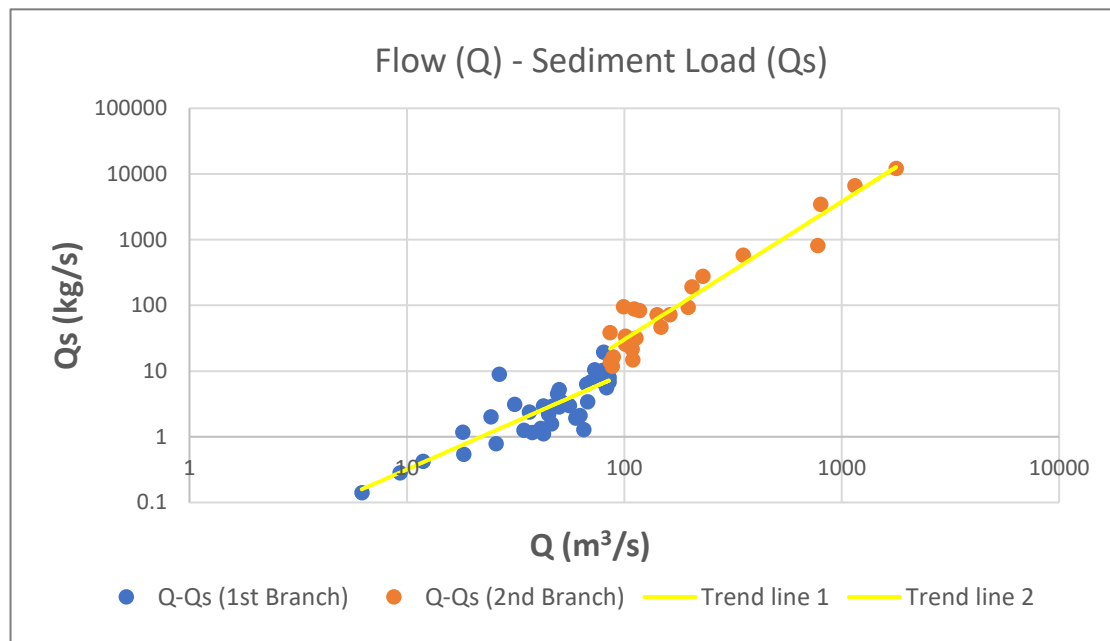
1st Branch			
<u>Slope (b)</u>	<u>Intercept</u>	<u>Correlation</u>	<u>a</u>
1,477	-4,620	0,871	0,010

$$\rightarrow Q_s = 0,0099 \cdot Q^{1,477}$$

2nd Branch			
<u>Slope (b)</u>	<u>Intercept</u>	<u>Correlation</u>	<u>a</u>
2,099	-6,260	0,960	0,002

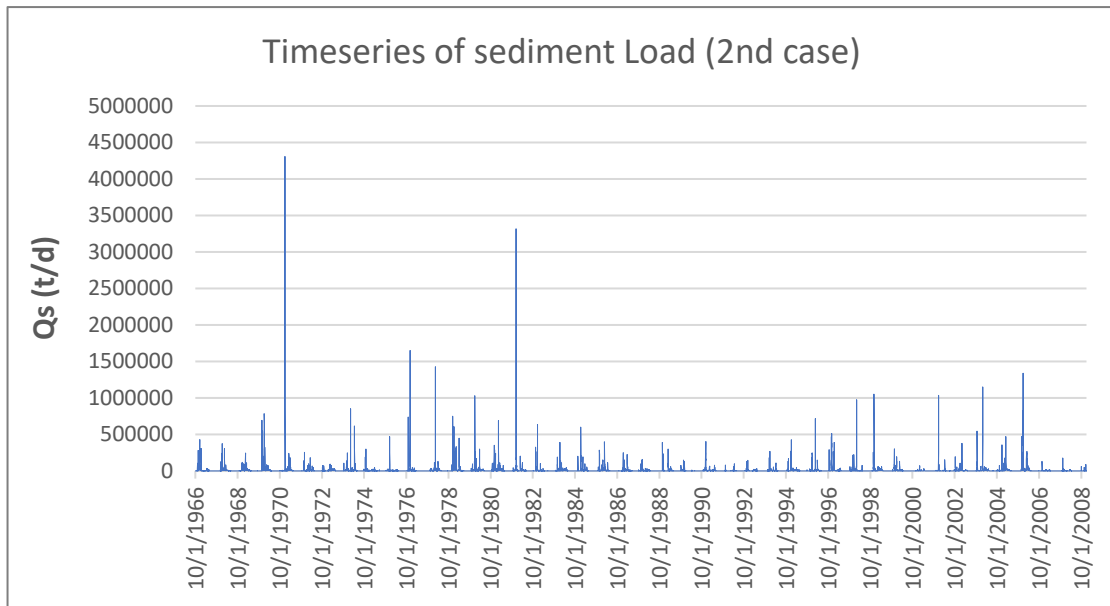
$$\rightarrow Q_s = 0,00191 \cdot Q^{2,099}$$

The graph below illustrates the relationship between flow and sediment load, occurred from several measurements that took place in 4 different locations inside the watershed. Points are separated into low (blue) and high (orange) values, shaping 2 exponential curves (Graph 4.2-3):



**Graph 4.2-3:** Double logarithmic plot of: Flow (m<sup>3</sup>/s) - Sediment Load (kg/s)

By generalizing and applying this formula to the flow data presented at Table 4.1-1 from 1966 to 2008, the fluctuation of daily values of sediment load Q<sub>s</sub> (t/d) that flows into the reservoir from Acheloos and its tributaries, for this specific time period is revealed in Graph 4.2-4 below.



**Graph 4.2-4:** Timeseries of sediment yield flowing into the reservoir (1966-2008)

Table 4.2-5 below shows the mean annual value of sediment yield flowing into Kremasta reservoir in tons and in tons divided by the area of the watershed. These are calculated by using measurement data from 4 different hydrometric stations inside the watershed (2<sup>nd</sup> case):

**Table 4.2-5:** Mean annual value of sediment yield (Sy)

1st Branch		2nd Branch	
a1 =	0,00986	a2 =	0,00191
b1 =	1,47678	b2 =	2,09918
A (km <sup>2</sup> ) =	3.292	A (km <sup>2</sup> ) =	3.292
Sy (t) = 3.654.937			
Sy (t/km <sup>2</sup> ) = 1.110,2			

In Graphs 4.2-2 and 4.2-4, an evident and important feature is that in both 1<sup>st</sup> and 2<sup>nd</sup> case, some extreme river flow phenomena result in exceedingly high values of sediment yield flushing into the reservoir in one day. Consequently, the mean daily value of sediment yield is forced to increase at a remarkable rate by these individual incidents of extreme flows. As it comes to mind, these extreme events comprise a critical part of the mean annual figure of sediment yield that settles into the reservoir.

### 4.2.3 Comparison with Zarris (2019) study

The two cases examined reveal a significant difference in terms of the resulted value of sediment yield. More specifically, the 1<sup>st</sup> case gave the value of 444,8 (t/km<sup>2</sup>), while the 2<sup>nd</sup> one concluded on 1.110,2 (t/km<sup>2</sup>) of annual sediment yield entering the reservoir every year. It would of course be interesting and meaningful to display here the equivalent value occurred by the hydrographic survey of Zarris et al. (2001) which is 1.005,6 (t/km<sup>2</sup>). In addition, Zarris (2019) created also flow - sediment load rating curves using a simple regression method and concluded on 1.332 (t/km<sup>2</sup>) of predicted mean annual sediment yield.

The 1<sup>st</sup> scenario utilizes data only from the hydrometric station of Kremasta near the dam (great proximity to the study area), whereas the calculations of the 2<sup>nd</sup> case are based on a bigger dataset from 4 stations across the watershed. Besides, in the 2<sup>nd</sup> case the process contains the figuration of two curves (two formulas) in order to describe better the extreme values of flow and sediment load. For these two reasons, we conclude that the outcome of the 2<sup>nd</sup> scenario is more reliable and closer to the real situation presented by the hydrographic survey.

In Table 4.2-6 below there is a presentation and comparison between the flow - sediment load rating curves of Zarris (2019) study and the present thesis project, while the above-mentioned values of sediment yield (Sy) are also appearing below.

**Table 4.2-6:** Comparison of the rating curves and the values of mean annual sediment yield between the two studies

	Curve 1st Branch	Curve 2nd Branch	Sy (t/km <sup>2</sup> )
<b>1<sup>st</sup> Case</b>	$Q_s = 0,00045 \cdot Q^{2,323}$	-	444,8
<b>2<sup>nd</sup> Case</b>	$Q_s = 0,0099 \cdot Q^{1,477}$	$Q_s = 0,00191 \cdot Q^{2,099}$	1.110,2
<b>Zarris (2019) study</b>	$Q_s = 0,0012 \cdot Q^{2,1107}$	-	1.332

It is evident that even short-term flow - sediment load measurements can describe sufficiently the actual situation and estimate accurately the sediment volume that was measured by Zarris et al. (2001) hydrographic survey. Moreover, the 1<sup>st</sup> case scenario uses an enormously small dataset, so it is not suggested to be used for further research. As opposed to that, considering that the 2<sup>nd</sup> case dataset is much larger and was obtained from several locations inside the watershed is safer and more accurate way to predict the sediment yield.

Lastly, the fact that the hydrographic survey of Zarris et al. (2001) showed that the annual measured sediment yield that enters the reservoir of Kremasta is 1.005,6 (t/km<sup>2</sup>), is another indicator for the high proximity and accuracy of the values predicted in the 2<sup>nd</sup> case of rating curves method. More specifically, Zarris et al. (2001) calculated that in Acheloos sub catchment area (1.733 km<sup>2</sup>) the mean annual sediment yield -after 35 years of operation- is 1.184,6 (t/km<sup>2</sup>), for Agrafiotis area (320 km<sup>2</sup>) the same value is 2.034,8 (t/km<sup>2</sup>) and for Tavropos (1.239 km<sup>2</sup>) it is 489,4 (t/km<sup>2</sup>). Thus, the total value for all the basin of Kremasta (3.292 km<sup>2</sup>) is 1.005,6 (t/km<sup>2</sup>). In the subject of sediment transport these disparities are negligible because of the unpredictable nature of these procedures.

### 4.3 Comparison of the four methodologies developed

After the calculation of sediment yield using 4 different methodologies, the next step is the estimation of sediment volume (Sv) that enters the reservoir through the years for each one of them. At Table 4.3-1 below, Total Sy is the total sediment yield of the watershed in tons,  $\rho$  is a mean value of density of the transferred sediment material, so it is feasible to estimate the dead sediment volume of the reservoir for long-term operation period:

**Table 4.3-1:** Comparison of the results of the 4 methodologies

	<b>Sy (t/km<sup>2</sup>)</b>	<b>Total Sy (t)</b>	<b>Annual Sv (hm<sup>3</sup>)</b>	<b>30-year Sv (hm<sup>3</sup>)</b>	<b>100-year Sv (hm<sup>3</sup>) *Predicted</b>
<b>RUSLE</b>	210,7	693.760	0,555	16,65	<b>55,5</b>
<b>GIS and RUSLE</b>	127	418.156	0,335	10,05	<b>33,46</b>
<b>Koutsoyiannis &amp; Tarla</b>	492,6	1.621.639	1,297	38,9	<b>129,7</b>
<b>Rating curves</b>	1.110,2	3.654.780	2,92	87,6	<b>292,4</b>
<b>Hydrographic survey</b>	1.005,6	3.310.435	2,65	79,5	<b>264,8</b>

The rating curves methodology concluded on 1.110,2 (t/km<sup>2</sup>) of sediment yield entering the reservoir every year. A value that is remarkably close to the equivalent value occurred by Zarris et al. (2001) hydrographic survey, which is 1.005,6 (t/km<sup>2</sup>), and indicates the real situation inside the reservoir. Furthermore, the 100-year dead sediment volume predicted by the rating curves method is also close to the predicted sediment volume based on the hydrographic survey.

The discrepancy though in the resulted sediment yield among the four methods and in comparison, with the hydrographic survey is attributed to the empirical factor of the first three methodologies. The RUSLE and Koutsoyiannis & Tarla (1987) methods consist of a series of empirical equations and in combination with Vanoni (1975) empirical formula, the results often appear to have a major variance between them. Moreover, the uncertainty and difficulty to predict the response of each soil type, land use and soil loss protection technique to extreme climate phenomena usually leads to an underestimation of the sediment yield. For instance, Panagos et al. (2015) research made an estimation of 89% lower than the hydrographic survey. This variance derived from the uncertainty in the computation of R-factor, because of the different time step used due to lack of frequent precipitation data (Vachaviolos, 2014).

The RUSLE method in the current study underestimated the sediment yield by 79% while the GIS and RUSLE method by 87%. Moreover, this disparity among the results is not attributed to any mistakes in one of the above methods and each one of them is well-structured. Nevertheless, the prediction of soil loss inside a watershed can be an exceedingly difficult task. This is evident considering that the initial design study for Kremasta dam predicted that for a design period of 100 years of operation, 17,4 % of the total storage capacity of the reservoir would have been filled up by the deposits volume which would be 784 (hm<sup>3</sup>) which is almost 300 % higher than the prediction of Zarris et al. (2001) based on the hydrographic survey that was 264,8 (hm<sup>3</sup>).

## 5 Sediment transport analysis in Kremasta reservoir

In order to perform a sediment transport analysis in HEC-RAS it is necessary to prepare the input geometric data for the program. More specifically, the calculation of the flow of each river that contributes to the total inflows of the reservoir is meaningful and will be useful for the following sediment transport analysis in HEC-RAS. In addition, the geometric data that will be input to HEC-RAS is going to be prepared in Civil 3D design software. Furthermore, flow and sediment data will be imported in the model to run the reservoir sediment transport simulation. Below in Chapters 5.1 - 5.3 these procedures are thoroughly described.

### 5.1 Calculation of each river flow

At this point and by having the dataset of the total daily inlets of the reservoir we can calculate the flow of each one of the three main basins (Acheloois, Agrafiotis, Tavropos/Megdovas) that Kremasta basin includes (Figure 5.1-1). Due to the lack of specific long-term measurements, the daily water flow of each river/basin is estimated by using a simple hydrological method based on the area of each basin, namely:

$$Q_i/Q_{total} = A_i/A_{total} \quad (5.1-1)$$

where  $i = 1 - 3$ ,  $A_i$ : basin area ( $m^2$ ) and  $A_{total}$ : total basin area ( $m^2$ )

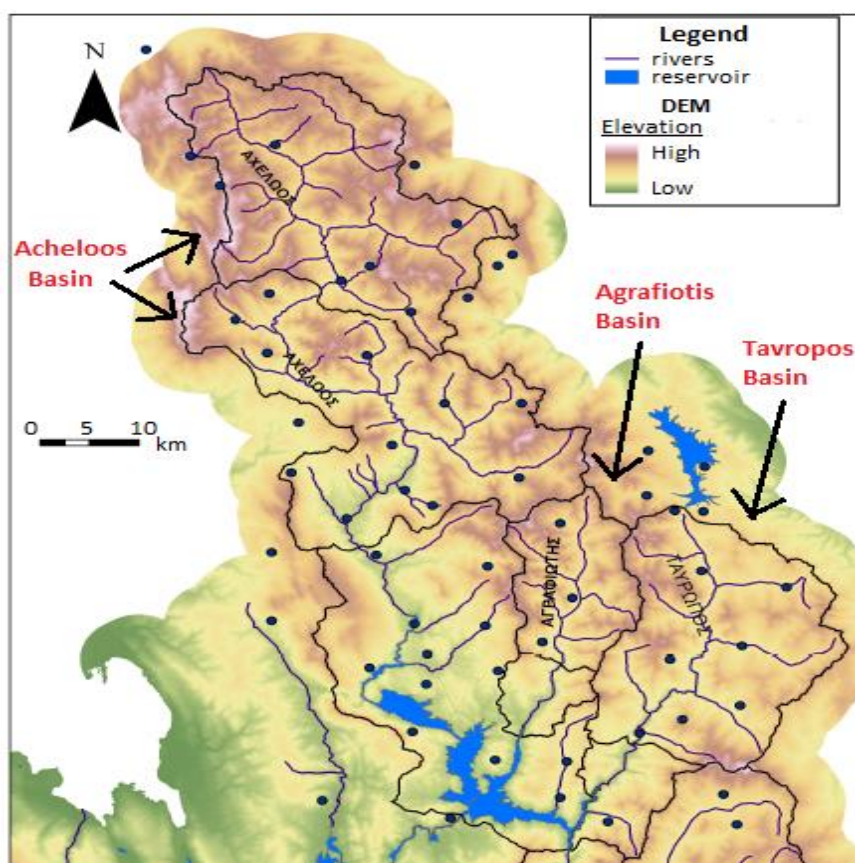


**Figure 5.1-1:** Digital Elevation Model (DEM) showing the 3 different basins of the area (Obtained by Zarris, 2019)

Below are displayed the percentages of area comprising the watershed of Kremasta:

- Acheloos river basin:  $A_1 = 1.733 \text{ (km}^2\text{)}$  and  $A_1 / A_{total} = 0,526 = 52,6 \%$
- Agrafiotis river basin:  $A_2 = 320 \text{ (km}^2\text{)}$  and  $A_2 / A_{total} = 0,097 = 9,7 \%$
- Tavropos/Trikeriotis river basin:  $A_3 = 1.239 \text{ (km}^2\text{)}$  and  $A_3 / A_{total} = 0,376 = 37,6 \%$

where  $A_{total} = A_1 + A_2 + A_3 = 3.292 \text{ (km}^2\text{)}$ .

Considering the above, Acheloos accounts for more than half of the total inlet that enters the reservoir each year. Moreover, given the percentage of its basin it is now easy to estimate the inlets attributed to each river using the timeseries of the total inlets of the reservoir (Table 5.1-1). It is critical to divide the total inflows into the inflow of each river because they will be used in further HEC-RAS calculations.

**Table 5.1-1:** Division of total inflows into flow of each river

Area:	$A_{total} = 3.292 \text{ (km}^2\text{)}$	$A_1 = 1.733 \text{ (km}^2\text{)}$	$A_2 = 320 \text{ (km}^2\text{)}$	$A_3 = 1.239 \text{ (km}^2\text{)}$
Date	Total Inflows ( $\text{m}^3/\text{s}$ )	Acheloos Inflow ( $\text{m}^3/\text{s}$ )	Agrafiotis Inflow ( $\text{m}^3/\text{s}$ )	Tavropos Inflow ( $\text{m}^3/\text{s}$ )
10/1/1966	32.5	17.1	3.2	12.2
10/2/1966	24.9	13.1	2.4	9.4
10/3/1966	39.6	20.8	3.8	14.9
10/4/1966	43.0	22.6	4.2	16.2
10/5/1966	46.3	24.4	4.5	17.4
10/6/1966	42.2	22.2	4.1	15.8
10/7/1966	38.0	20.0	3.7	14.3
10/8/1966	17.7	9.3	1.7	6.7
10/9/1966	17.7	9.3	1.7	6.7
10/10/1966	38.8	20.4	3.8	14.6
10/11/1966	32.5	17.1	3.2	12.2
10/12/1966	10.8	5.7	1.0	4.1
10/13/1966	18.5	9.8	1.8	7.0
10/14/1966	23.6	12.4	2.3	8.9
10/15/1966	30.4	16.0	2.9	11.4
10/16/1966	30.4	16.0	2.9	11.4
10/17/1966	30.4	16.0	2.9	11.4
10/18/1966	30.4	16.0	2.9	11.4
10/19/1966	163.4	85.9	15.8	61.4
10/20/1966	81.8	43.0	7.9	30.8
10/21/1966	22.8	12.0	2.2	8.6
10/22/1966	23.9	12.6	2.3	9.0

\*The provided table is just a sample of a 42-year dataset of inflows at Kremasta reservoir. The aim of its presentation is to observe how the total inflow dataset is divided into the runoff of each river (each basin). The total daily hydrograph is not displayed in the present study due to its length, though it is the main and most necessary dataset for the completion of the current thesis.

## 5.2 Preparation of geometric data using Civil 3D modeling

### 5.2.1 Description

Civil 3D is an engineering design software used for a variety of construction and design projects. The environment is quite similar to AutoCAD and is simple and useful for purposes such as roadway, railway, hydraulic design etc. Another main activity taking place in Civil 3D 2019 is the processing and design of surfaces, digital elevation models (DEM) and bathymetry grids, while it contains a useful series of tools and procedures (Figures 5.2-1).

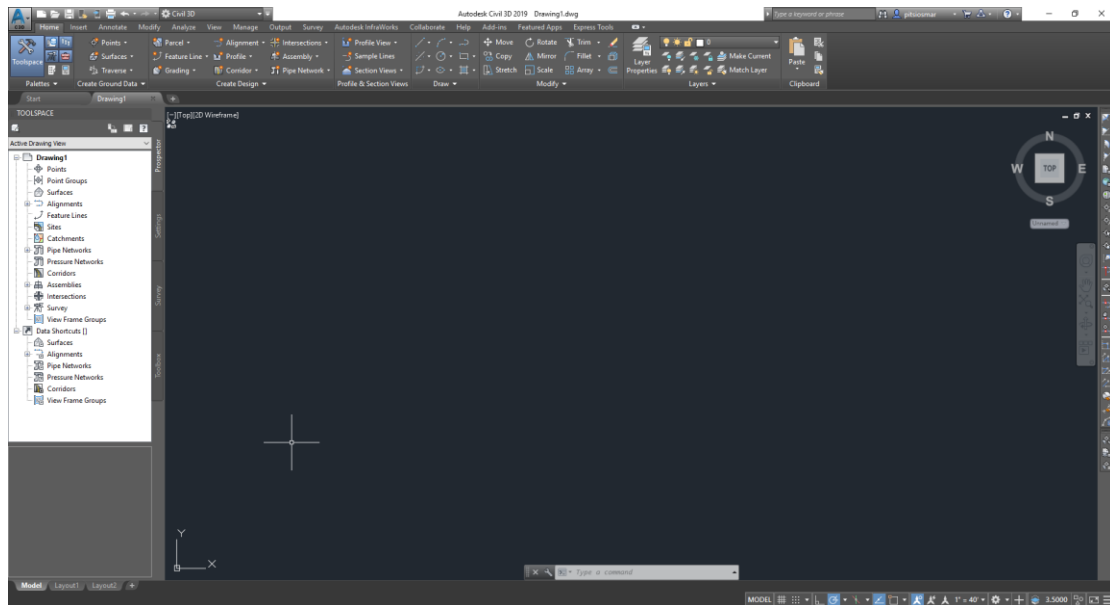


**Figure 5.2-1:** Civil 3D 2019 Interface

The usage of Civil 3D is undoubtedly decisive and meaningful for the progress of this project. It is the steppingstone for the transition to HEC-RAS and an especially useful tool that helps in the process of preparing the geometric data for the HEC-RAS model by creating cross sections that show the bathymetry of the reservoir. This 1D geometric illustration of the bathymetry will subsequently be exported to HEC-RAS to perform a 1D sediment transport simulation. Hence, the cross sections -of the initial bathymetry- will be needed to observe how the bed of the reservoir changes throughout the years due to sediment deposition.



**Figure 5.2-2:** Civil 3D 2019 Home panel

Figure 5.2-2 displays the toolbar of the home panel in Civil 3D where there is a specific tab called “Profile & Section Views” which will be useful for the creation of the cross sections.

## 5.2.2 Geometric data

The 1D sediment transport simulation inside the reservoir is a process that requires the possession of geometric data, namely the initial bathymetry of the reservoir. This was a challenging procedure and after a thorough research and collaboration with professors and researchers from N.T.U.A., the team managed to find a grid (mesh) of the initial bathymetry (Figure 5.2-3) before the beginning of the operation of the dam (1966).

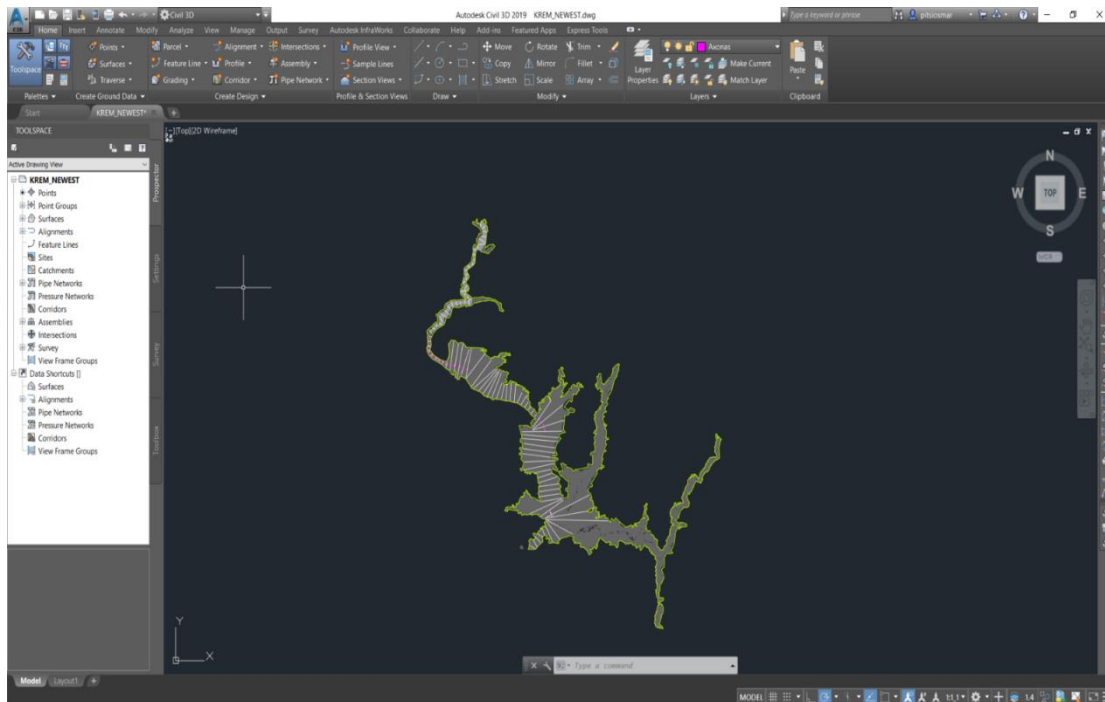


Figure 5.2-3: Grid of the initial bathymetry of the reservoir (Civil 3D 2019)

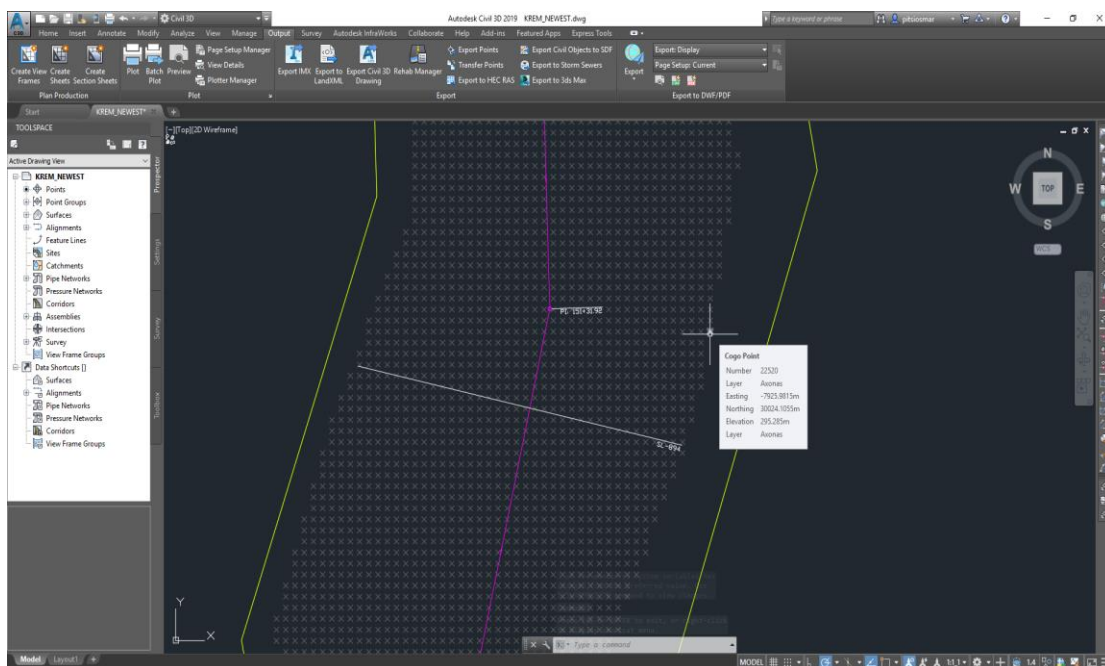


Figure 5.2-4: “Cogo Points” (Civil 3D 2019)

The bathymetry grid mainly consists of “Cogo Points” (Figure 5.2-4), but also some “Block References” and “Polylines” all of them containing the geographical coordinates (x, y, z) of each point.

### 5.2.3 Creation of cross sections

The goal of the Civil 3D usage is to cut and view cross sections across the reservoir. For this purpose, it is necessary to define a main axis that goes through the reservoir. This will be the purple line presented in Figure 5.2-5 which starts from the mouth of Acheloos river and reaches the dam of Kremasta. However, first step is the creation of a surface which includes all the features of the given grid: “Block references”, “Polylines” and “Cogo Points” that contain geographical coordinates. What follows next is the design of the aforementioned axis which in terms of Civil 3D software is called “Alignment”.



**Figure 5.2-5:** “Alignment” and “Sample Lines” (Civil 3D 2019)

The Figure 5.2-5 above illustrates a part of the bathymetry grid with the geometric characteristics created in Civil 3D 2019. More specifically, it shows the “Alignment” (Purple color), the “Sample Lines” (White color) and “Surface Boundary” (Yellow color). The cross sections begin from the upstream of the reservoir (mouth of Acheloos) and finish right upstream of Kremasta dam following the designed alignment as shown in Figures 5.2-6 and 5.2-7 which is 39,2 (km) long.

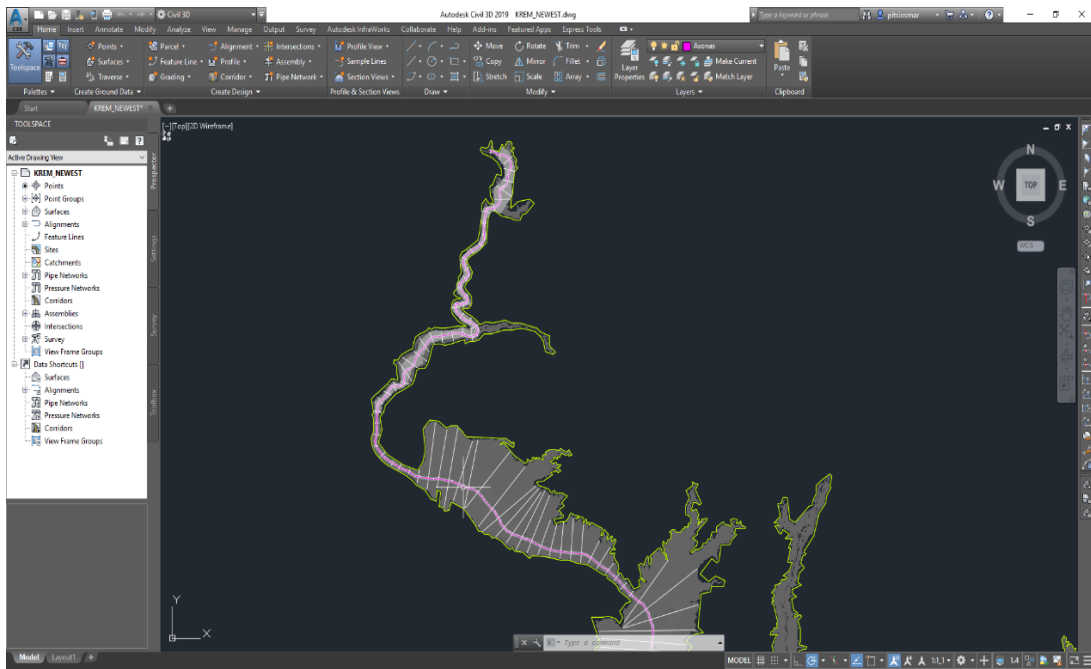


**Figure 5.2-6:** The beginning of the alignment as Acheloos river (Civil 3D 2019)

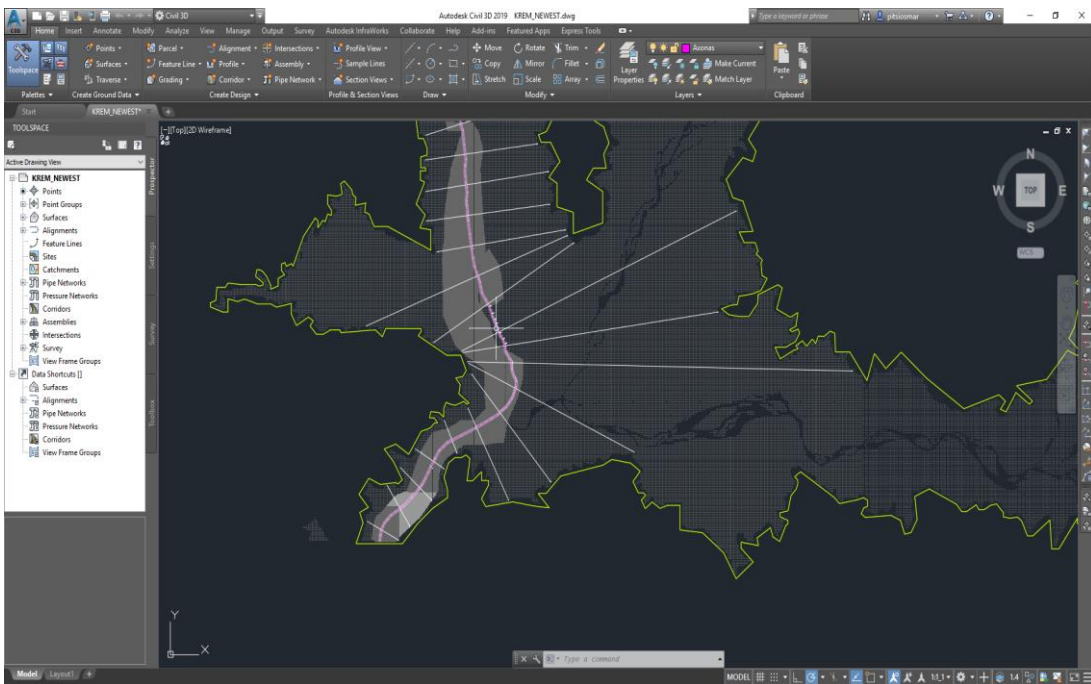


**Figure 5.2-7:** The end of the alignment just upstream of the dam (Civil 3D 2019)

The alignment here is designed by hand and follows a path so that the sample lines will not be tangent with each other. The cutting and creation of the cross sections is made by clicking the “Sample Line” command and selecting the designed alignment.

Next step is to choose the “By range of stations” option to create a group of cross sections and then define the distance between the cross sections which will be 400 (m). After that and in order to view the cross sections we press the “View Cross Sections”

tool and the results are displayed in Figures 5.2-8 and 5.2-9. What is shown below is the bed geometry of the reservoir on the year 1966.

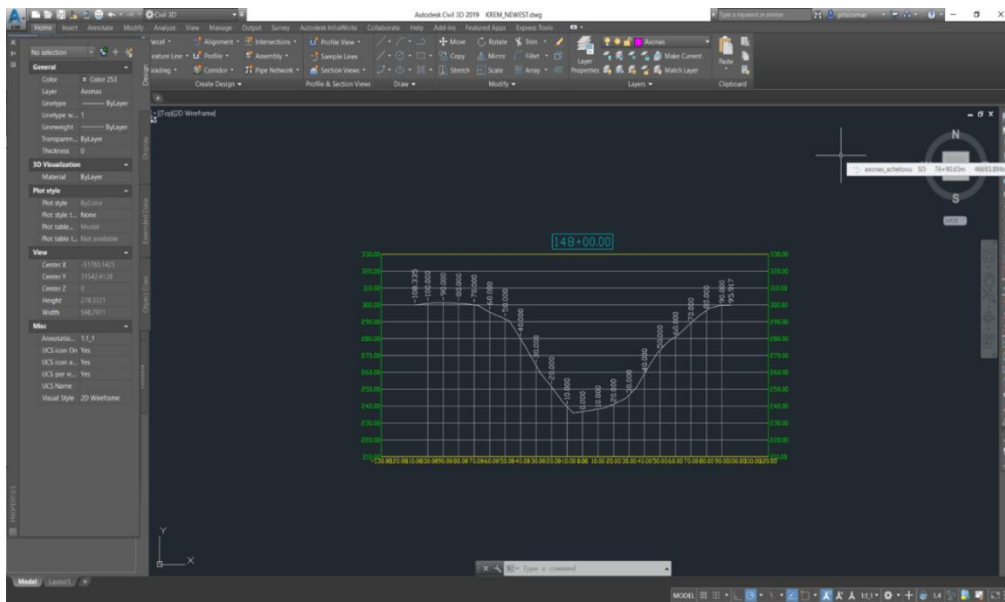


**Figure 5.2-8:** Cross section at 14.8 km from the beginning of the alignment (Civil 3D 2019)

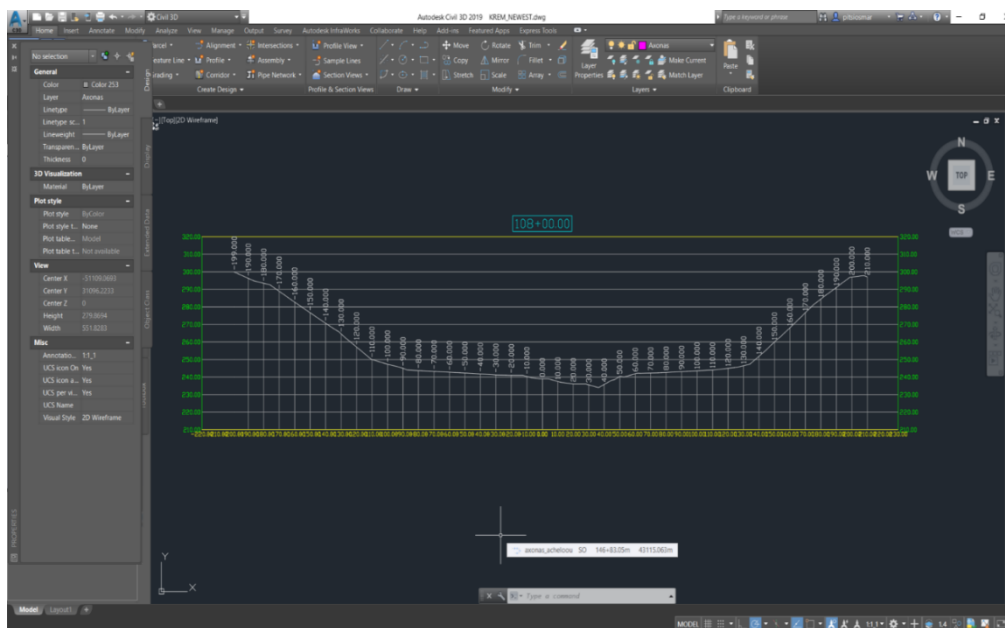


**Figure 5.2-9:** Cross section at 10.8 km from the beginning of the alignment (Civil 3D 2019)

Finally, the prepared geometry is a Civil 3D shapefile that contains all the cross sections and is exported to HEC-RAS by using the “Export to HEC RAS” icon inside the “Output” tab.

## 5.3 Theoretical background of HEC-RAS

### 5.3.1 General

The study for the sediment transport analysis in Kremasta reservoir is carried out using the hydraulic program HEC-RAS, which was composed by U.S. Corps of Engineers, Hydrologic Engineering Center. The version used here is HEC-RAS 5.0.7 and provides the capability to calculate the water surface under a one-dimensional, steady or unsteady, non-uniform flow in natural or artificial channels with fixed riverbed. It uses the 1D conservation of energy principle as the basic computational process for the simulation of the flow in a river (Dedousis, 1999). Hydraulic models are generally divided into one-dimensional, two-dimensional, and three-dimensional according to the dimension of the vectors of the calculated hydraulic characteristics.

One-dimensional models usually use the Manning equation and the solution of the model involves calculating the average flow depth and average velocity perpendicular to the cross section of the river which is evenly distributed in the cross section (or in parts) with a common friction coefficient. Based on the topography of the area, the flood map is produced, with flood areas those with lower altitudes than that of the calculated free water surface.

The two-dimensional models attempt to simulate flood phenomena in the dimensions of length and width. The flow depth is estimated at each point of the study area and the calculation of the flow velocity distribution in two dimensions, with the flow of the river and in the transvers direction.

Three-dimensional models are used in more complex hydraulic applications such as in cases where the vertical velocity is significant -hydraulic jumps analyses, spillway design, etc. These models use complex computational formulas and achieve the most accurate flow calculation (Oikonomou, 2013).

The estimation of the water level can be held for supercritical, subcritical or critical flow. The analysis for a subcritical flow is held from the downstream to the upstream while for the supercritical is the opposite. HEC-RAS has the capability to control the situation of the flow based on Froude number and to simulate cases where there is a change of the flow situation (such as a hydraulic jump). During the calculations it can simulate several hydraulic structures and obstacles along the river such as bridges, culverts, and levees. Moreover, there is a capability to define different Manning's values for the main riverbed and the floodplains, calculating separately the flow for each part of the cross-section and finally estimate the total flow as a sum of the several flows.

In order to achieve a complete supervision of the process of calculating the level of the free water surface and the correct evaluation of the results, an extensive presentation of the theoretical background of the hydraulic program is displayed below, with special emphasis on the basic hydraulic equations that it solves and the assumptions on which it is based under permanent and non-permanent flow treatments (Dedousis, 1999).

### 5.3.2 Steady flow

HEC-RAS determines the elevation levels of surface runoff at selected points (cross sections) under certain flow conditions. Geometric data of cross-sections as well as flow data (boundary conditions) are required as input elements. The flow state is controlled according to the Froude number, based on which, cases where alternations of flow states occur, are examined. The water surface level is determined for subcritical, supercritical or mixed flow.

Solving the equation of energy in one-dimensional analysis, HEC-RAS calculates in conditions of steady flow the water surface successively from cross section to cross section with a repetitive process which is based on five steps as described below:

- (i) Initially, the flow surface level (WS) is assumed at the upstream cross-section.
- (ii) Flow and kinetic energy height are calculated.
- (iii) Friction losses and total energy losses are calculated.
- (iv) The energy equation is solved.
- (v) The initial case of the flow surface height is compared to the calculated value.

Steps (i) to (v) are repeated until the two values are equal with a predetermined tolerance (default value 0,003 m). In the first attempt, the choice of the initial estimate of the water surface level is obtained from the flow depth of the previous cross-section after adapting to the flow depth of the examined cross-section. In the second iteration, the level is selected equal to the initially selected level plus 70% of the error of the first attempt. From the third repetition onwards, the “secand method” is followed. Basically, the difference between the calculated and the assumed level of the two previous repetitions is reduced by reducing the initial level by  $\pm 50\%$  from the previous repetition. Up to 20 repetitions are performed and if the required convergence is not achieved, then the critical depth is used in the examined cross section. Below there is a presentation of the theory behind the simulations and calculations of HEC-RAS.

#### Calculation of water surface

In addition to the assumption of one-dimensional flow analysis, the application considers a slope of less than 1:10. The basic hydraulic equation solved by HEC-RAS is the conservation of energy principle between two successive cross sections which is formulated as:

$$Z_2 + Y_2 + \frac{\alpha_2 \cdot V_2^2}{2 \cdot g} = Z_1 + Y_1 + \frac{\alpha_1 \cdot V_1^2}{2 \cdot g} + h_e \quad (5.3-1)$$

where

$Z_1, Z_2$  are the riverbed altitudes in two successive cross-sections 1 and 2,

$Y_1, Y_2$  are the water depths in two successive cross-sections 1 and 2,

$\alpha_1, \alpha_2$  are correction factors of the kinetic energy,

$V_1, V_2$  are the mean flow velocities in cross-sections 1 and 2 ( $Q/A$ ),

$g$  is the gravitational acceleration,

$h_e$  is the total energy loss.

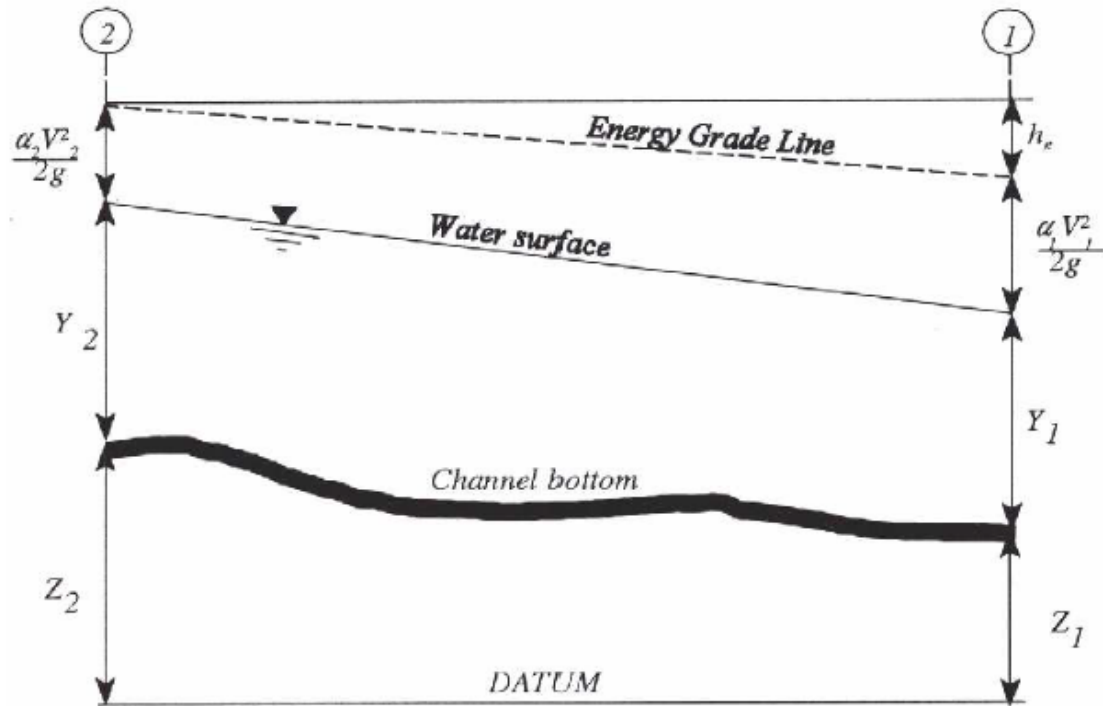


**Figure 5.3-1:** Open channel flow (Obtained by Dedousis, 1999)

The Figure 5.3-1 above presents the characteristic sizes of an open channel flow.

The total amount of energy losses between two cross sections is their linear losses - losses due to friction- which are calculated as the product the slope of the piezometric line and the length of the examined section and in amount of local losses -losses due to narrowing and widening- according to relationship:

$$h_e = L \cdot \overline{Sf} + C \cdot \left| \frac{a_2 \cdot V_2^2}{2 \cdot g} - \frac{a_1 \cdot V_1^2}{2 \cdot g} \right| \quad (5.3-2)$$

where

L is the mean distance between two successive cross sections 1 and 2,

$\overline{Sf}$  is the slope of the piezometric line,

C is local energy losses coefficient (0,1 or 0,3),

$\left| \frac{a_2 \cdot V_2^2}{2 \cdot g} - \frac{a_1 \cdot V_1^2}{2 \cdot g} \right|$  is the variation of hydrostatic pressure between cross sections 1 and 2 due to flow velocity.

With this methodology it is possible to handle various hydraulic problems such as hydraulic jumps, estimation of altitude hydraulic profiles of channels and the determination of the effects of various constructions such as bridges etc.

The weighted average distance (L) between two successive cross sections is calculated according to the following equation:

$$L = \frac{L_{lob} \cdot \bar{Q}_{lob} + L_{ch} \cdot \bar{Q}_{ch} + L_{rob} \cdot \bar{Q}_{rob}}{\bar{Q}_{lob} + \bar{Q}_{ch} + \bar{Q}_{rob}} \quad (5.3-3)$$

where  $L_{lob}$ ,  $L_{ch}$ ,  $L_{rob}$  are the distances between two successive from sections for the left, main and right part of the channel and  $\bar{Q}_{lob}$ ,  $\bar{Q}_{ch}$ ,  $\bar{Q}_{rob}$  are the mean flows for the same parts of the cross section.

### Calculation of flow capacity of the channel

The calculation of the flow capacity of the channel and hydraulic features of the cross section is based on its subdivision into units in which speed can considered uniformly distributed. The technique used by HEC-RAS is the subdivision of the cross section in the central riverbed and in the floodplains through changing the Manning's roughness factor (Figure 5.3-2). The total flow is the sum of the individual flow of each section. According to Manning's equation the flow is calculated as:

$$Q = K \cdot S_f^{1/2}, K = \frac{1,486}{n} \cdot A \cdot R^{2/3} \quad (5.3-4), (5.3-5)$$

where

- K is the flow capacity,
- Sf is the slope of the piezometric line,
- n is the Manning's roughness coefficient,
- A is the area of the wetted part of the cross section,
- R is the hydraulic radius (area A / wetted perimeter P).

The sections in which the cross section is divided are considered to have evenly distributed velocities.

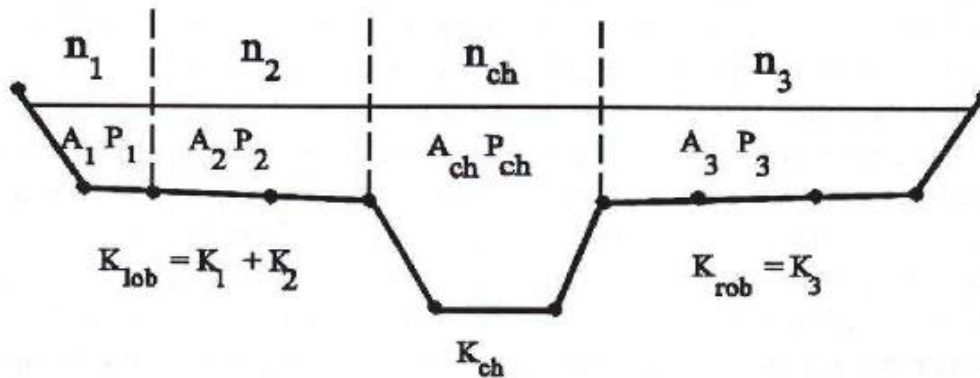


**Figure 5.3-2:** Subdivision of cross section into sections based on Manning's values  
(Obtained by Dedousis, 1999)

In case that in the several sections there is a different roughness coefficient, then the following equation is used to estimate an equivalent roughness coefficient (Dedousis, 1999):

$$nc = \left[ \frac{\sum_{i=1}^N (P_i \cdot n_i^{1.5})}{P} \right]^{2/3} \quad (5.3-6)$$

where

$n_c$  is the Manning's equivalent roughness coefficient,  
 $P$  is the wetted perimeter of the cross section,  
 $P_i$  is the wetted perimeter of the  $i$  part of the cross section,  
 $n_i$  is the roughness coefficient of the  $i$  part of the cross section.

### Calculation of the mean height of kinetic energy

In order to estimate the local energy loss in two successive cross sections, the mean kinetic energy needs to be calculated for each part of the cross section as shown in Figure 5.3-3. In every cross section only one water surface level and one mean height of kinetic energy are calculated because HEC-RAS only solves the one-dimensional flow case. Consequently, for a fixed water level the mean height of kinetic energy is the average of each section's kinetic energy (Oikonomou, 2013).

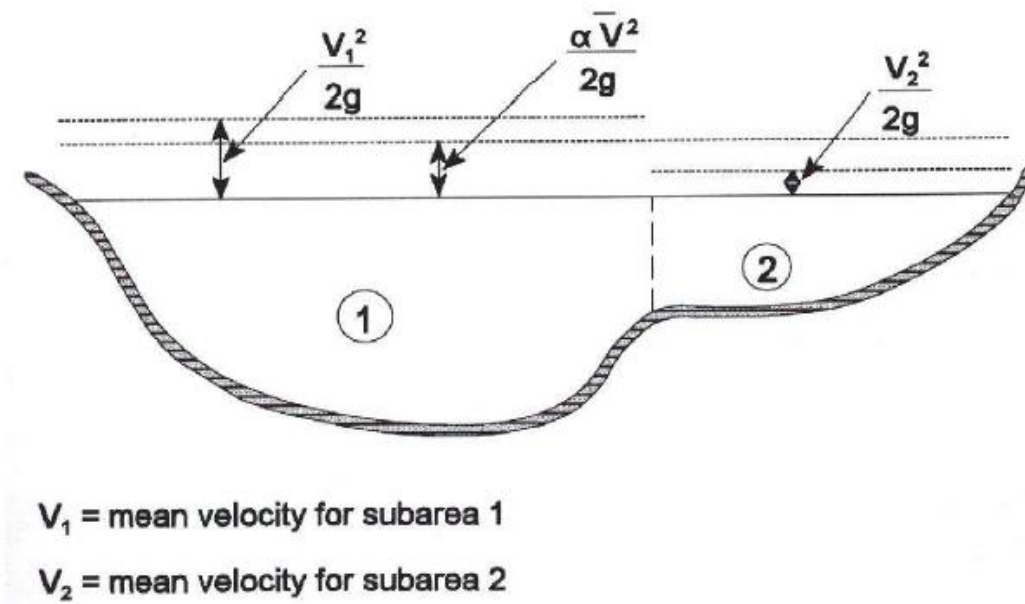


Figure 5.3-3: Estimation of mean kinetic energy (Obtained by Dedousis, 1999)

The “ $a$ ” coefficient must be calculated so that the kinetic energy height is estimated. It can be calculated based on the flow capacity of each section of the channel (Equation 5.3-7) (main riverbed and floodplains) or the flow capacity and the wetted area of the cross section (Equation 5.3-8):

$$a = \frac{[Q_1 \cdot V_1^2 + Q_2 \cdot V_2^2 + \dots + Q_N \cdot V_N^2]}{Q \cdot \bar{V}^2} \quad (5.3-7)$$

$$a = \frac{(A_t)^2 \cdot \left[ \frac{(K_{lob})^3}{(A_{lob})^2} + \frac{(K_{ch})^3}{(A_{ch})^2} + \frac{(K_{rob})^3}{(A_{rob})^2} \right]}{K_t^3} \quad (5.3-8)$$

where

$A_t$  is the total wetted area of the cross section,

$A_{lob}$ ,  $A_{ch}$ ,  $A_{rob}$  are the wetted areas of left part, the main channel and right part accordingly,

$K_t$  is the total flow capacity,

$K_{lob}$ ,  $K_{ch}$ ,  $K_{rob}$  are the flow capacities of left part, the main channel and right part accordingly.

### Calculation of the critical depth

The calculation of the critical depth is held through a repetitive application of the total energy relationship for each cross section which can be done by two possible methods: the “parabolic method” and the “second method”. The parabolic method (faster and is the default of the program) gives the chance to calculate only one minimum value in the energy curve. The total energy height is as follows:

$$H = WS + \frac{a \cdot V^2}{2 \cdot g} \quad (5.3-9)$$

where

WS is the water surface level,

$\frac{a \cdot V^2}{2 \cdot g}$  is the kinetic energy.

The critical depth ( $WS_{crit}$ ) is the water surface level for which the total energy is minimum as indicated in Figure 5.3-4 below.

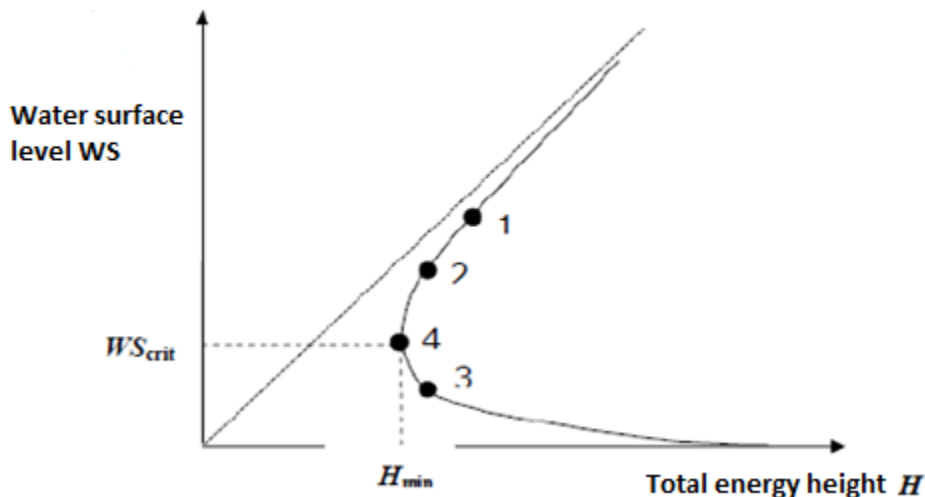


**Figure 5.3-4:** Variation of total energy depending on the water level  
(Obtained by Oikonomou, 2013)

### Application of the conservation of momentum principle

In cases when the conservation of energy principle cannot be applied such as abrupt change in slope, bridge narrowing, falling channel or in channel junction etc., then the principle of conservation of momentum (accelerator principle) can be applied (requires gradually changing flow state), as follows:

$$P_2 - P_1 + W_x - F_f = Q \cdot \rho \cdot \Delta V_x \quad (5.3-10)$$

where

P is the hydrostatic pressure in two successive cross section 1 and 2,

W<sub>x</sub> is the force from the weight of water in x direction,

F<sub>f</sub> is the force due to external friction energy losses (linear losses) from cross section 2 to 1,

Q is the water flow,

ρ is the density of water,

ΔV<sub>x</sub> is the differentiation of flow velocities from cross section 2 to 1 in x direction.

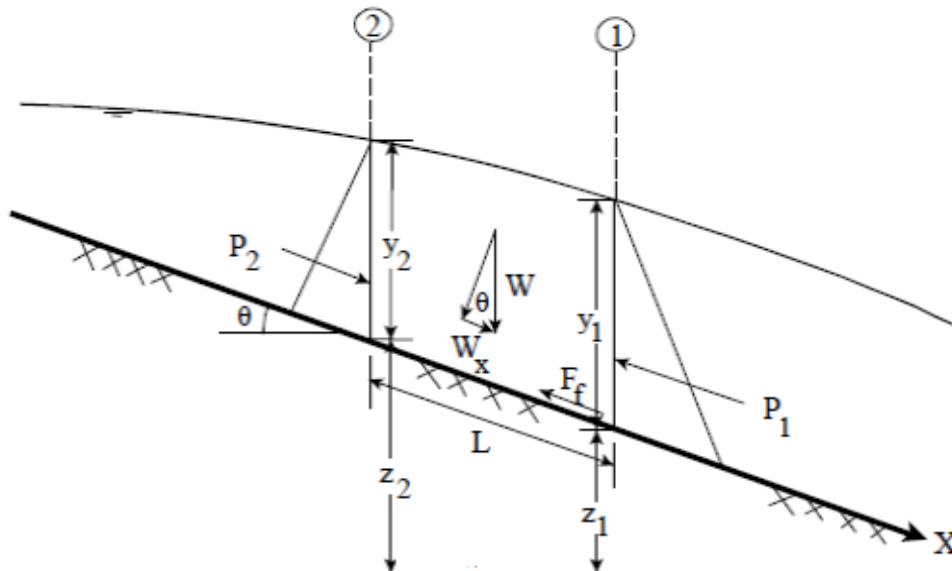


**Figure 5.3-5:** Presentation of the terms of the conservation of momentum equation  
(Obtained by Dedousis, 1999)

The terms of the equation are presented in Figure 5.3-5 above and their formulas are displayed below.

**A.** More specifically the hydrostatic pressure is defined as follows:

$$P = \gamma \cdot A \cdot \bar{Y} \cdot \cos\theta \quad (5.3-11)$$

where

P is the hydrostatic pressure,

γ is the specific gravity of water,

A is the wetted surface area of the cross section,  
 $\bar{Y}$  is the depth from the water surface to the center of gravity.

**B.** The weight of water in x direction ( $W_x$ ) between the cross sections 1 and 2 is:

$$W_x = \gamma \cdot \left( \frac{A_1 + A_2}{2} \right) \cdot L \cdot S_o \quad (5.3-12)$$

where

$\gamma$  is the specific gravity of water,  
 $A_i$  is the wetted surface area of each cross section,  
 L is the distance between cross sections 1 and 2,  
 $S_o$  is the slope of the riverbed.

**C.** The force due to external friction ( $F_f$ ) is:

$$F_f = \tau \cdot \bar{P} \cdot L \quad (5.3-13)$$

where

$\bar{P}$  is the mean wetted perimeter between cross sections 1 and 2,  
 L is the distance between cross sections 1 and 2,  
 $\tau$  is the shearing stress.

**D.** The differentiation of velocity from cross section 2 to 1 ( $\Delta V_x$ ) is:

$$\Delta V_x = \beta_1 \cdot V_1 - \beta_2 \cdot V_2 \quad (5.3-14)$$

where

$\beta$  is the correction coefficient of the velocity distribution and V are the flow velocities.

Finally, the conservation of energy equation is the following:

$$\frac{Q_2^2 \cdot \beta_2}{g \cdot A_2} + A_2 \cdot \bar{Y}_2 + \left( \frac{A_1 + A_2}{2} \right) \cdot L \cdot S_o - \left( \frac{A_1 + A_2}{2} \right) \cdot L \cdot \bar{Sf} = \frac{Q_1^2 \cdot \beta_1}{g \cdot A_1} + A_1 \cdot \bar{Y}_2 \quad (5.3-15)$$

### Calculation of linear losses (due to friction)

The linear losses are calculated as the product of the slope of piezometric line  $S_f$  and the length L of the examined section. The slope is calculated from Manning's equation as follows:

$$\bar{Sf} = \left( \frac{Q}{K} \right)^2 \quad (5.3-16)$$

The program has the capability to use other relationships as well for the computation of the mean slope of the piezometric line. The prevalent of all these equations is presented below:

$$\bar{Sf} = \left( \frac{Q_1}{K_1} + \frac{Q_2}{K_2} \right)^2 \quad (5.3-17)$$

### Calculation of losses due to changes in geometry

The losses due to changes in the geometry of the channel such as narrowing and widening spots are computed by HEC-RAS as follows:

$$h_o = c \cdot \left| \frac{a_1 \cdot V_1^2}{2 \cdot g} + \frac{a_2 \cdot V_2^2}{2 \cdot g} \right| \quad (5.3-18)$$

where  $c$  is the coefficient of narrowing or widening of the channel's cross section.

HEC-RAS “understands” that there is a narrowing in geometry when the kinetic energy load on the downstream cross section is higher than the one on the upstream ( $V_2 > V_1$ ). Correspondingly, when the kinetic energy is higher on the upstream then HEC-RAS “perceives” this as a widening of the channel.

All the theoretical hydraulic principles, relationships, and explanations above were obtained from Dedousis (1999) and Oikonomou (2013) studies and describe the theoretical background of HEC-RAS 5.0.7. Of course, this theoretical framework does not display all the functions or equations of HEC-RAS 5.0.7, but the basic ones.

### Initial conditions - Boundary conditions - Flow data

The water surface level is required to be input in HEC-RAS as a boundary condition to start the simulation. In subcritical flow, the boundary condition is defined on the downstream, while in supercritical on the upstream. In mixed flow they are input both upstream and downstream. There are four types of boundary conditions that can be input in the program:

- The Water Surface: in this type of condition, the water surface level for each profile should be input.
- The Critical Depth: in this type of condition, the program calculates the critical depth and uses it as boundary condition. No extra information is needed.
- The Normal Depth: in this type of condition, the value for the slope of the energy grade line should be input in order to calculate the normal depth in this position. Generally, the energy grade line is approached as the mean slope of the riverbed.
- Rating Curve: in this type of condition, curves between the flow and the water surface are input for every profile.

If there are no data for the water surface level, then we can assume it or put the critical or normal depth instead. The assumption of a water surface level includes an error rate, so it is necessary to import extra cross sections in the program. In case of subcritical flow, the extra cross sections are added on the downstream, in supercritical flow on the upstream and in mixed flow on both upstream and downstream of the river. The flow data is substantial to be imported for each cross section in order to calculate the profile of the water surface. The value of flow given on the upstream of the river, remains stable unless a lateral flow is added in another cross section (Paresidou and Plitsi, 2005).

### 5.3.3 Unsteady flow

The physical laws that rule the flow in a river are:

1. The conservation of mass principle,
2. The conservation of momentum principle.

These laws are mathematically expressed using partly differential equations, and more specifically the continuity and momentum equations that will be mentioned further below.

#### Continuity equation

The flow and the wetted area are symbolized as  $Q(x, t)$  and  $Ax$  accordingly. The total wetted area  $Ax$  is the sum of the effective area  $A$  and the floodplain  $S$ . According to the conservation of mass principle, the change in mass per time unit inside the control volume equals to the total net mass inflow from the area  $Ax$  that surrounds the control volume.

Assuming that  $\Delta x$  has a low value, the change in mass inside the control volume is:

$$p \cdot \frac{\partial A_t}{\partial t} \cdot \Delta x = p \cdot \left[ \left( Q - \frac{\partial Q}{\partial x} \cdot \frac{\Delta x}{2} \right) - \left( Q + \frac{\partial Q}{\partial x} \cdot \frac{\Delta x}{2} \right) + Q_s \right] \quad (5.3-19)$$

where

$Q - \frac{\partial Q}{\partial x} \cdot \frac{\Delta x}{2}$  is the percentage of water inlet,

$Q + \frac{\partial Q}{\partial x} \cdot \frac{\Delta x}{2}$  is the percentage of water outlet,

$p$  is the density of the fluid,

$\frac{\partial A_t}{\partial t} \cdot \Delta x$  is the percentage of control volume change,

$Q_s$  is the lateral inflow on the control volume.

#### Application of the conservation of momentum principle

The principle of conservation of momentum is expressed by Newton's 2<sup>nd</sup> law as follows:

$$\sum F_x = \frac{\overline{dM}}{dt} \quad (5.3-20)$$

According to the conservation of momentum theory, the sum of the external forces exerted on the fluid, which in time moment  $t$  takes the aforementioned control volume, equals to the change of quantity of motion (per unit time) inside the control volume minus the net inlet of quantity of motion that enters the control volume from  $Ax$  area. That is a vector equation applied in  $x$  direction. Three kinds of forces will be examined here: (A) Pressure forces (B) Gravity forces (C) Friction forces:

##### A. Pressure forces

$$F_{p_n} = -\rho \cdot g \cdot A \cdot \frac{\partial h}{\partial x} \cdot \Delta x \quad (5.3-21)$$

where

$Fp_n$  is the net pressure force in the control volume,  
 $\rho$  is the density of the fluid,  
 $g$  is the gravitational acceleration,  
 $A$  is the area of the cross section,  
 $\frac{dh}{dx} \cdot \Delta x$  is the percentage of height differentiation inside the control volume.

#### B. Gravity forces

$$Fg = -\rho \cdot g \cdot A \cdot \frac{dz_o}{dx} \cdot \Delta x \quad (5.3-22)$$

where

$Fg$  is the net gravity force in the control volume,  
 $\rho$  is the density of the fluid,  
 $g$  is the gravitational acceleration,  
 $A$  is the area of the cross section,  
 $Z_o$  is the bed lifting,  
 $\frac{dz_o}{dx} \cdot \Delta x$  is the percentage of bed lifting inside the control volume.

#### C. Friction forces

$$Ff = -\rho \cdot g \cdot A \cdot Sf \cdot \Delta x \quad (5.3-23)$$

where

$Ff$  is the friction force in the control volume,  
 $\rho$  is the density of the fluid,  
 $g$  is the gravitational acceleration,  
 $A$  is the area of the cross section,  
 $Sf$  is the friction due to slope and is positive for the x axis and is defined as follows:

$$Sf = \frac{Q \cdot |Q| \cdot n^2}{2,208 \cdot R^{4/3} \cdot A^2} \quad (5.3-24)$$

where

$R$  is the hydraulic radius  
 $n$  is the Manning's coefficient.

The final form of the conservation of momentum equation is as follows:

$$\frac{dQ}{dt} + \frac{d(QV)}{dx} + g \cdot A \cdot \left( \frac{dz}{dx} + Sf \right) = 0 \quad (5.3-25)$$

#### Initial conditions - Boundary conditions - Flow data

Boundary conditions can be simulated in all the free openings of the river environment. For the case of an unsteady flow simulation, the program allows the input of all the following types of boundary conditions at the upstream boundary of the river:

1. Flow Hydrograph
2. Stage Hydrograph
3. Stage/Flow Hydrograph

The downstream boundary conditions that can be input during an unsteady flow simulation are the following:

1. Flow-Stage Rating Curve
2. Normal Depth (Manning's equation)
3. Flow Hydrograph
4. Stage Hydrograph
5. Stage/Flow Hydrograph

Moreover, there is a possibility to import boundary conditions such as lateral inflow hydrograph and groundwater interflow, in intermediate locations (cross sections). The initial flow conditions can be input with two possible ways. The first and most common is to input the flow data for each river and then the program calculates the water surface in steady flow conditions. The second method is applied by setting as initial conditions the results (flow and depth) from a previous run of the program (Dedousis, 1999· Paresidou and Plitsi, 2005· Oikonomou, 2013).

#### 5.3.4 Quasi-unsteady flow

The quasi-unsteady modeling is a more stable process than the unsteady flow simulation. Furthermore, unsteady flow modeling usually requires specialized expertise from the user. Unsteady models can be unstable, and often require skillful trouble shooting by an experienced practitioner. Worth mentioning is also that movable cross-sections add an additional degree of freedom which can exacerbate stability issues and hence, in most cases, the quasi-unsteady assumption is easier to use (Gibson et al., 2017). Another fact is that quasi-unsteady simulations can be faster under certain circumstances. The unsteady flow analysis solves each time step significantly faster than the quasi-unsteady. Nevertheless, the variable time step available in quasi-unsteady flow, which focuses computational time on periods of maximum bed change, can make quasi-unsteady simulations more efficient for long term runs. Therefore, in some systems, with minor storage, errors introduced by the quasi-unsteady simulation may be acceptable, as they are justified by the simpler and faster solution (Gibson et al., 2017).

#### **Boundary conditions - Flow data**

For the case of a quasi-unsteady flow simulation, the program allows the input of a flow series as an upstream boundary condition (at the first river station). The downstream boundary conditions that can be input in a quasi-unsteady flow simulation are the following: 1) Flow-Stage Rating Curve, 2) Normal Depth, 3) Stage Series.

There is a possibility also to import boundary conditions such as Lateral Flow Series, Internal Stage BC and Uniform Lateral Flow in intermediate locations (cross sections). Moreover, in a quasi-unsteady simulation the computational increment should be defined (it is the time step of the calculations) along with the flow duration which indicates the duration of each one of the flow values. Finally, it is necessary to set the temperature series for the whole period of the simulation.

## 5.4 Application of HEC-RAS

### 5.4.1 General

The US Army Corps of Engineers' (USACE) Hydrologic Engineering Center (HEC) recently released version 5.0 of their River Analysis System (HEC-RAS) in 2016 (USACE, 2016). HEC-RAS 5.0 included a variety of hydraulic and water quality advances over previous versions, most notably a two-dimensional hydrodynamic model. HECRAS version 5.0 also included several important sediment transport developments (Gibson et al., 2017).

HEC-RAS first included 1D sediment transport computations in version 4.0 (Gibson et al., 2006). The original capabilities computed sediment continuity over cross-section-centered control volumes with the Exner equation. Versions 4.0 and 4.1 used a quasi-unsteady hydrodynamic model and computed the cross-sectional bed change using the “veneer method”. The veneer method applies erosion and deposition evenly over all wet cross section nodes between user-specified movable bed limits. These earlier versions also included bed mixing algorithms and other physical and empirical limiters to constrain the theoretical continuity equation with practical, morphological, limitations (Gibson et al., 2017).

HEC-RAS 5.0 expanded its capabilities. The two most important developments are firstly the capability to perform a sediment transport analysis using an unsteady flow model and secondly the possibility to add lateral bank failure and toe scour capabilities by coupling the vertical bed change model with the USDA-ARS Bank Scour and Toe Erosion Model (BSTEM). The new versions also include several new features such as the Copeland (1992) bed mixing and armoring algorithm, bed roughness predictors, and Specific Gage Analysis capabilities (Gibson et al., 2017). All these new capabilities of HEC-RAS can not only be used for a river sediment transport analysis but also for reservoir sediment modeling as presented in the current study.

The interface of HEC-RAS 5.0.7 (the version that is used for the present thesis) is displayed below in Figure 5.4-1. More specifically, the project file and all the types of files imported to the project are shown, along with a series of icons on the toolbar concerning data input and edit, the different simulations that can be performed and several data and output view options. The unit system was set to S.I. Units.

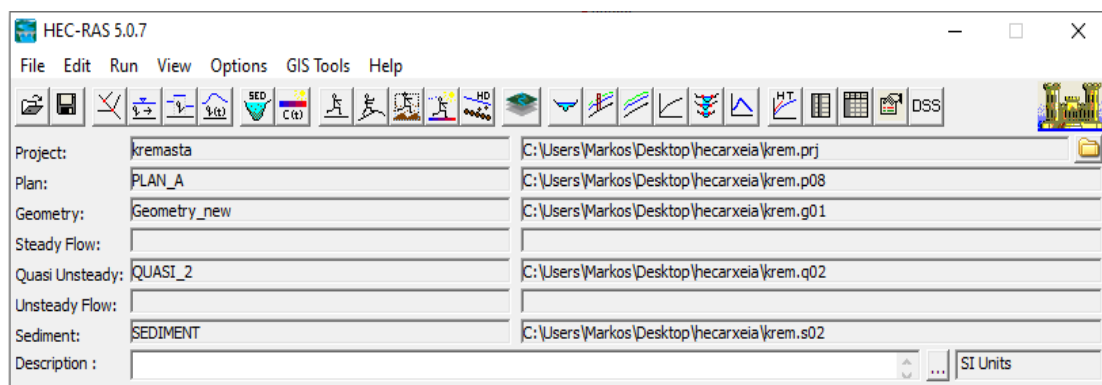


**Figure 5.4-1:** The interface of HEC-RAS (home page) (HEC-RAS 5.0.7)

## 5.4.2 Input data

The input data consist of the geometric, quasi-unsteady flow and sediment data of Acheloos river. Acheloos is the river that will be examined due to its magnitude for the dam. The process of importing all these data is described thoroughly further below.

### 5.4.2.1 Geometric data

The present study focuses on the one-dimensional analysis of sediment transport inside Kremasta reservoir. As it was mentioned above, the rivers that inflow inside the reservoir are Acheloos, Agrafiotis and Tavropos/Megdovas. The flow of Acheloos comprises roughly 50% of the total inflows that enter the reservoir every year, hence it is the main source of water and a critical supplier of sediment for the reservoir. Bearing this in mind and in order to simplify the analysis (by avoiding the junction of two or axes which would be difficult to process in the current study) Acheloos river is chosen as the main axis (channel) to examine and build the geometry of the reservoir around it. The same concept was used in Civil 3D when for the preparation of the geometric data was required to define a main alignment (axis) and this was Acheloos river.

The “View/Edit geometric data” icon on the home page is used to import the geometric data and next the buttons “File”, “Import Geometry Data” and “GIS Format” are pressed arow to import the GEO file prepared in Civil 3D. During this process it is critical to invert the river stations because in Civil 3D they are vice versa. The geometric data (Figure 5.4-2) for this study consists of the axis of Acheloos river, which is 39,2 (km) long, and 109 cross sections across this river, some of which were “built” in Civil 3D and others interpolated in HEC-RAS to fill some geometric gaps. The tool of cross section points filter (from the “Tools” tab) is used in some cross sections to reduce the points per XS (cross section) -the limit is 500 points- because some of them are very wide. As it is mentioned, Kremasta is the biggest reservoir in Greece, so this filter was needed in locations where the reservoir is extremely wide and the cross sections had to cover all this width in order to describe accurately the reservoir.

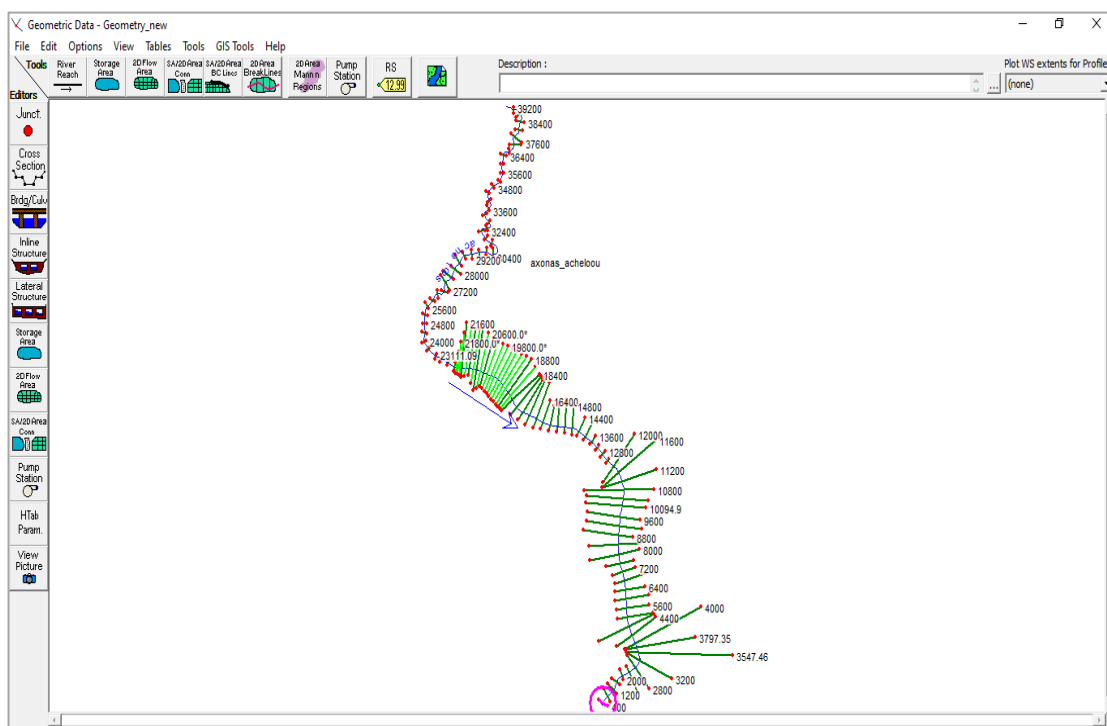


**Figure 5.4-2:** Geometric data – Acheloos river and cross sections (HEC-RAS 5.0.7)

Below in Figures 5.4-3 and 5.4-4, two cross sections are presented as a sample (filled with water because the simulation has already run). The first one has a width of approximately 2 (km), while the second one is roughly 200 (m) wide indicating the width variations of the reservoir which contains lots of narrow passages.

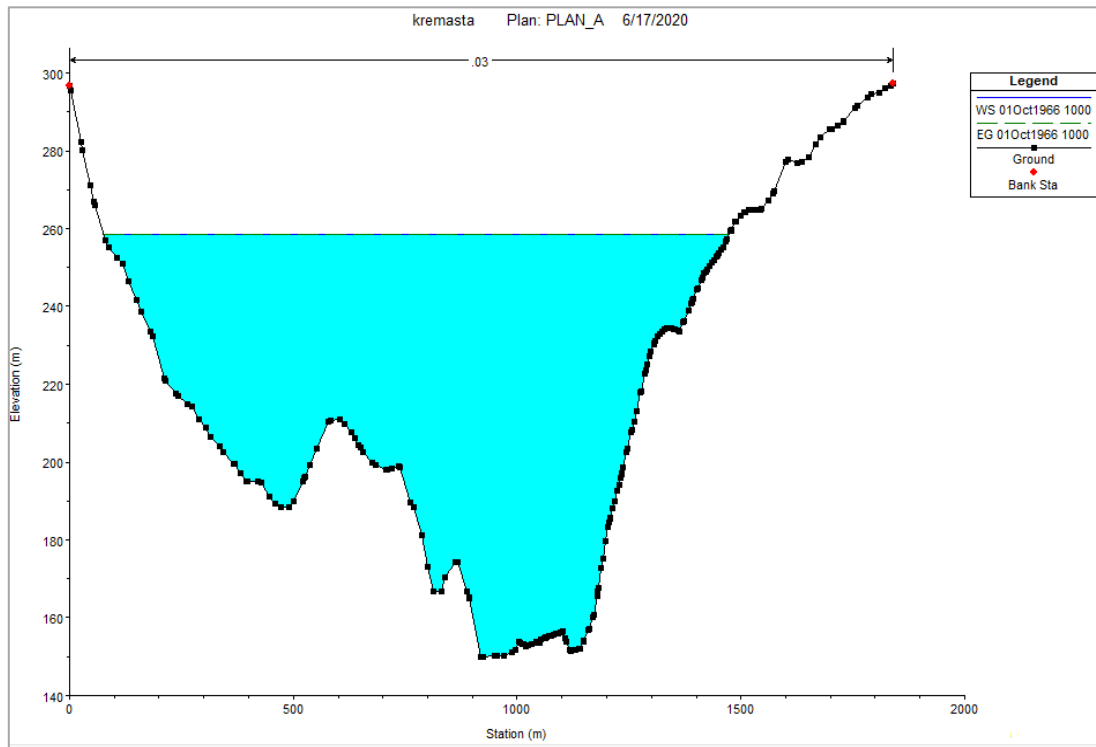


**Figure 5.4-3:** Cross section in river station 2800 (m) (HEC-RAS 5.0.7)

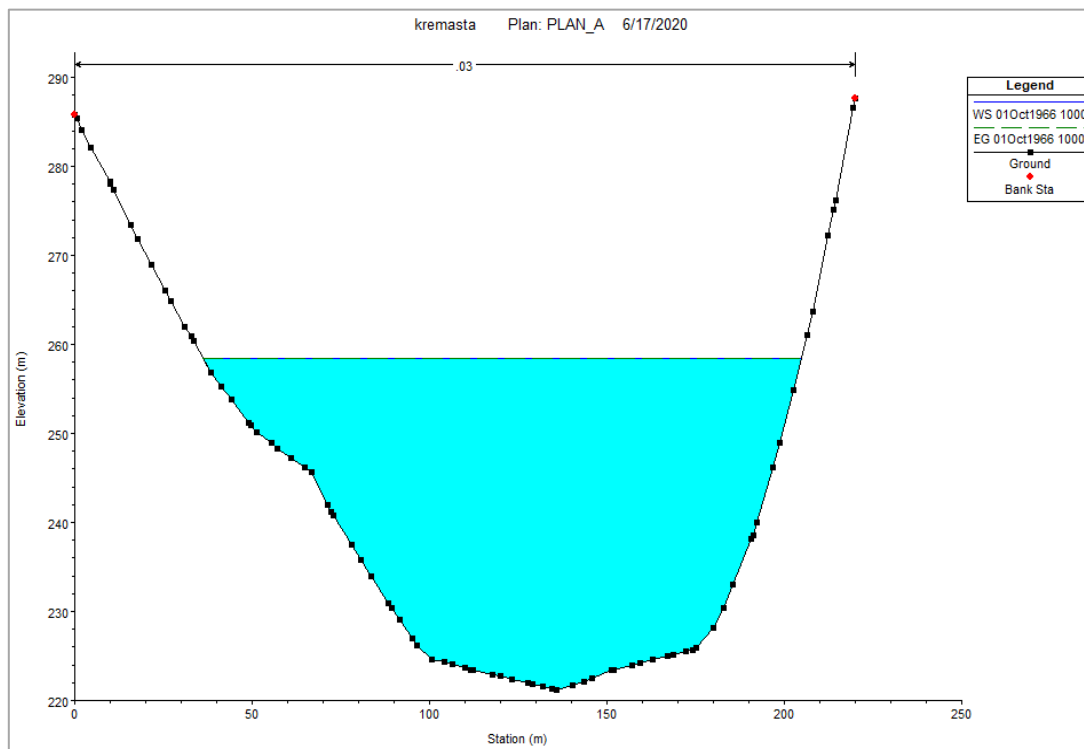


**Figure 5.4-4:** Cross section in river station 22400 (m) (HEC-RAS 5.0.7)

Using the “Tables” tab, the manning’s n roughness values are defined as 0,03 for all the cross sections and riverbanks, a value that occurs from Zarris et al. (2001) and other international literature (Figures 5.4-5 and 5.4-6). Moreover, from the “Tables” tab the reach lengths (distance among cross sections) are generally set at 400 (m) due to the large reservoir, except from the locations where an interpolation was required, and the reach lengths are lower.

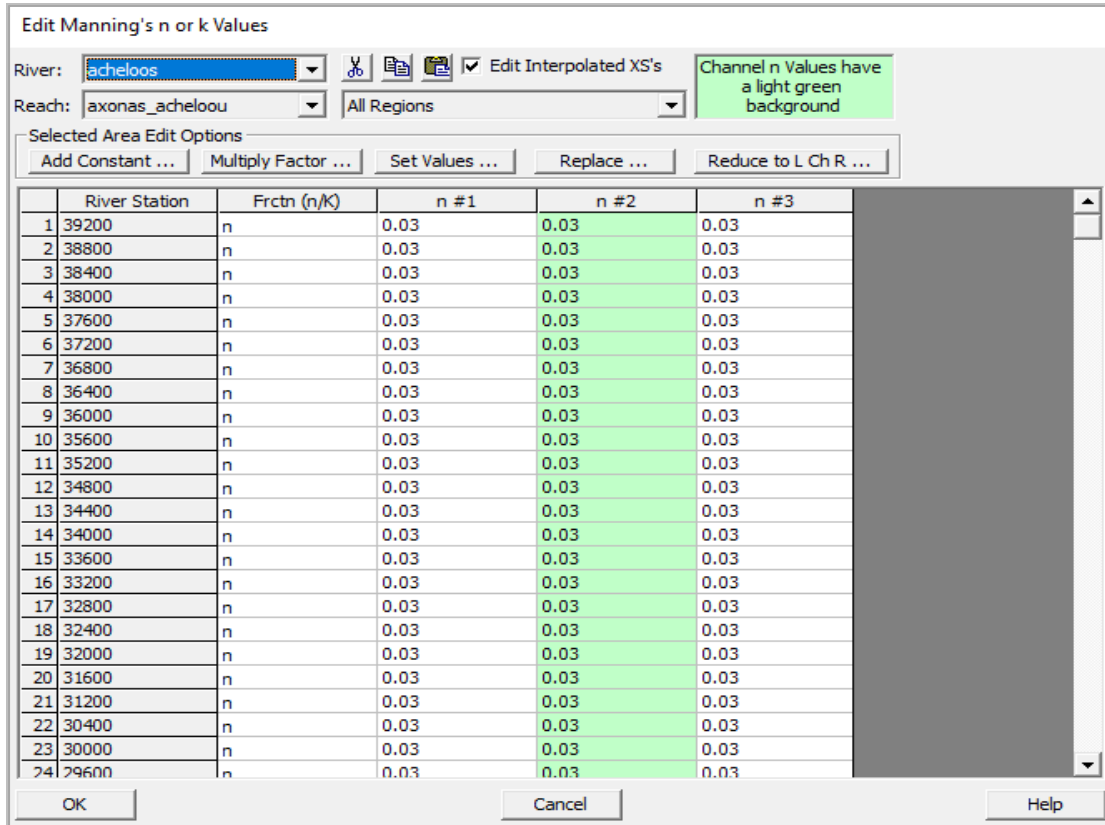


Figure 5.4-5: Manning’s roughness n factor (HEC-RAS 5.0.7)

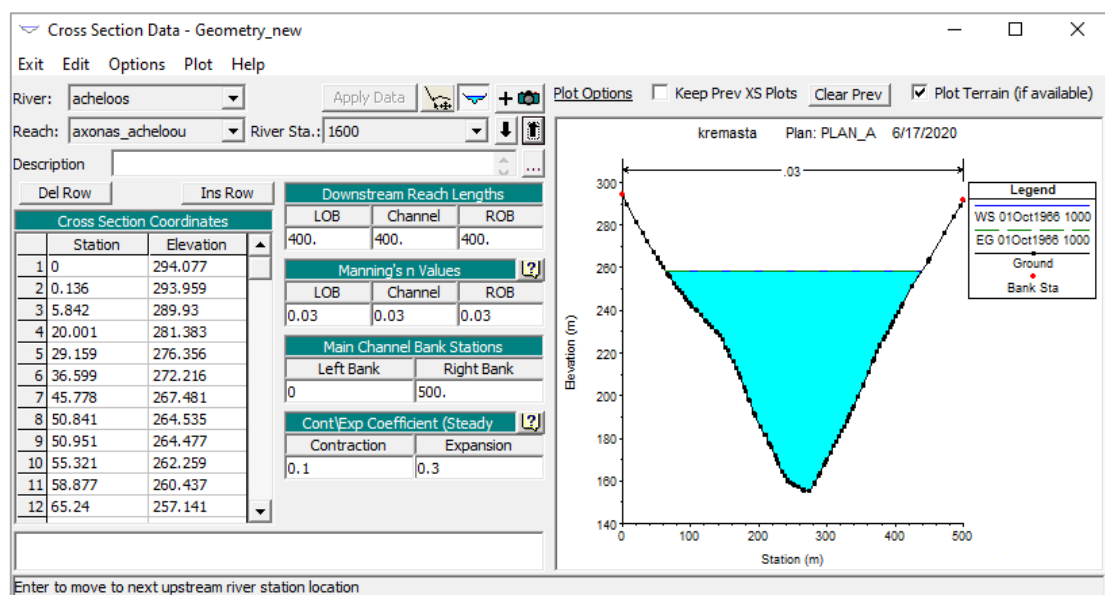


Figure 5.4-6: Reach lengths and other characteristics of the cross section (HEC-RAS 5.0.7)

### 5.4.2.2 Flow data

The performance of a one-dimensional sediment transport simulation can be carried out either using quasi-unsteady or unsteady flow data. Quasi-unsteady modeling is a more stable process and can be faster under certain circumstances. The unsteady flow analysis solves each time step significantly faster than the quasi-unsteady. Nevertheless, the variable time step available in quasi-unsteady flow, which focuses computational time on periods of maximum bed change, can make quasi-unsteady simulations more efficient for long term runs. (Gibson et al., 2017). Keeping these in mind, quasi-unsteady modeling is chosen for the present study.

More specifically, the boundary conditions for the quasi-unsteady flow dataset included a daily flow series for the upstream boundary (first cross section) and a monthly stage series for the downstream boundary (last cross section). The flow series are the daily inflows of Acheloos river, while the stage series are the water level of the reservoir. In addition, lateral flow series are added in two cross sections (10.800 m and 4.000 m) which are the locations where the rivers Agrafiotis and Tavropos meet the main channel of Acheloos inside the reservoir. Each river flow dataset was calculated above in Chapter 5.1. All these data are available thanks to the hard-long-term work and measurements of scientists and professors from the National Technical University of Athens and the Public Power Corporation of Greece. The Figure 5.4-7 below shows the quasi-unsteady flow editor in HEC-RAS environment.

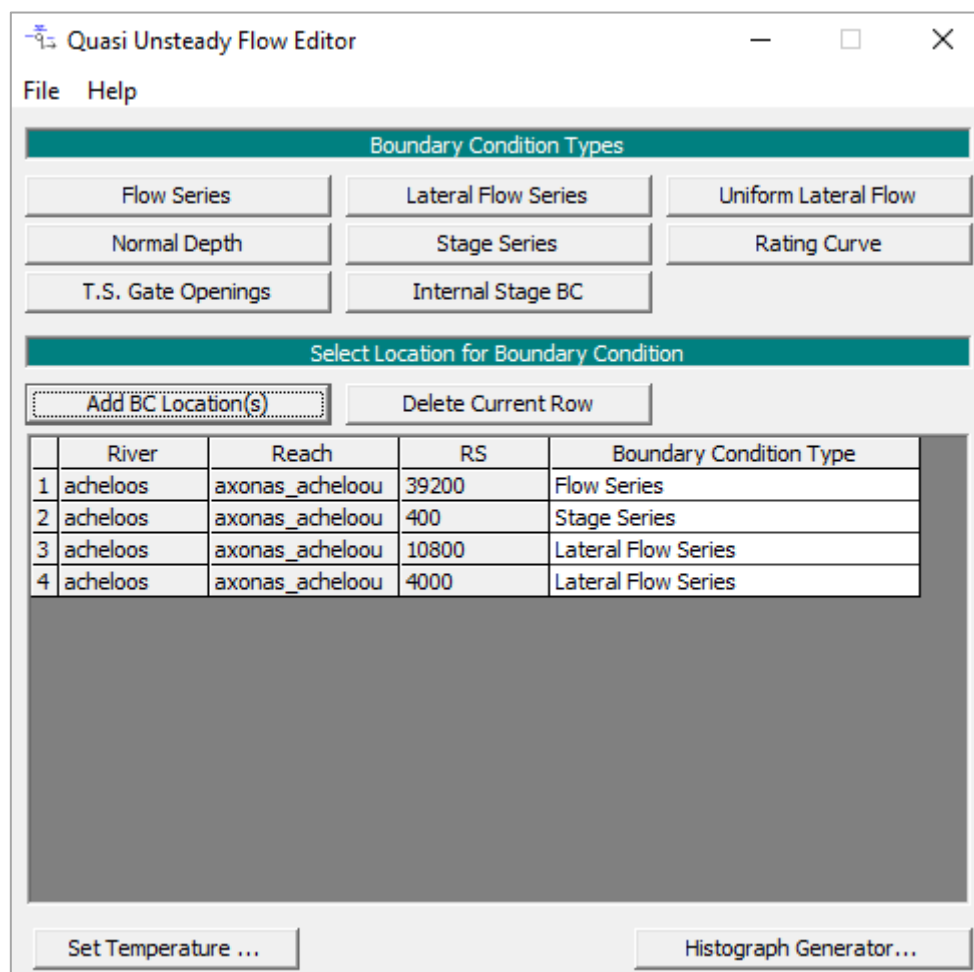


Figure 5.4-7: Quasi-unsteady flow editor (HEC-RAS 5.0.7)

Figure 5.4-8 below indicates the flow series where a fixed start date -which is 01/10/1966 and is the beginning of the simulation- has been defined, along with the flow duration which is 24 hours according to the available daily flow series. The computational increment is the time step of the calculations and is defined as 24 hours for flow from 0,01 to 500 (m<sup>3</sup>/s), and 1 hour for flow higher than 500 (m<sup>3</sup>/s) to avoid errors during the run. More specifically, when there are large amounts of sediment on a single cross section and the program becomes unstable, the solution is to decrease the computation increment for high values of flow because some cross sections cannot handle the large sediment loads. In that case the run might be slower, but it will also be more accurate.

Flow Series for ACHELOOS axonas\_achelouu 39200

Select/Enter the Data's Starting Time Reference

Use Simulation Time: Date: 01OCT1966 Time: 10:00

Fixed Start Time: Date: 01OCT1966 Time: 10:00

Hydrograph Data

No. Ordinates Interpolate Values Del Row Ins Row

	Simulation Time	Elapsed Time (hours)	Flow Duration (hours)	Computation Increment (hours)	Flow (m <sup>3</sup> /s)
1	01Oct1966 1000	24	24	24	17.1
2	02Oct1966 1000	48	24	24	13.1
3	03Oct1966 1000	72	24	24	20.8
4	04Oct1966 1000	96	24	24	22.6
5	05Oct1966 1000	120	24	24	24.4
6	06Oct1966 1000	144	24	24	22.2
7	07Oct1966 1000	168	24	24	20
8	08Oct1966 1000	192	24	24	9.3
9	09Oct1966 1000	216	24	24	9.3
10	10Oct1966 1000	240	24	24	20.4
11	11Oct1966 1000	264	24	24	17.1
12	12Oct1966 1000	288	24	24	5.7
13	13Oct1966 1000	312	24	24	9.8

Compute computation increments based on flow

	Qlow	Qhigh	CI
1	0.01	500	24
2	500	10000	1
3			
4			
5			
6			
7			

Plot ... OK Cancel

**Figure 5.4-8:** Setting of flow series data (HEC-RAS 5.0.7)

The lateral flow series for Agrafiotis and Tavropos rivers contain the same characteristics (except from the flows) and are determined in the same way. Now in the stage series (Figure 5.4-9) the stage duration is defined as 730 hours because as mentioned earlier, the stage data is monthly. Additionally, another mandatory feature to determine is the temperature of the area which is set at 16°C (the mean annual temperature of Kremasta). The number of coordinates for the flow and temperature data is 15.422, while for the stage series is 508 to cover all the dataset.

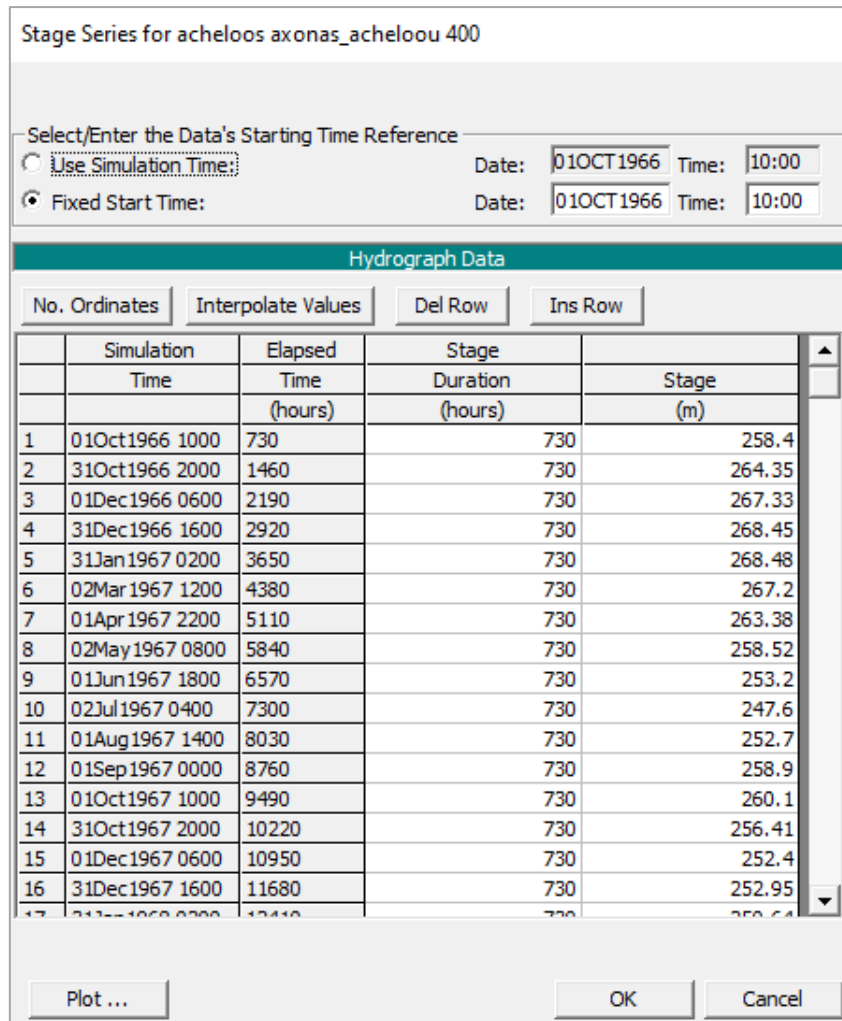


**Figure 5.4-9:** Setting of stage series data (HEC-RAS 5.0.7)

The filling of the reservoir started just after the diversion tunnel was closed in July 1965. In that day, the water level was at 144 (m). The next six months, the increase rate of the water level was high, and it is worth mentioning that by the end of January 1966 the water level was roughly at 255 (m) altitude.

In May 1966, the water level of the reservoir was at 269 (m) altitude, which is significantly lower than the maximum allowed water level of 284 (m), and subsequently it started decreasing. For the next 3 years apart from some fluctuations, it remained stable. For instance, the water level reached its lower value at roughly 230 (m) in August 1967. The cause for that were the drainage works that had to be done so that the extensive leaks of the first months of operation would stop.

Subsequently, the water level fluctuated periodically with higher values appearing during May and June and the lower ones at November-December period. The max value of water level recorded until August 2004, showed up in May 1994 and accounted for a mean monthly value of water level of 276,5 (m) (Kalfountzos, 2013).

### 5.4.2.3 Sediment data

The sediment data initially requires the definition of a max depth (due to erosion) which is set at 5 (m) and considered as a reasonable value, left and right banks in which we used the “use banks for extents” option. Furthermore, the bed gradation curve required, was obtained by Zarris (2019) study (Figure 5.4-11). Moreover, the transport function of Laursen (Copeland) is chosen in the present study, along with Thomas (Ex5) sorting method and Ruby fall velocity method which are the most common for the case of reservoir modeling. Additionally, HEC-RAS 5.0.7 introduces several bed change options for deposition: no bed change allowed outside of the movable bed limits, allow deposition outside of the bed limits and a reservoir option for sediment to deposit more in deeper parts of the cross sections and for the erosion as well: max width, side slope and center station. From all these, the option that allows deposition outside of the bed limits is chosen for this study. Moreover, the selected routing method is the one that limits sediment velocity to water velocity (usually suggested for reservoirs).

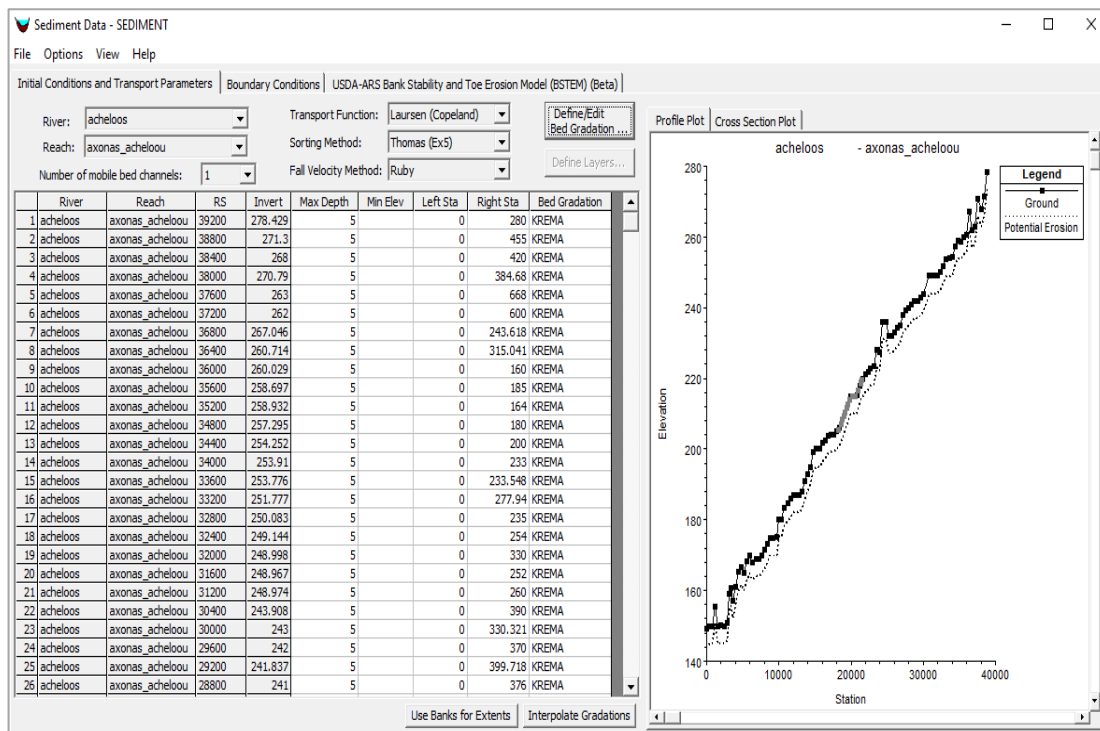
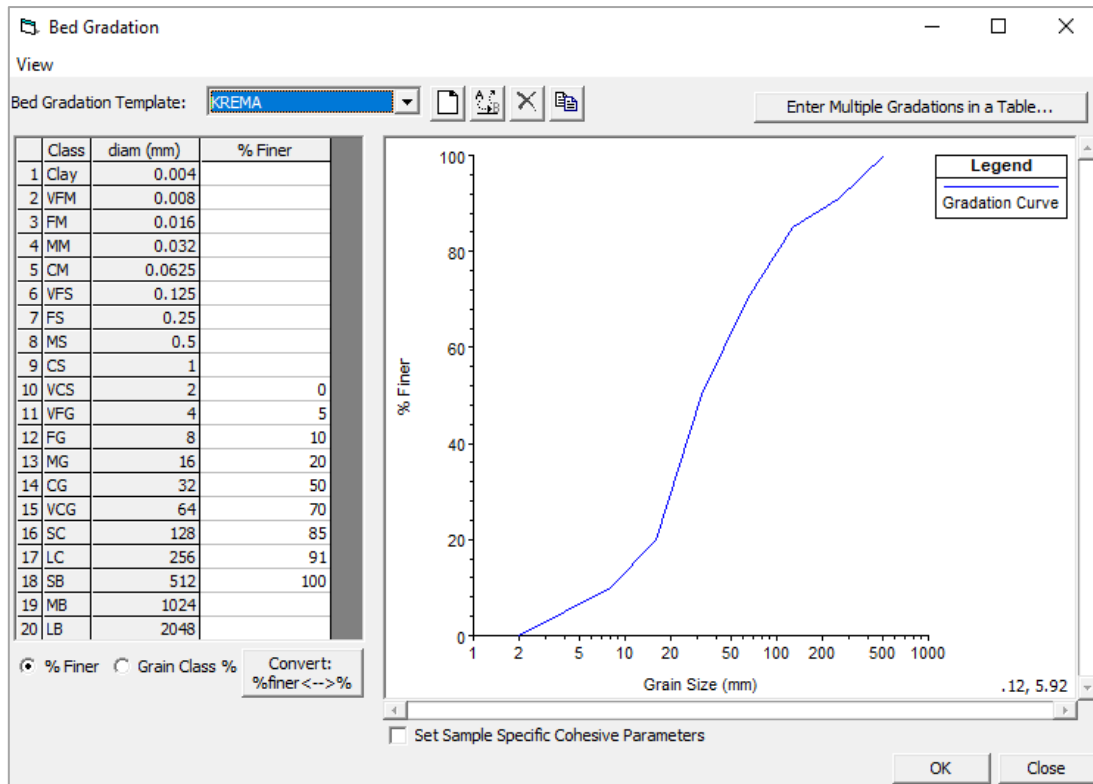


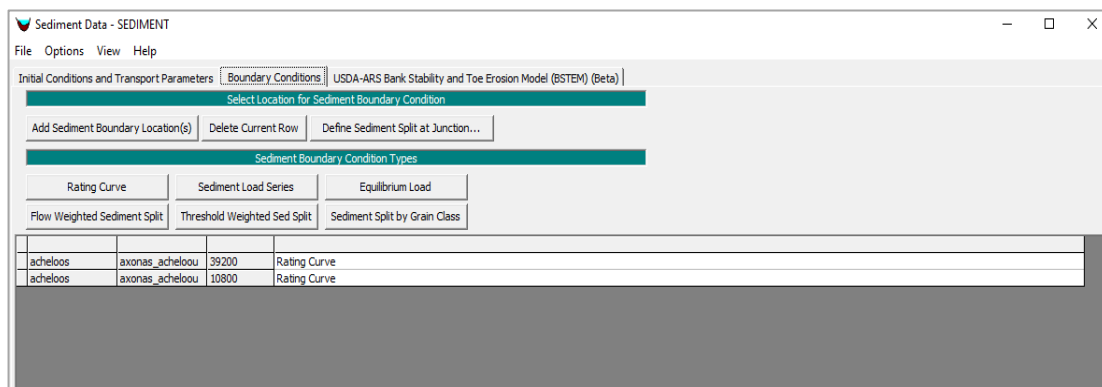
Figure 5.4-10: Definition of initial conditions (HEC-RAS 5.0.7)

Figure 5.4-10 presents the sediment data interface and shows the several data for each cross section which can differentiate among them, but for the present study they are the same. On the right side of the image is evident the current ground and the ground under a future potential erosion after the simulation.



**Figure 5.4-11:** Definition of bed gradation (HEC-RAS 5.0.7)

Another substantial feature concerning the sediment data (after the set the initial conditions) is the setting of the boundary conditions. Regarding the upstream boundary (1<sup>st</sup> cross section) a flow-sediment load rating curve is chosen. When it comes to the intermediate cross sections there are the options to import a rating curve or a sediment load series. For the present thesis, an intermediate rating curve is used for the cases of Agrafiotis where there is a lateral inflow of water and sediment.



**Figure 5.4-12:** Definition of boundary conditions (HEC-RAS 5.0.7)

Figure 5.4-12 reveals the defined sediment boundary conditions which are an initial rating curve (cross section 39.200 m) and an intermediate one (cross section 10.800 m) where Agrafiotis “meets” the axis of Achelous. The rating curves include 2 sets of flow-sediment load and the percentages of different bed materials and are presented in Figure 5.4-13 below:

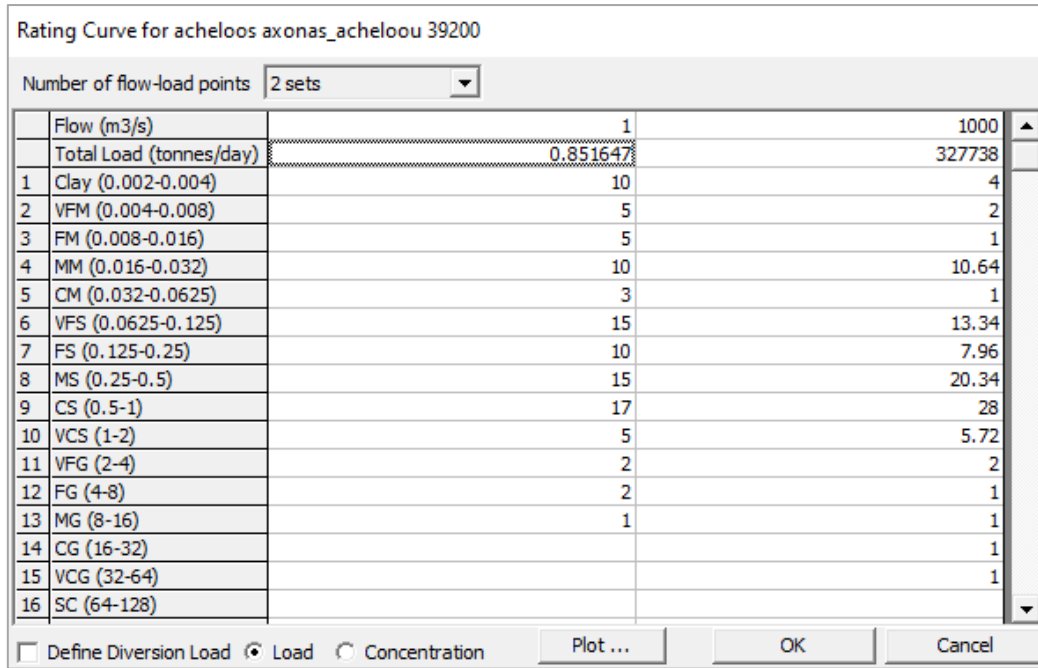


**Figure 5.4-13:** Definition of rating curve as boundary condition (HEC-RAS 5.0.7)

The rating curve that is input to HEC-RAS as a sediment data boundary condition is a product of the previous analysis in Chapter 4 (2<sup>nd</sup> Case) where the flow-sediment load relationship was built. This relationship consists of two branches, one for the low and one for the high values of flow. As observed for 1 (m<sup>3</sup>/s) flow there are 0,85 (t/d) of sediment load and for a river flow of 1.000 (m<sup>3</sup>/s) the river carries 327.738 (t/d) of sediment load; these numbers occur from the following relationships:

$$Qs = 0,0099 \cdot Q^{1,477} \quad \text{when } Q < 86 \text{ (m}^3\text{/s)} \quad (5.4-1)$$

$$Qs = 0,00191 \cdot Q^{2,099} \quad \text{when } Q > 86 \text{ (m}^3\text{/s)} \quad (5.4-2)$$

Under the frame of Zarris et al. (2001) study two drillings in Acheloos river (inside the reservoir) were held in order to investigate the bed gradation and more specifically to identify the material of the transported sediment (gradation). The following Table 5.4-1 presents the results of the drilling processes that are used for the present study to determine the gradation of the transported material shown in Figure 5.4-13:

**Table 5.4-1:** Types and percentages of transported material (Gradation) by Zarris et al. (2001)

Description	Diameter (mm)	1 <sup>st</sup> Drilling (%)	2 <sup>nd</sup> Drilling (%)
Gravel	2-64	1	4
Very coarse sand	1-2	3,35	6,72
Coarse sand	0,5-1	8,78	28
Medium sand	0,25-0,5	24,97	22,34
Fine sand	0,125-0,25	39,87	9,96
Very fine sand	0,065-0,125	10,91	15,34
Medium/Coarse mud	0,016-0,065	11	13,67
<i>Total:</i>	-	<b>100</b>	<b>100</b>

### 5.4.3 Sediment transport simulation

Thus, after all data are defined, next step is to click the “perform a sediment transport simulation” button in order to determine some extra data before the program is ready for the one-dimensional sediment transport analysis inside the reservoir. These data are shown in Figures 5.4-14 and 5.4-15 and firstly concern the starting and ending date of the simulation which are 01/10/1966 and 20/12/2008 accordingly. Moreover, the creation of a plan file was necessary as well as the setting of the sediment output options.

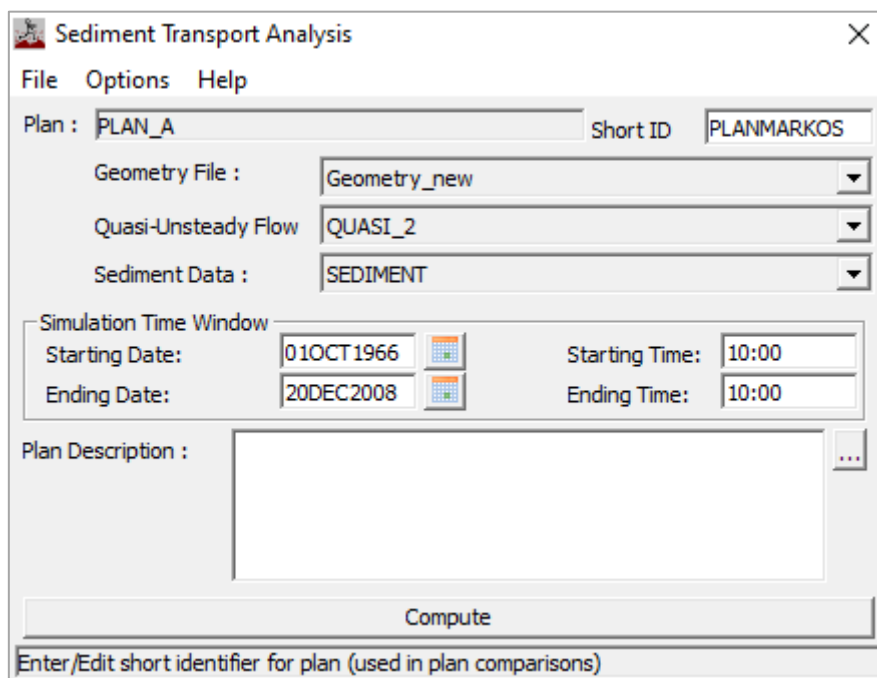


**Figure 5.4-14:** Performing a sediment transport simulation (HEC-RAS 5.0.7)

The output options (Figure 5.4-15) initially concern the output level. It ranges from 1 to 6 and the higher that level is, the more detailed the sediment output will be. For the present study level 4 is chosen, considering that it contains all the meaningful information we need. Moreover, someone can define whether the sediment output will be in mass or volume and if the output increment will coincide with the computation increment (default). Finally, it offers the option to view how the bed of each cross section changes throughout the years. Several other output options are offered but not examined during the current thesis. The choices made are shown in Figure 5.4-15.

The present study faced many errors, warnings or instabilities concerning the ineffective areas, computation increment problems and big datasets which overloaded the program. More specifically, in some locations where the width difference between two cross sections is huge, an interpolation is needed so that it smooths the terrain, reduces the ineffective areas, and allows sediment to pass through. Additionally, the computation increment had to decrease in extreme cases of inflows so that it handles the high flow and sediment load values. Eventually, all these problems were solved by fixing specific data problems and selections.

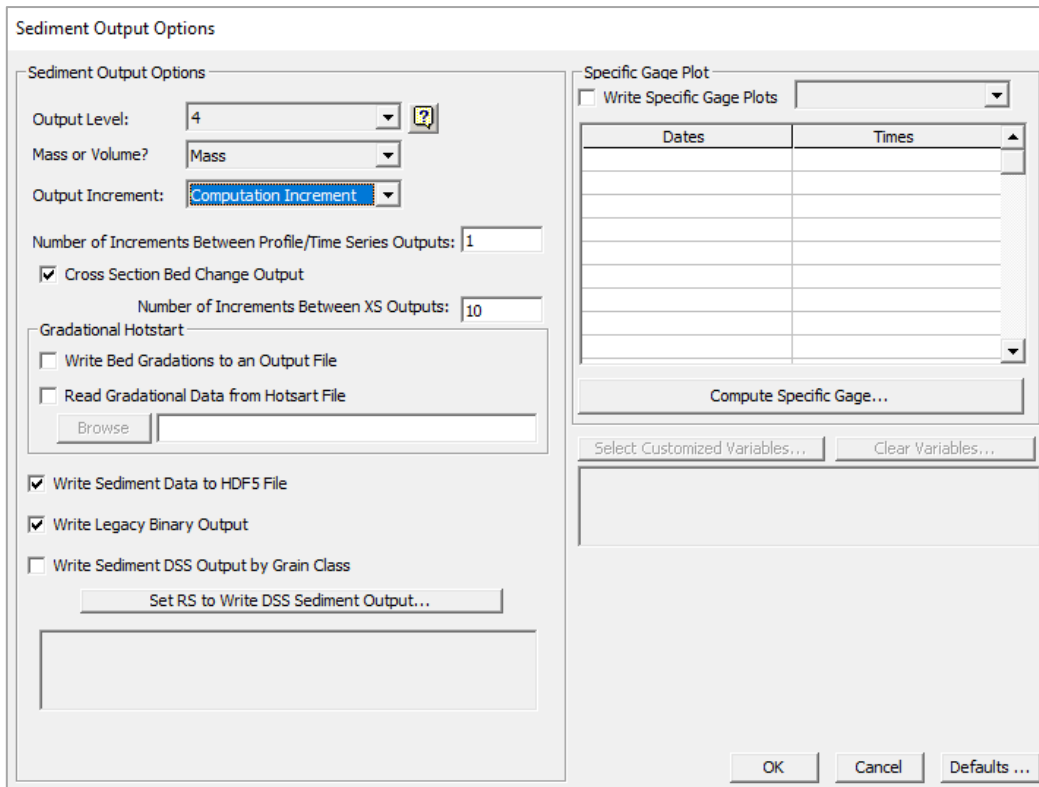


**Figure 5.4-15:** Sediment output options (HEC-RAS 5.0.7)

After all these settings and data input, the model was ready, so the run of the simulation began (Figure 5.4-16). The cumulative results and conclusions of the simulation are presented in the next chapter of the present thesis and in the Appendix.

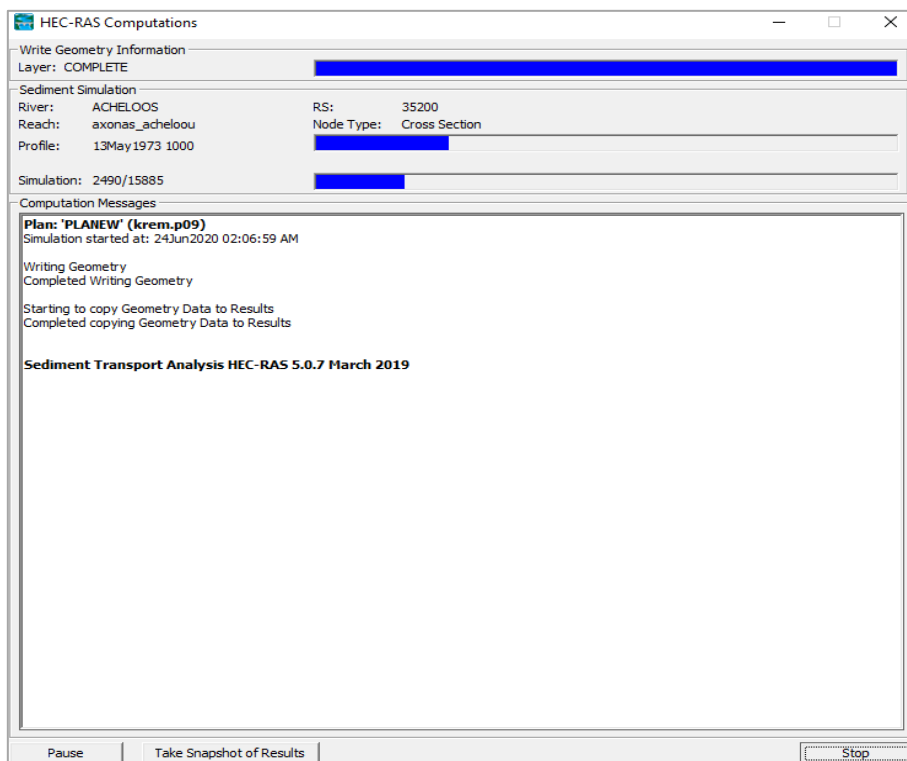


**Figure 5.4-16:** Run of the sediment transport simulation (HEC-RAS 5.0.7)

## 6 Results and Conclusions

### 6.1 Sediment deposition

Sediment deposition in a reservoir pool, and the longitudinal deposition areas, are commonly divided into three main zones -the topset bed, the foreset bed and the bottomset bed- which are described below and shown in Figure 6.1-1. *Topset beds* correspond to delta deposits of rapidly settling sediment. The downstream limit of the topset bed corresponds to the break in slope between the topset and foreset beds which is also the downstream limit of bed material transport in the reservoir. *Foreset deposits* represent the steep face of the delta advancing into the reservoir and are differentiated from topset beds by an increase in slope and decrease in grain size. *Bottomset beds* consist of fine sediments which are deposited beyond the delta by turbidity currents or nonstratified flow. They may also include organic material produced by algae or aquatic plants within the reservoir (Morris and Fan, 1998· U.S. Society on Dams, 2015).

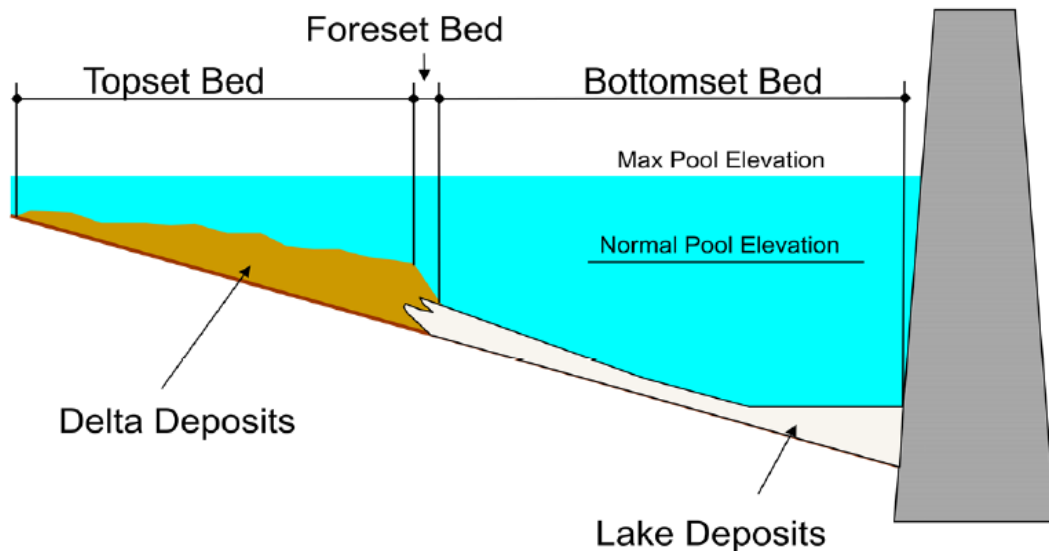


**Figure 6.1-1:** Main zones of deposition (Obtained by U.S. Society on Dams, 2015)

The first result from HEC-RAS one-dimensional sediment transport simulation is the Figure 6.1-2 below which shows how the longitudinal profile of Kremasta reservoir changes after 42 years of dam operation (old sediment output view is used). More specifically the graph below concerns the part of Acheloos river. The output shows that the deltaic deposits are evident and after the cross section at 21.200 (m) only the finer material is transported to the downstream of this specific cross section causing insignificant changes to the bed geometry. This deltaic deposit form is a reasonable output because when a river enters the reservoir pool, the flow velocities decrease along with the capability of the river to carry the sediment further beyond close to the dam. Older research projects supported that sediment deposits near the dam, while this proved to be wrong after a series of studies across the U.S.A. and South Africa that concluded on an even distribution of sediment across the reservoir except from the first part with the deltaic deposits. This happens also in the case of Kremasta, where the bed changes after cross section 21.200 (m) -where the reservoir is nearly 5 (km) wide- are not obvious. Delta deposits are also the most visible component of sedimentation and

in this case, they occupy an area of roughly 18 (km) at the beginning of the reservoir pool.

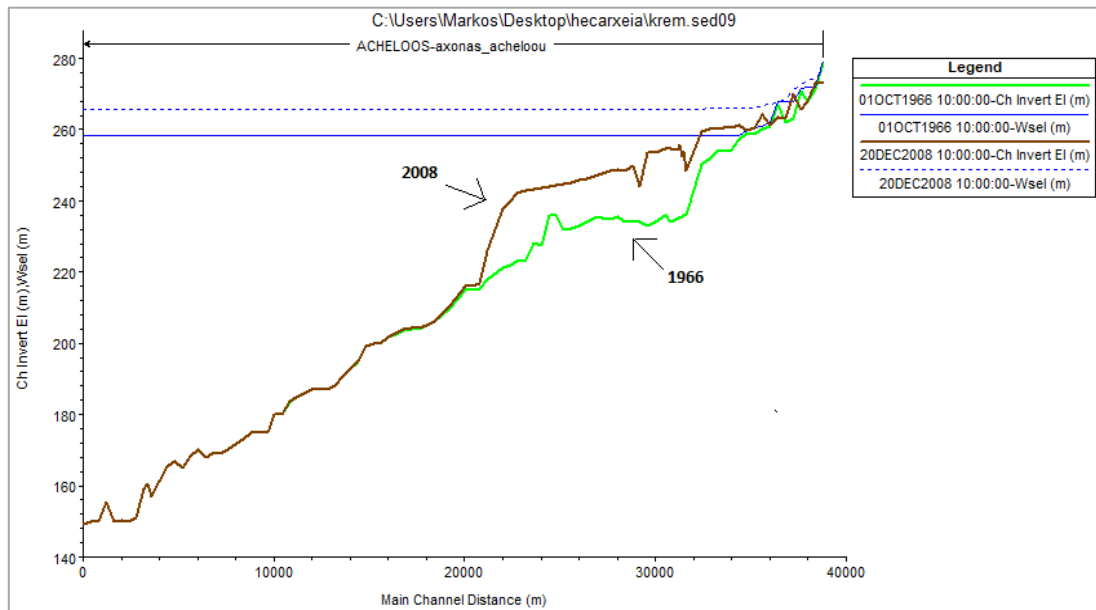


**Figure 6.1-2:** Changes in the longitudinal profile of Acheloos river after 42 years of simulation (HEC-RAS 5.0.7)

Comparing Figures 6.1-1 and 6.1-2, there is an evident similarity between the theory and the results of the sediment transport modeling inside the reservoir pool. Figure 6.1-2 displays a deltaic depositional pattern which ends at the point where the cross sections get wider and deeper (roughly 18 km away from the upstream boundary at cross section 20.800 m). Due to the fact that delta deposition is focused in the shallow upstream reaches of reservoirs where the width tends to be the narrowest and storage volume is small, reservoir deltas can be problematic from the standpoint of upstream aggradation (U.S. Society on Dams, 2015). More specifically, the existence of large sediment volumes as deltaic deposits creates an uplift of the river water stage on the upstream.

Whereas delta deposits may contain both coarse and fine material, the bottomset beds are characteristically fine-grained. However, tributary inflows, reservoir drawdown, slope failures, and extreme floods can all deliver coarser material into zones where finer-grained material normally predominates, resulting in layering of deposits or localized variations in grain size. The bed load and coarse fraction of the suspended load are deposited first to form delta deposits, while fine sediments with lower settling velocities are transported deeper into the reservoir by either stratified or nonstratified flow.

Depositional patterns vary with differences in hydrologic conditions, sediment grain size, and reservoir geometry. In reservoirs with fluctuating water levels, previously deposited sediments may be extensively eroded and reworked by streamflow, failure of exposed slopes, and wave action. Most sediments are transported within reservoirs to points of deposition by three processes: (1) transport of coarse sediment as bed load along the delta surface or topset, (2) transport of fine sediment in turbid density currents, and (3) transport of fine sediment as nonstratified flow, closer to the dam (Morris and Fan, 1998· U.S. Society on Dams, 2015).

Moreover, below (Figure 6.1-3) is presented the change of a cross section -which is located at the reservoir delta at the branch of Acheloos river- throughout the period of simulation due to sediment deposition. There is an aggradation of nearly 15 (m) after 42 years.

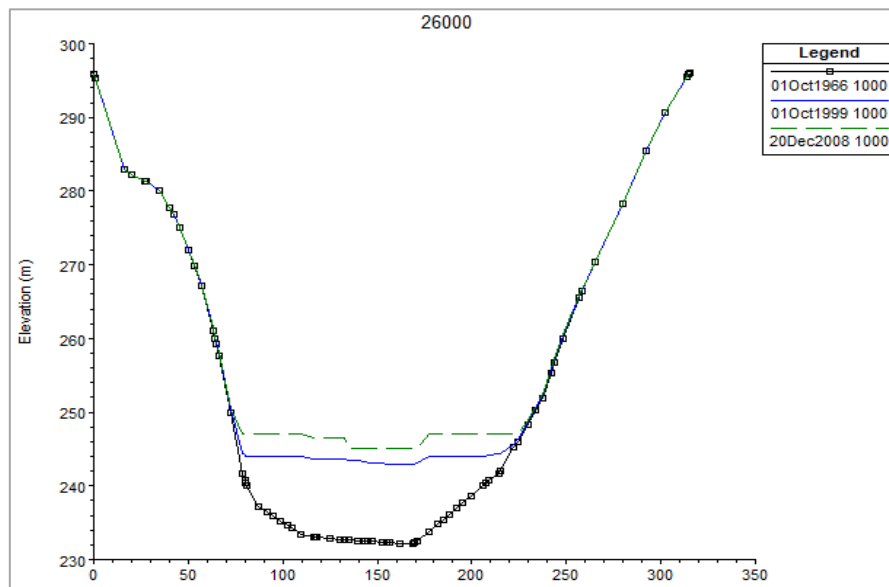


**Figure 6.1-3:** Cross section (26.000 m) change throughout the period of simulation due to deposition (HEC-RAS 5.0.7)

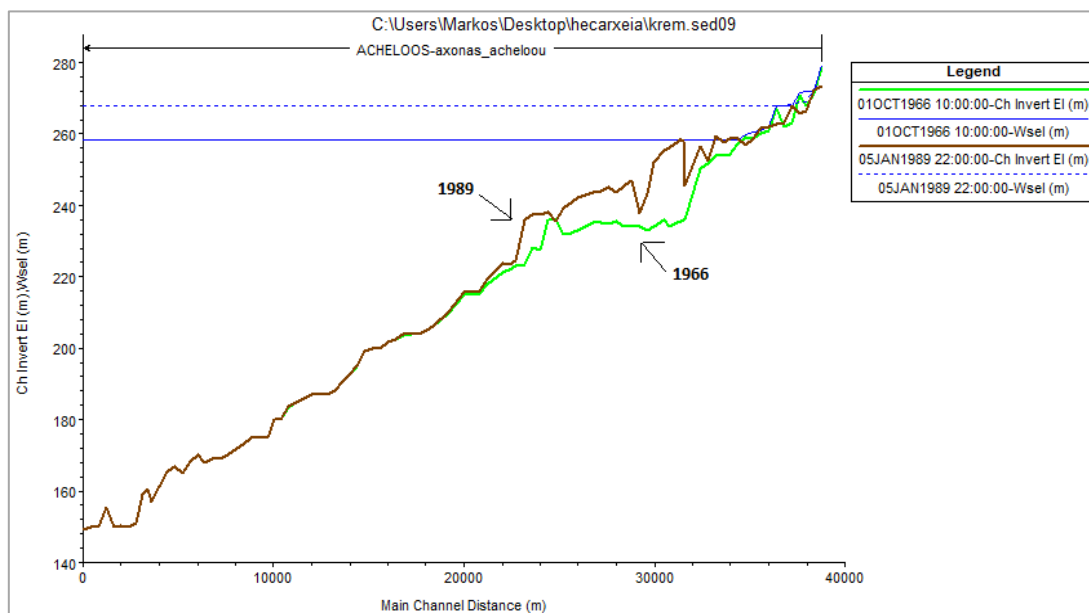


**Figure 6.1-4:** Changes in the longitudinal profile of Kremasta reservoir (Acheloos part) at an intermediate simulation moment (HEC-RAS 5.0.7)

Figure 6.1-4 exhibits an intermediate situation where the delta deposits have begun to form. While the deposits increase, the topset bed rises. With the ongoing sediment inflow throughout the years, the topset bed expands inside the reservoir of Kremasta and the slope of the frontset bed grows. The point of intersection between the topset and the frontset bed is created by the maximum annual decrease of the water stage elevation of the reservoir, and especially when this event coincides with the beginning

of the wet period (Zarris et al., 2001). Thus, the area of the expansion of the delta deposits depends on the amount of the river sediment yield, the material of the transported sediment, but also on the water stage variations when the wash load appears. Figure 6.1-5 below shows the evolution of the delta deposits at Kremasta reservoir (Acheloos part) which agrees with the deposition theory presented above.

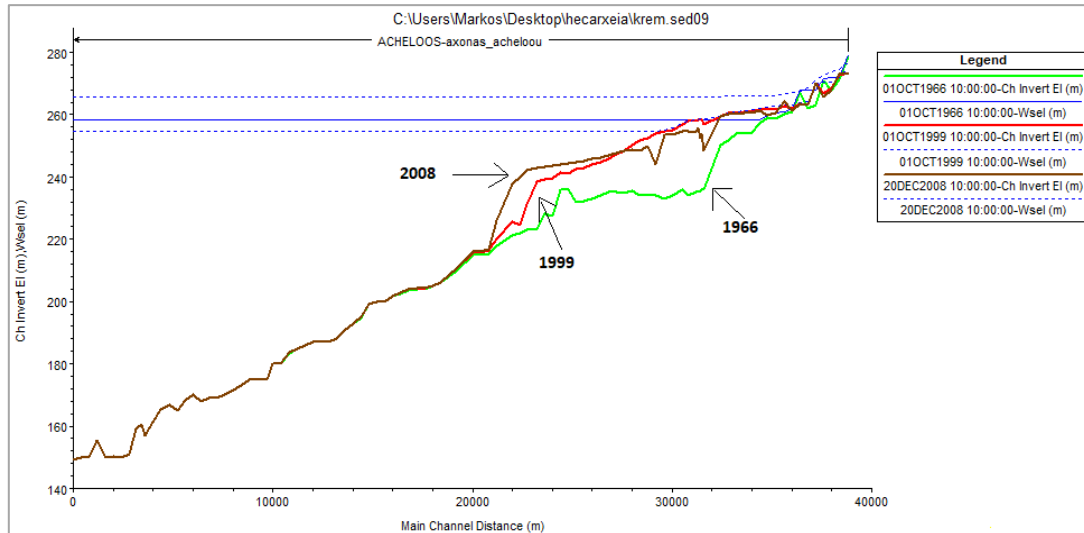


**Figure 6.1-5:** Evolution of the deposits at Kremasta reservoir (Acheloos part) from 1966 to 2008 (HEC-RAS 5.0.7)

## 6.2 Comparison with other studies

This chapter compares the results of the present study with these of Zarris et al. (2001, 2003, 2019). The study of Zarris et al. (2001) and hydrographic survey (Figure 6.2-1) identified the main areas of deposition in Kremasta reservoir pool, concluding that sediment mostly deposits at the reservoir deltas which confirms the validity of the output of the current simulation and the theoretical assumptions.

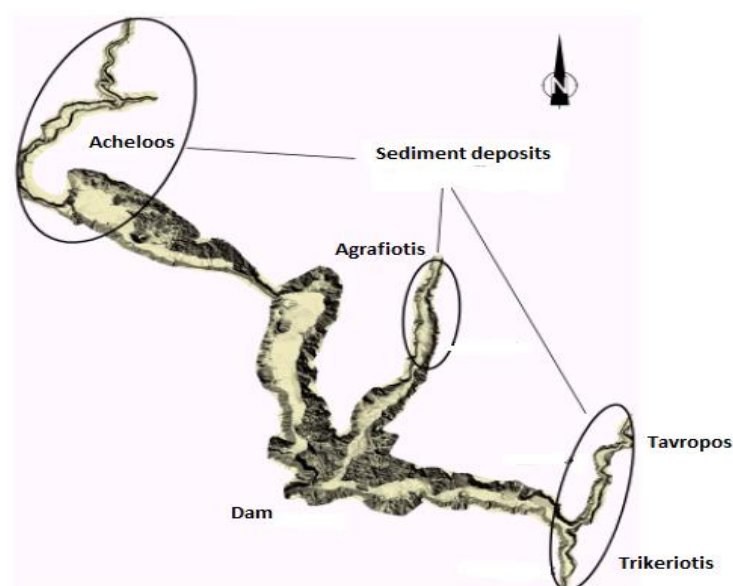


**Figure 6.2-1:** Spatial distribution of sediment deposits in Kremasta reservoir (Obtained by Zarris et al., 2001)

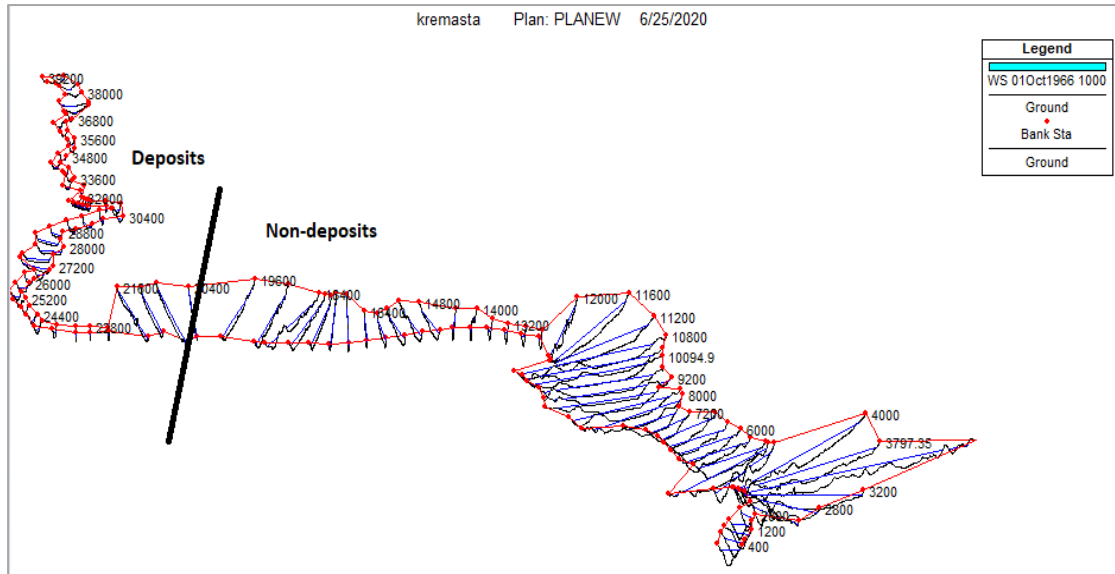


**Figure 6.2-2:** 3D Plot of the reservoir pool (Acheloos river branch) (HEC-RAS 5.0.7)

The Figure 6.2-2 above shows a 3D plot of the Acheloos river branch and the cross sections, using the command “X-Y-Z Perspective Plot” in HEC-RAS. As observed in Figure 6.2-3, the deposits are located at the reservoir deltas which enhances the results from HEC-RAS shown in Figure 6.2-2 for Acheloos river branch. Downstream of the black marked locations the deposits are insignificant, and some areas display a bed erosion.

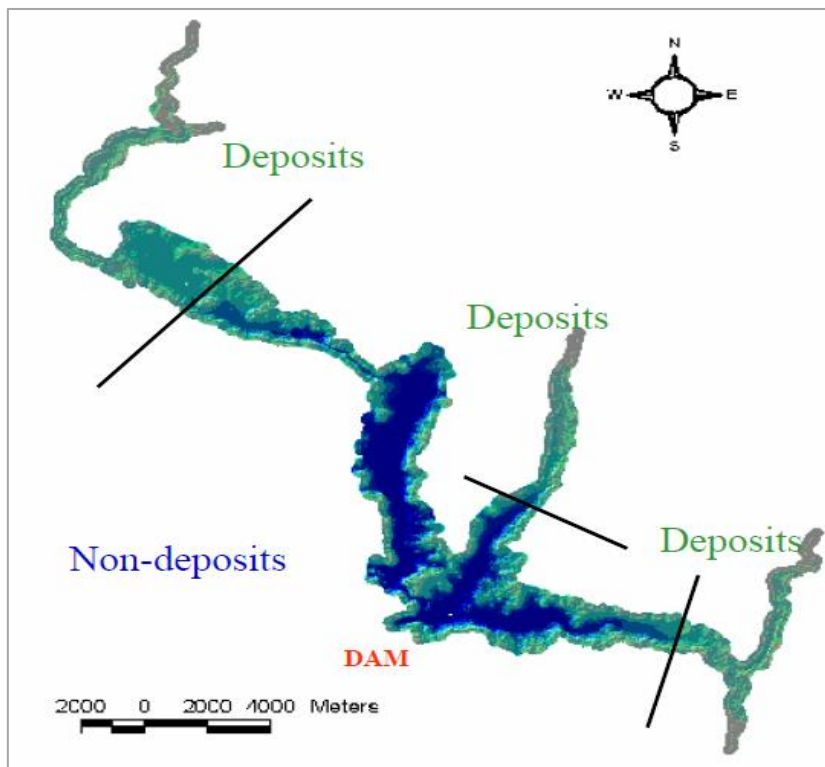


**Figure 6.2-3:** Locations of deposits occurred from Zarris et al. (2001) study (Obtained by Zarris et al., 2003)

Moreover, Zarris (2019) performed a hydrographic survey and cut cross sections across the reservoir pool to observe how the bed changed from 1966 to 1999 due to sediment deposition, similarly to the present study. Therefore, below (Figures 6.2-4 and 6.2-5) there is a comparison between the bed change calculations of the two studies for the cross section 22.400 (m) and there is an evident similarity between them.

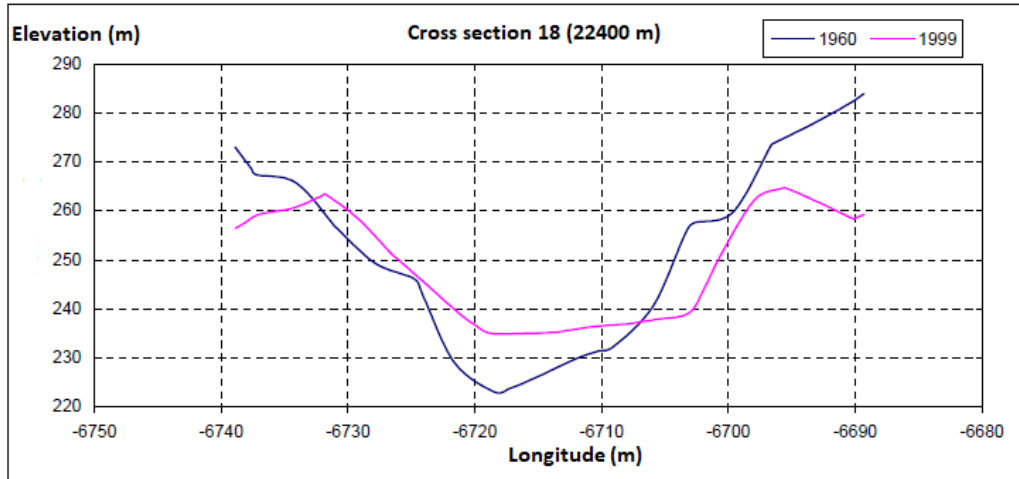


**Figure 6.2-4:** Bed changes in cross section +22400 (m) according to the Zarris study (Obtained by Zarris, 2019)

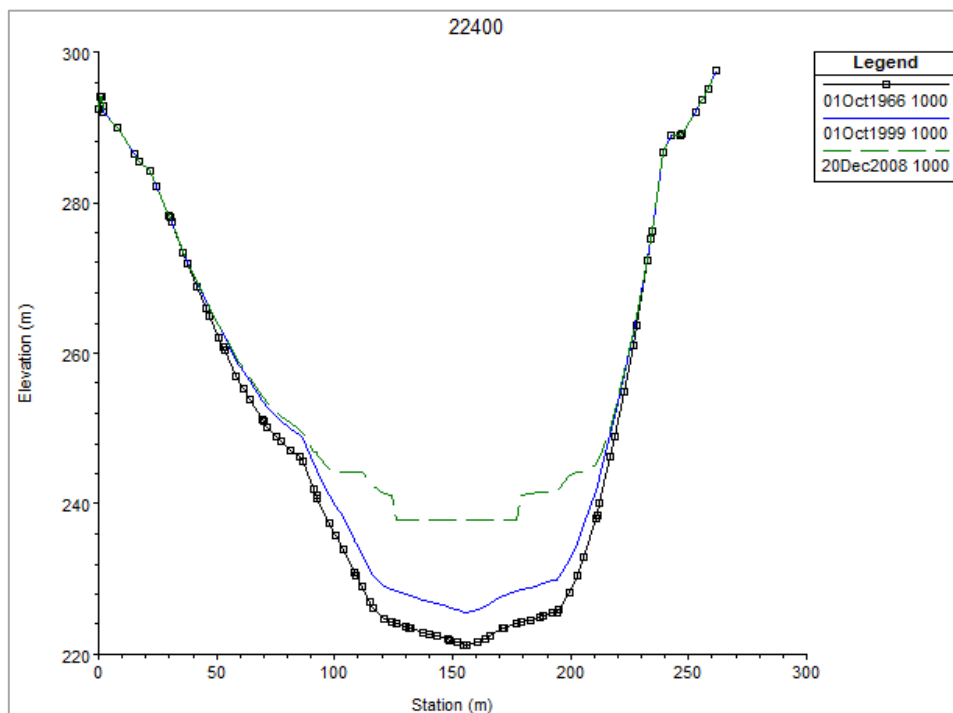


**Figure 6.2-5:** Bed changes in cross section +22400 (m) according to the present study (HEC-RAS 5.0.7)

As observed, Zarris (2019) study showed a maximum aggradation of roughly 12 (m), while the HEC-RAS simulation of the present study revealed a deposition of about 5 (m). In the next decade, the bed of the cross section (in HEC-RAS) uplifted to reach nearly 240 (m) elevation (15 m aggradation).

### 6.3 Hydrodynamic characteristics

The Table 6.3-1 below illustrates the hydrodynamic characteristics of the flow inside the reservoir pool for each cross section (River Station). This table is a snapshot of a specific intermediate moment of the simulation (31/05/2000). Another table, concerning the day with the highest inflow (a significant moment of the simulation), is presented in the Appendix of the present study.

**Table 6.3-1:** Hydrodynamic characteristics of the flow inside the reservoir on 31/05/ 2000 (HEC-RAS 5.0.7)

Reach	River Sta	Profile	Q Total (m3/s)	Min Ch El (m)	W.S. Elev (m)	Crit W.S. (m)	E.G. Elev (m)	E.G. Slope (m/m)	Vel Chnl (m/s)	Flow Area (m2)	Top Width (m)	Froude # Chl
axonas_acheloo	39200	31May2000 1000	22.30	273.43	274.61		274.69	0.001746	1.25	17.84	20.23	0.43
axonas_acheloo	38800	31May2000 1000	22.30	272.70	273.03	273.03	273.15	0.014659	1.52	14.66	63.15	1.01
axonas_acheloo	38400	31May2000 1000	22.30	268.67	270.61		270.63	0.000165	0.55	40.67	23.55	0.13
axonas_acheloo	38000	31May2000 1000	22.30	266.33	270.56		270.58	0.000090	0.56	39.67	11.99	0.10
axonas_acheloo	37600	31May2000 1000	22.30	270.15	270.35	270.35	270.45	0.015423	1.39	16.06	82.20	1.00
axonas_acheloo	37200	31May2000 1000	22.30	262.78	264.74		264.75	0.000143	0.55	40.36	22.76	0.13
axonas_acheloo	36800	31May2000 1000	22.30	263.42	264.27	264.27	264.54	0.011750	2.29	9.72	18.16	1.00
axonas_acheloo	36400	31May2000 1000	22.30	261.03	263.74		263.75	0.000070	0.44	50.66	21.83	0.09
axonas_acheloo	36000	31May2000 1000	22.30	263.16	263.53	263.53	263.64	0.015202	1.49	14.99	68.60	1.02
axonas_acheloo	35600	31May2000 1000	22.30	260.06	262.12		262.14	0.000238	0.72	30.93	16.38	0.17
axonas_acheloo	35200	31May2000 1000	22.30	259.93	262.05		262.07	0.000143	0.58	38.48	19.16	0.13
axonas_acheloo	34800	31May2000 1000	22.30	261.44	261.94		261.96	0.000688	0.55	40.84	82.17	0.25
axonas_acheloo	34400	31May2000 1000	22.30	260.63	261.65		261.69	0.000664	0.83	26.86	27.23	0.27
axonas_acheloo	34000	31May2000 1000	22.30	260.60	261.36		261.38	0.000885	0.58	38.65	86.61	0.28
axonas_acheloo	33600	31May2000 1000	22.30	260.22	261.07		261.10	0.000569	0.70	32.06	38.56	0.24
axonas_acheloo	33200	31May2000 1000	22.30	260.27	260.80		260.82	0.000809	0.62	35.98	67.42	0.27
axonas_acheloo	32800	31May2000 1000	22.30	259.26	259.78	259.78	259.98	0.012616	1.99	11.20	28.26	1.01
axonas_acheloo	32000	31May2000 1000	22.30	256.38	258.74		258.78	0.000385	0.92	24.12	11.94	0.21
axonas_acheloo	31900.0*	31May2000 1000	22.30	258.44	258.68		258.70	0.001805	0.55	40.78	169.58	0.36
axonas_acheloo	31800.0*	31May2000 1000	22.30	258.21	258.52		258.54	0.001442	0.58	38.78	126.16	0.33
axonas_acheloo	31700.0*	31May2000 1000	22.30	258.11	258.37		258.39	0.001533	0.53	41.87	160.19	0.33
axonas_acheloo	31600	31May2000 1000	22.30	257.54	258.25		258.28	0.000766	0.72	30.84	43.66	0.27
axonas_acheloo	31200	31May2000 1000	22.30	257.56	257.86		257.88	0.001363	0.55	40.72	136.83	0.32
axonas_acheloo	30934.19	31May2000 1000	22.30	257.15	257.43		257.45	0.001942	0.62	36.22	133.26	0.38
axonas_acheloo	30400	31May2000 1000	22.30	255.56	256.47		256.49	0.001664	0.64	34.82	107.31	0.36
axonas_acheloo	30000	31May2000 1000	22.30	255.27	255.56		255.58	0.003286	0.60	37.10	210.06	0.46
axonas_acheloo	29600	31May2000 1000	22.30	254.05	254.77		254.78	0.001343	0.48	46.72	191.12	0.31
axonas_acheloo	29200	31May2000 1000	22.30	253.74	254.17		254.18	0.001700	0.47	47.33	235.76	0.34
axonas_acheloo	28800	31May2000 1000	22.30	253.03	253.38		253.41	0.002167	0.76	29.18	84.35	0.41
axonas_acheloo	28400	31May2000 1000	22.30	251.66	251.76		251.79	0.010260	0.73	30.46	301.67	0.74
axonas_acheloo	28000	31May2000 1000	22.30	248.97	249.09		249.10	0.004719	0.51	43.67	414.72	0.50
axonas_acheloo	27600	31May2000 1000	22.30	247.11	247.26		247.27	0.004436	0.51	43.86	400.10	0.49
axonas_acheloo	27200	31May2000 1000	22.30	246.19	246.35		246.35	0.001398	0.32	68.72	517.26	0.28
axonas_acheloo	26800	31May2000 1000	22.30	245.42	245.95		245.96	0.000710	0.49	45.17	108.95	0.24

Reach	River Sta	Profile	Q Total (m3/s)	Min Ch El (m)	W.S. Elev (m)	Crit W.S. (m)	E.G. Elev (m)	E.G. Slope (m/m)	Vel Chnl (m/s)	Flow Area (m2)	Top Width (m)	Froude # Chl
axonas_acheloo	26400	31May2000 1000	22.30	244.16	245.92		245.92	0.000039	0.18	123.55	152.67	0.06
axonas_acheloo	26000	31May2000 1000	22.30	243.01	245.92		245.92	0.000002	0.08	291.05	145.29	0.02
axonas_acheloo	25600	31May2000 1000	22.30	242.47	245.91		245.92	0.000001	0.07	297.41	109.74	0.01
axonas_acheloo	25200	31May2000 1000	22.30	240.87	245.91		245.91	0.000008	0.20	112.63	33.72	0.03
axonas_acheloo	24800	31May2000 1000	22.30	241.27	245.91		245.91	0.000004	0.15	153.05	44.60	0.03
axonas_acheloo	24400	31May2000 1000	22.30	239.42	245.91		245.91	0.000001	0.10	232.32	59.91	0.02
axonas_acheloo	24000	31May2000 1000	22.30	239.39	245.91		245.91	0.000000	0.06	403.81	89.74	0.01
axonas_acheloo	23600	31May2000 1000	22.30	238.57	245.91		245.91	0.000000	0.04	584.63	105.95	0.01
axonas_acheloo	23111.09	31May2000 1000	22.30	231.07	245.91		245.91	0.000000	0.02	933.50	98.71	0.00
axonas_acheloo	22800	31May2000 1000	22.30	224.48	245.91		245.91	0.000000	0.01	2015.70	127.85	0.00
axonas_acheloo	22400	31May2000 1000	22.30	225.65	245.91		245.91	0.000000	0.01	1792.11	123.63	0.00
axonas_acheloo	21600	31May2000 1000	22.30	220.04	245.91		245.91	0.000000	0.00	21648.69	1722.90	0.00
axonas_acheloo	21200	31May2000 1000	22.30	216.43	245.91		245.91	0.000000	0.00	42368.69	1819.97	0.00
axonas_acheloo	20800	31May2000 1000	22.30	215.84	245.91		245.91	0.000000	0.00	55764.46	2352.15	0.00
axonas_acheloo	20400	31May2000 1000	22.30	215.87	245.91		245.91	0.000000	0.00	52715.06	1981.74	0.00
axonas_acheloo	19600	31May2000 1000	22.30	210.40	245.91		245.91	0.000000	0.00	45845.05	1712.77	0.00
axonas_acheloo	18800	31May2000 1000	22.30	206.08	245.91		245.91	0.000000	0.00	38086.72	1693.87	0.00
axonas_acheloo	18400	31May2000 1000	22.30	205.10	245.91		245.91	0.000000	0.00	23760.38	1223.56	0.00
axonas_acheloo	18000	31May2000 1000	22.30	204.13	245.91		245.91	0.000000	0.00	44691.96	1750.19	0.00
axonas_acheloo	17600	31May2000 1000	22.30	204.11	245.91		245.91	0.000000	0.00	45566.60	1629.38	0.00

Reach	River Sta	Profile	Q Total (m <sup>3</sup> /s)	Min Ch El (m)	W.S. Elev (m)	Crit W.S. (m)	E.G. Elev (m)	E.G. Slope (m/m)	Vel Chnl (m/s)	Flow Area (m <sup>2</sup> )	Top Width (m)	Froude # Chl
axonas_acheloo	17200	31May2000 1000	22.30	203.83	245.91		245.91	0.000000	0.00	41689.90	1733.74	0.00
axonas_acheloo	16800	31May2000 1000	22.30	202.65	245.91		245.91	0.000000	0.00	28892.32	1227.58	0.00
axonas_acheloo	16400	31May2000 1000	22.30	201.71	245.91		245.91	0.000000	0.00	26035.22	1030.77	0.00
axonas_acheloo	16000	31May2000 1000	22.30	200.06	245.91		245.91	0.000000	0.00	32911.82	900.18	0.00
axonas_acheloo	15600	31May2000 1000	22.30	200.04	245.91		245.91	0.000000	0.00	27870.29	964.16	0.00
axonas_acheloo	15200	31May2000 1000	22.30	199.08	245.91		245.91	0.000000	0.00	25586.55	863.89	0.00
axonas_acheloo	14800	31May2000 1000	22.30	194.97	245.91		245.91	0.000000	0.00	29470.00	893.30	0.00
axonas_acheloo	14400	31May2000 1000	22.30	193.02	245.91		245.91	0.000000	0.00	20997.00	667.25	0.00
axonas_acheloo	14000	31May2000 1000	22.30	190.85	245.91		245.91	0.000000	0.00	5232.38	160.78	0.00
axonas_acheloo	13600	31May2000 1000	22.30	188.00	245.91		245.91	0.000000	0.00	9141.98	241.29	0.00
axonas_acheloo	13200	31May2000 1000	22.30	187.12	245.91		245.91	0.000000	0.00	6145.40	178.51	0.00
axonas_acheloo	12800	31May2000 1000	22.30	187.00	245.91		245.91	0.000000	0.00	6437.88	172.85	0.00
axonas_acheloo	12400	31May2000 1000	22.30	187.01	245.91		245.91	0.000000	0.00	6694.77	164.14	0.00
axonas_acheloo	12000	31May2000 1000	22.30	185.96	245.91		245.91	0.000000	0.00	46623.64	1697.37	0.00
axonas_acheloo	11600	31May2000 1000	22.30	184.92	245.91		245.91	0.000000	0.00	28341.40	3024.98	0.00
axonas_acheloo	11200	31May2000 1000	22.30	183.61	245.91		245.91	0.000000	0.00	23676.80	2580.68	0.00
axonas_acheloo	10800	31May2000 1000	22.30	180.04	245.91		245.91	0.000000	0.00	22017.00	2992.58	0.00
axonas_acheloo	10400	31May2000 1000	22.30	180.03	245.91		245.91	0.000000	0.00	05209.10	2323.80	0.00
axonas_acheloo	10094.9	31May2000 1000	22.30	175.03	245.91		245.91	0.000000	0.00	21006.40	2534.16	0.00
axonas_acheloo	9600	31May2000 1000	22.30	174.85	245.91		245.91	0.000000	0.00	17720.20	2257.66	0.00
axonas_acheloo	9200	31May2000 1000	22.30	174.87	245.91		245.91	0.000000	0.00	03860.70	1971.99	0.00
axonas_acheloo	8800	31May2000 1000	22.30	173.05	245.91		245.91	0.000000	0.00	01685.90	2022.62	0.00
axonas_acheloo	8400	31May2000 1000	22.30	171.46	245.91		245.91	0.000000	0.00	99511.71	1986.34	0.00
axonas_acheloo	8000	31May2000 1000	22.30	170.00	245.91		245.91	0.000000	0.00	02565.90	2154.07	0.00
axonas_acheloo	7600	31May2000 1000	22.30	169.00	245.91		245.91	0.000000	0.00	68660.45	1168.39	0.00
axonas_acheloo	7200	31May2000 1000	22.30	169.00	245.91		245.91	0.000000	0.00	52705.36	932.81	0.00
axonas_acheloo	6800	31May2000 1000	22.30	168.00	245.91		245.91	0.000000	0.00	71477.81	1285.62	0.00
axonas_acheloo	6400	31May2000 1000	22.30	170.00	245.91		245.91	0.000000	0.00	63749.22	1226.32	0.00
axonas_acheloo	6000	31May2000 1000	22.30	168.12	245.91		245.91	0.000000	0.00	71164.55	1297.81	0.00
axonas_acheloo	5600	31May2000 1000	22.30	164.91	245.91		245.91	0.000000	0.00	57900.14	1388.37	0.00
axonas_acheloo	5200	31May2000 1000	22.30	166.72	245.91		245.91	0.000000	0.00	84943.30	1505.22	0.00
axonas_acheloo	4800	31May2000 1000	22.30	165.19	245.91		245.91	0.000000	0.00	022614.20	2394.07	0.00
axonas_acheloo	4400	31May2000 1000	22.30	161.16	245.91		245.91	0.000000	0.00	66495.08	1612.19	0.00
axonas_acheloo	4000	31May2000 1000	22.30	157.08	245.91		245.91	0.000000	0.00	45868.30	3522.85	0.00
axonas_acheloo	3797.35	31May2000 1000	38.30	160.70	245.91		245.91	0.000000	0.00	36858.20	3298.95	0.00
axonas_acheloo	3547.46	31May2000 1000	38.30	159.19	245.91		245.91	0.000000	0.00	98328.90	4793.71	0.00
axonas_acheloo	3200	31May2000 1000	38.30	151.00	245.91		245.91	0.000000	0.00	38278.00	2430.24	0.00
axonas_acheloo	2800	31May2000 1000	38.30	150.00	245.91		245.91	0.000000	0.00	67445.73	1272.56	0.00
axonas_acheloo	2400	31May2000 1000	38.30	150.17	245.91		245.91	0.000000	0.00	19757.82	351.31	0.00
axonas_acheloo	2000	31May2000 1000	38.30	150.00	245.91		245.91	0.000000	0.00	16446.20	314.17	0.00
axonas_acheloo	1600	31May2000 1000	38.30	155.37	245.91		245.91	0.000000	0.00	14956.73	323.99	0.00
axonas_acheloo	1200	31May2000 1000	38.30	149.94	245.91		245.91	0.000000	0.00	20898.11	365.02	0.00
axonas_acheloo	800	31May2000 1000	38.30	150.00	245.91		245.91	0.000000	0.00	21967.43	416.40	0.00
axonas_acheloo	400	31May2000 1000	38.30	149.10	245.91	150.06	245.91	0.000000	0.00	19211.79	366.63	0.00

The table indicates the total flow (Q in m<sup>3</sup>/s), the minimum channel and water stage elevations (Min Ch El and W.S. Elev in meters), the flow velocities (Vel Chnl in m/s), the flow area (m<sup>2</sup>), the top width (m), the critical depth (Crit W.S. in meters) and the Froude number for each cross section.

As observed, the flow velocities are generally low due to the slow movement of the water inside the reservoir pool, and they decrease approaching the dam, where the reservoir pool is wider and deeper. More specifically, the width of the reservoir is increasing dramatically after the cross section 21.600 (m) where the flow velocities approach zero. The water stage on the 31<sup>st</sup> of May 2000 was 245,91 (m). It is remarkable that five cross sections (38.800 m, 37.600 m, 36.800 m, 36.000 m, 32.800 m) have a Froude number which is 1 or higher and the flow is characterized as critical / almost supercritical. Therefore, in those five river stations, the water stage elevation is equal to the critical depth (m). The wider and deeper parts of the reservoir pool display a Froude number close to zero due to low flow velocities which shows that there is no water movement in these areas.

Another way (a more detailed one) to view the hydrodynamic results of the model is by using the “View detailed output” button which creates the Table 6.3-2 below that presents some other hydrodynamic characteristics at a specific moment and place.

**Table 6.3-2: Other hydrodynamic characteristics (HEC-RAS 5.0.7)**

Cross Section Output					
File Type Options Help					
River:	ACHELOOS	Profile:	01Oct1966 1000		
Reach	axonas_achelouo	RS:	36400	Plan:	krem
Plan: krem ACHELOOS axonas_achelouo RS: 36400 Profile: 01Oct1966 1000					
E.G. Elev (m)	262.40	Element	Left OB	Channel	Right OB
Vel Head (m)	0.18	Wt. n-Val.		0.030	
W.S. Elev (m)	262.22	Reach Len. (m)	400.00	400.00	400.00
Crit W.S. (m)	262.17	Flow Area (m2)		9.17	
E.G. Slope (m/m)	0.008555	Area (m2)		9.17	
Q Total (m3/s)	17.10	Flow (m3/s)		17.10	
Top Width (m)	19.35	Top Width (m)		19.35	
Vel Total (m/s)	1.87	Avg. Vel. (m/s)		1.87	
Max Chl Dpth (m)	0.92	Hydr. Depth (m)		0.47	
Conv. Total (m3/s)	184.9	Conv. (m3/s)		184.9	
Length Wtd. (m)	400.00	Wetted Per. (m)		19.48	
Min Ch El (m)	261.30	Shear (N/m2)		39.48	
Alpha	1.00	Stream Power (N/m s)		73.63	
Frctn Loss (m)	1.52	Cum Volume (1000 m3)		1764062.00	
C & E Loss (m)	0.04	Cum SA (1000 m2)		39469.68	

More specifically, it presents the friction and C&E losses (m), the hydraulic depth (m), the wetted perimeter (m), the shear ( $N/m^2$ ), the stream power ( $N/m \cdot s$ ) and the cumulative volume ( $1000 m^3$ ) and storage area ( $1000 m^2$ ) for each cross section.

## 6.4 Final Conclusions

- The RUSLE, GIS and Koutsoyiannis & Tarla (1987) methods consist of a series of empirical equations and in combination with Vanoni (1975) empirical formula, the results have a critical discrepancy among them and in comparison, with the hydrographic survey. Moreover, the uncertainty and difficulty to predict the response of each soil type, land use and soil loss protection technique to extreme climate phenomena leads to an underestimation of the sediment yield. This also happens due to the wide variety in the values attributed to C-factor for every land use and also the overestimation of R-factor in the analytical application of RUSLE, due to lack of long-term precipitation data.
- The rating curves methodology, used to estimate the sediment yield, proved to be a reliable tool considering that it concluded on 1110,2 (t/km<sup>2</sup>), while Zarris (2019) measured a 1005,6 (t/km<sup>2</sup>) value of mean annual sediment yield.
- The sediment deposition rate (dead volume) occurred from the present study and specifically the rating curves method (292,4 hm<sup>3</sup>) is significantly lower than the prediction of the initial study (784 hm<sup>3</sup>). Moreover, Zarris et al. (2001) predicted a value of 264,8 (hm<sup>3</sup>) for the 100-year dead sediment volume. This indicates that the initial study overestimated the dead sediment volume and probably some of the technical elements of the dam.
- The reservoir exhibits one of the highest values of sediment yield worldwide. This is mainly due to hydrological parameters (e.g. intense storms) and the dominant geological formation (e.g. highly erodible flysch) of the watershed.
- HEC-RAS sediment transport simulation reveals that some of the first narrow cross sections have a Froude Number slightly higher than 1. This means that the flow is critical or supercritical with high flow velocities. As the reservoir pool gets wider and deeper, the flow velocities decrease dramatically and fall roughly to 0.
- The simulation also indicates that the sediment deposition is mainly located at the river deltas and is close to zero in the main reservoir pool of Kremasta. This was expected because of the significant length and width of the reservoir and the four rivers that end up in it. Such conclusion regarding the spatial accumulation of the sediment agrees with the hydrographic survey and study of Zarris et al. (2001) that shows no deposition inside the reservoir. This also means that the reservoir has a sediment retention capacity close to 100%.
- At the point where the deltaic depositional pattern ends (roughly 18 km away from the upstream boundary), the flow velocities decrease, and the reservoir is not capable to carry the coarse sediment further downstream. Only, the finer sediment is transported by density currents to the downstream near the dam.
- After the 42-year sediment modeling of the reservoir, the theoretical dead volume of the reservoir remains empty while a part of the net storage is filled with sediment. Hence, dead volume principles, at least for large reservoirs, should be reconsidered in terms of spatial accumulation, because this affects the water abstraction elevation and the hydroelectric station.
- The existence of large sediment volumes as deltaic deposits creates an uplift of the river water stage which could increase the possibility of flood on the upstream areas during an intense storm episode.

## 6.5 Proposals for further research

- Firstly, it should be pointed out that there are several techniques such as cover management and support techniques of the land (e.g. cultivation patterns) which could help **reduce the soil loss** of the watershed of Kremasta that actually has a surprisingly high value.
- In order to minimize the uncertainties introduced by the empirical models that calculate the sediment yield, results should be enhanced by **future field measurements** (hydrometeorological data, stage level, flow velocity and water discharge, suspended and bedded sediment yield, aggregate grading analysis) and hydrographic surveys in order to propose a sustainable sediment management plan of Kremasta dam.
- The predicted 100-year dead Sv of 784 (hm<sup>3</sup>) accounts roughly for 17% of the storage capacity of the reservoir. However, the hydrographic survey of Zarris (2019) showed that in 35 years only 66 (hm<sup>3</sup>) of sediment deposited. This indicates the difficulty to predict sediment transport and emphasizes the necessity to reconsider the methods to **estimate the dead sediment volume**.
- The present study revealed that in large reservoirs, delta deposits predominate - it was not clear in the past- and therefore a change in strategy regarding the **design of the reservoir**, which affects the water abstraction and the inactive storage of the dam, should be applied so that future projects are more sustainable in monetary and environmental terms.
- A further research project could involve the performance of a **sediment transport analysis for the whole reservoir** and not just for Acheloos part, so that a comparison between the rivers' capability to carry sediment inside the reservoir will be held.
- Another proposal would be to **restart the sediment discharge measurements** in the four rivers of the area in order to reconsider the flow-sediment load rating curves using a bigger dataset.
- Considering that the present study predicted that 6% of the storage capacity of Kremasta reservoir will be covered with sediment by 2066, **dredging works or sediment abstraction** might be needed to free some of the capacity.

## References

- 1) Cooper, K. (2011). Evaluation of the relationship between the RUSLE R-Factor and mean annual precipitation.
- 2) Dedousis, S. (1999). Hydraulic calculations using HEC-RAS program. 2.2 Edition. (in Greek)
- 3) Efstratiadis, A., Michas, S., and Dermatas, D. (2015). Lecture 12 (Part B): Outlet flow and sediment management, Department of Water Resources and Environmental Engineering, National Technical University of Athens. (in Greek)
- 4) Efthimiou, N. (2020). The new assessment of soil erodibility in Greece, Faculty of Environmental Sciences, Czech University of Life Sciences Prague.
- 5) Gibson, S., Sanchez, A., Piper, S., and Brunner, G. New One – Dimensional Sediment Features in HEC-RAS 5.0 and 5.1. Hydrologic Engineering Center, Institute for Water Resources, U.S. Army Corps of Engineers, May 2017.
- 6) Kalfountzos, K. (2013). Geological research at the area of Alevrada and Kremasta hydroelectric station, Thesis Project, School of Geology, University of Patras, Patra, Greece. (in Greek)
- 7) Koutsoyiannis, D., and Tarla, K. (1987). Sediment yield estimations in Greece, pp. 127-154. (in Greek)
- 8) Lambrakis, N., Stournaras, G., and Katsanou, K. (2011). Advances in the Research of Aquatic Environment: Volume 2. Environmental Earth Sciences.
- 9) Michas, K., Nikolaou, K., Koukouvinos, A., and Mamassis, M. Estimation of sediment yield with MUSLE and monitoring. A case study for Tsiknias dam at Lesbos Island in Greece, Paper.
- 10) Mitasova, H., and Mitas, L. (2001). Modelling Physical Systems, In: Geographic Information Systems and Environmental Modelling, Parks B., Crane M. and Clarke, K eds., Prentice Hall.
- 11) Moore, I.D., and Burch, G.J. (1986). Physical basis of the length slope factor in the Universal Soil Loss Equation. Soil Science Society of America, 50, pp. 1294-1298.
- 12) Morris, G., and Fan, J. (1998). Reservoir Sedimentation Handbook, McGraw-Hill Book Co., New York, U.S.A.
- 13) Oikonomou, A. (2013). Investigation of the operation of hydraulic simulation software in the evolution of a flood event, Thesis Project, Interdepartmental Program of Postgraduate Studies: “Water Resources Science and Technology”, National Technical University of Athens. (in Greek)
- 14) Panagos, P., Borrelli, P., Meusburger, K., Van der Zanden, E., Poesen, J., and Alewell, C. (2015). Modelling the effect of support practices (P-factor) on the reduction of soil erosion by water at European scale.
- 15) Panagos, P., Meusburger, K., Alewell, C., and Montanarella, L. (2012). Soil erodibility estimation using LUCAS point survey data of Europe, Environmental Modelling & Software, Volume 30.
- 16) Panagos, P., Meusburger, K., Ballabio, C., Borrelli, P., and Alewell, C. (2014). Soil erodibility in Europe: A high-resolution dataset based on LUCAS, Science of the Total Environment, Volumes 479-480.
- 17) Papapetrou, M. (2017). Estimation of the soil erosion and the sediment discharge in Greece, Thesis Project, Interdepartmental Program of Postgraduate Studies:

- “Water Resources Science and Technology”, National Technical University of Athens. (in Greek)
- 18) Paresidou, A., and Plitsi, D. (2005). Mathematical simulation of flow in river using HEC-RAS program, Thesis Project, School of Civil Engineering, University of Thessalia, Volos, Greece. (in Greek)
  - 19) Renard, K.G., Foster, G.R., Weessies, G.A, and McCool, D.K. (1997). Predicting soil erosion by water: a guide to conservation planning with the Revised Universal Soil Loss Equation (RUSLE), U.S. Department of Agriculture, Agriculture Handbook 703.
  - 20) Renard, K.G., and Freimund, J.R. (1994). Using Monthly Precipitation Data to Estimate the R-Factor in the Revised USLE, *Journal of Hydrology*, 157, pp. 287-306.
  - 21) Römken, M., Young, R., Poesen, J., McCool, D.K., El-Swaify, M., and Bradford, J. (1986). Soil erodibility factor (K).
  - 22) United States Society on Dams (2015). Modeling Sediment Movement in Reservoirs, USSD Committee on Hydraulics of Dams, Subcommittee on Reservoir Sedimentation, Denver, USA.
  - 23) USACE, (2015). HEC-RAS River Analysis System, Version 5.0, Hydrologic Engineering Center User Manual. U.S. Army Corps of Engineers.
  - 24) Vachaviolos, T. (2014). Estimation of the soil erosion, the sediment yield and the reservoir deposition using empirical methods, Thesis Project, Interdepartmental Program of Postgraduate Studies: “Water Resources Science and Technology”, National Technical University of Athens. (in Greek)
  - 25) Van der Knijff, J.M., R.J.A. Jones, and Montanarella, L. (2000a). Soil erosion risk assessment in Europe, JRC Scientific and Technical Report - EUR 19022 EN, European Soil Bureau, European Commission.
  - 26) Van der Knijff, J.M., R.J.A. Jones, and Montanarella, L. (2000b). Soil erosion risk assessment in Italy, JRC Scientific and Technical Report - EUR 19044 EN, European Soil Bureau, European Commission.
  - 27) Vanoni, V.A. (1975). Sedimentation Engineering Practice, American Society of Civil Engineers, Manuals and Reports on Engineering Practice, No. 54, pp. 745.
  - 28) Wischmeier, W.H., and Smith, D.D. (1978). Predicting rainfall erosion losses - a guide to conservation planning, U.S. Department of Agriculture, Agriculture Handbook No. 537.
  - 29) Zarris, D., Lykoudi, E., and Koutsoyiannis, D. Final Report, Investigation of sediment deposition in hydroelectric reservoirs, Department of Water Resources and Environmental Engineering, National Technical University of Athens, October 2001. (in Greek)
  - 30) Zarris, D., Lykoudi, E., and Koutsoyiannis, D. Sediment yield estimation from a hydrographic survey: A case study for the Kremasta reservoir, Western Greece, Proceedings of the 5th International Conference of European Water Resources Association: “Water Resources Management in the Era of Transition”, Athens, Greece, September 2002.
  - 31) Zarris, D., Lykoudi, E., Koutsoyiannis, D., and Poulos, S.E. Channel change and sediment movement after a major level drawdown at Kremasta reservoir, Western Greece, EGS – AGU – EUG Joint Assembly, Nice, France, April 2003.

- 32) Zarris, D. (2019). Investigation of sediment deposition in hydroelectric reservoirs, PhD thesis, Department of Water Resources and Environmental Engineering, National Technical University of Athens. (in Greek)
- 33) <http://www.hydroscope.gr/>
- 34) <https://www.google.com/earth/>
- 35) <http://filotis.itia.ntua.gr/>
- 36) <http://geodata.gov.gr/>
- 37) <https://esdac.jrc.ec.europa.eu/>
- 38) <http://lakesnetwork.org/>
- 39) <https://www.naturagraeca.com/ws/>
- 40) <https://www.limnikremaston.gr/>
- 41) <https://www.agriniopress.gr/>

## Appendix

**Table A.1:** Field measurements of flow and sediment load at Kremasta area  
(Obtained by Zarris, 2019)

Date	Flow (m <sup>3</sup> /s)	Sediment Flow (kg/s)
22/1/1964	85	7.92
23/1/1964	88	11.75
24/1/1964	85	6.79
25/1/1964	80	6.72
26/1/1964	79	8.45
27/1/1964	76	9.56
29/1/1964	70	6.78
30/1/1964	73	10.37
31/1/1964	86	38.19
1/2/1964	101	25.46
2/2/1964	101	33.80
15/2/1964	800	3460.65
16/2/1964	352	581.02
17/2/1964	205	190.39
28/2/1964	230	274.31
1/3/1964	775	806.71
2/3/1964	1780	12094.91
3/3/1964	1150	6585.65

**Table A.2:** Field measurements of flow and sediment load at Mesochora area  
(Obtained by Zarris, 2019)

Date	Flow (m <sup>3</sup> /s)	Sediment Flow (kg/s)
12/12/69	50.08	2.82
12/17/69	55.95	2.95
4/10/70	51.3	3.41
4/13/70	79.97	10.17
2/7/72	18.25	0.54
2/14/72	42.52	1.11
2/24/72	42.49	2.94
5/3/72	36.61	2.36
6/7/72	11.88	0.42
6/14/72	9.3	0.28
2/24/73	25.66	0.78
2/26/73	34.55	1.25

**Table A.3:** Field measurements of flow and sediment load at Avlaki area  
(Obtained by Zarris, 2019)

Date	Flow (m <sup>3</sup> /s)	Sediment Flow (kg/s)
11/7/66	110.9	88.09
6/3/67	37.67	1.15
6/16/67	26.57	8.86
6/4/68	117.32	82.83
6/15/68	31.26	3.09
1/25/67	80.42	19.32
3/24/67	44.79	2.19
3/28/67	46.27	1.56
4/8/67	41.34	1.34
4/12/67	78.66	8.08
4/17/67	113.05	31.53
4/20/67	88.97	16.41
5/24/67	67.07	6.29
3/27/68	82.86	5.58
4/4/68	109.34	14.83
5/9/68	59.71	1.92
5/29/68	46.59	2.9
1/13/69	49.35	4.51
1/17/69	162.18	72.09
1/20/69	86.13	13.59
1/24/69	50.16	5.17
4/24/69	141.27	71.8
4/29/69	108.43	21.39
12/17/69	196.24	93.23
1/26/70	67.83	3.4
1/27/70	62.42	2.1
4/13/70	147.43	46.26
4/15/70	98.98	95.15
12/2/70	24.32	2
12/7/70	18.05	1.17
9/22/76	6.2	0.14
4/12/83	65.15	1.28

**Table A.4:** Field measurements of flow and sediment load at Megdovas area  
(Obtained by Zarris, 2019)

Date	Flow (m <sup>3</sup> /s)	Sediment Flow (kg/s)
7/11/2000	14.1	0.36
12/12/2000	11.48	0.06
16/1/2001	31.66	0.05
6/2/2001	61.97	0.15
6/3/2001	103.3	0.57
3/4/2001	28.62	0.03

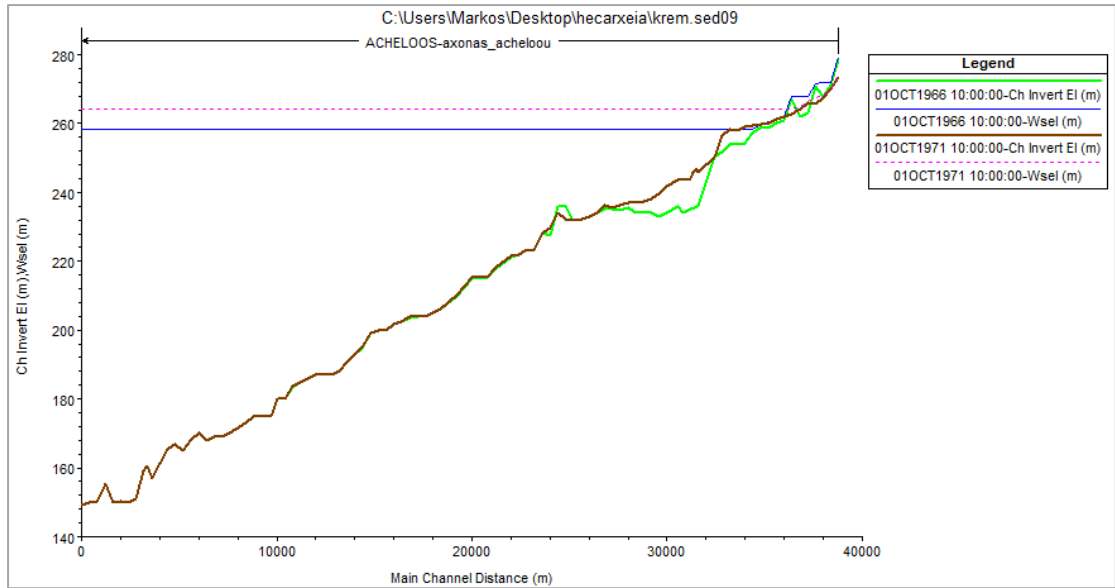


**Figure A.1:** Evolution of the deposits at Kremasta reservoir (Achelous part) from 1966 to 1971 (HEC-RAS 5.0.7)

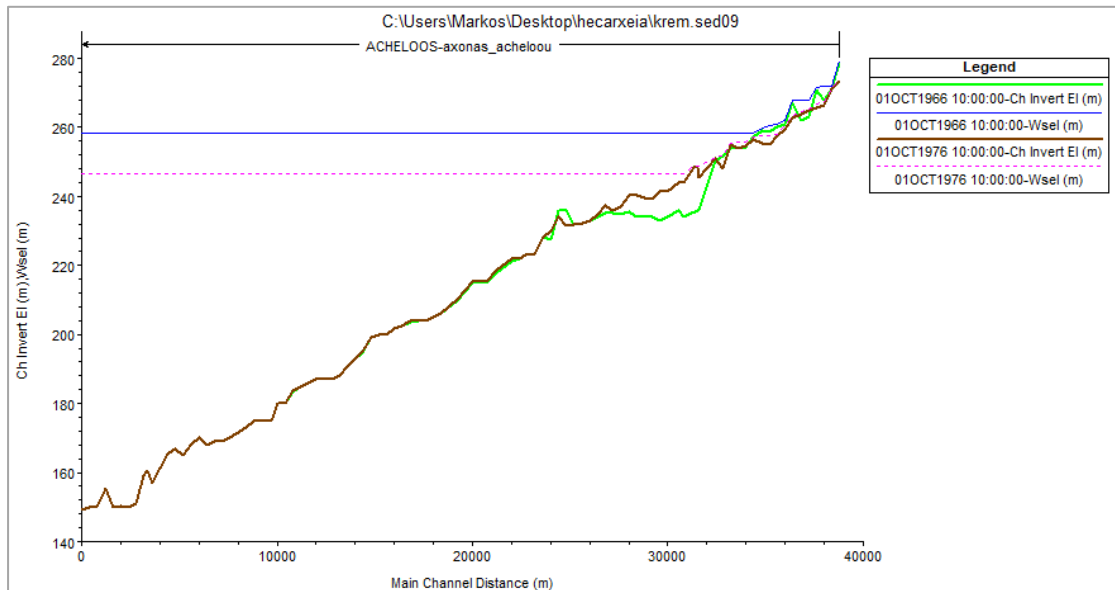


**Figure A.2:** Evolution of the deposits at Kremasta reservoir (Achelous part) from 1966 to 1976 (HEC-RAS 5.0.7)

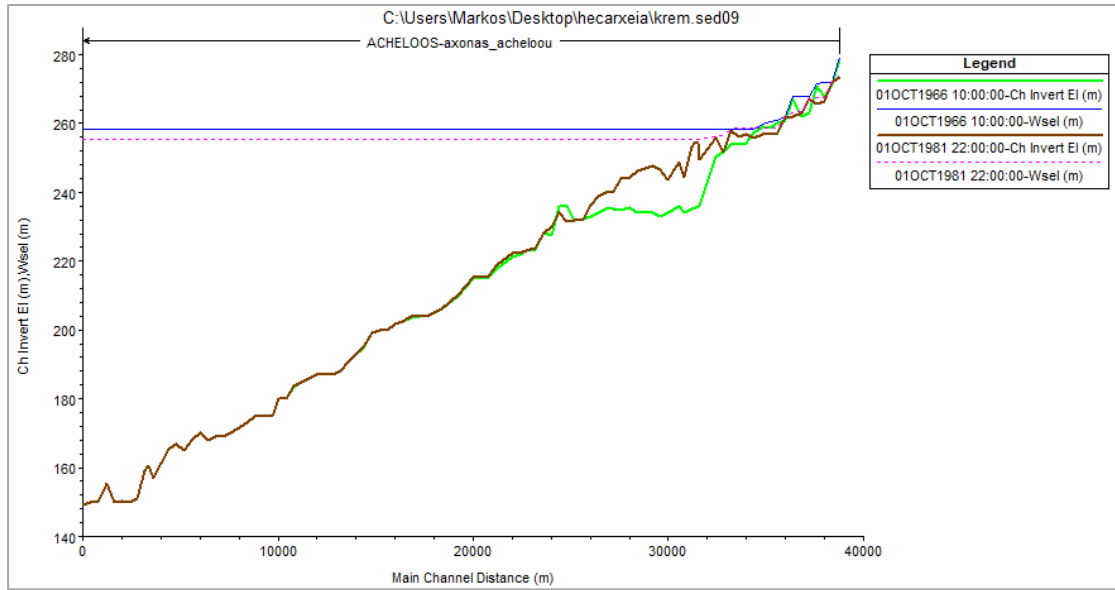


**Figure A.3:** Evolution of the deposits at Kremasta reservoir (Acheloo part) from 1966 to 1981 (HEC-RAS 5.0.7)

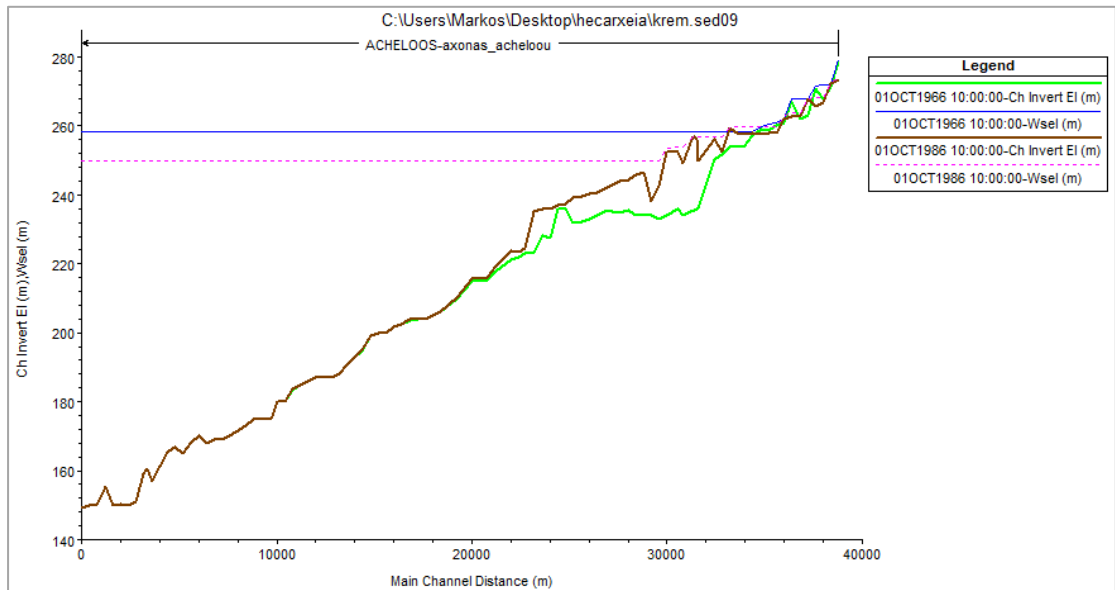


**Figure A.4:** Evolution of the deposits at Kremasta reservoir (Acheloo part) from 1966 to 1986 (HEC-RAS 5.0.7)

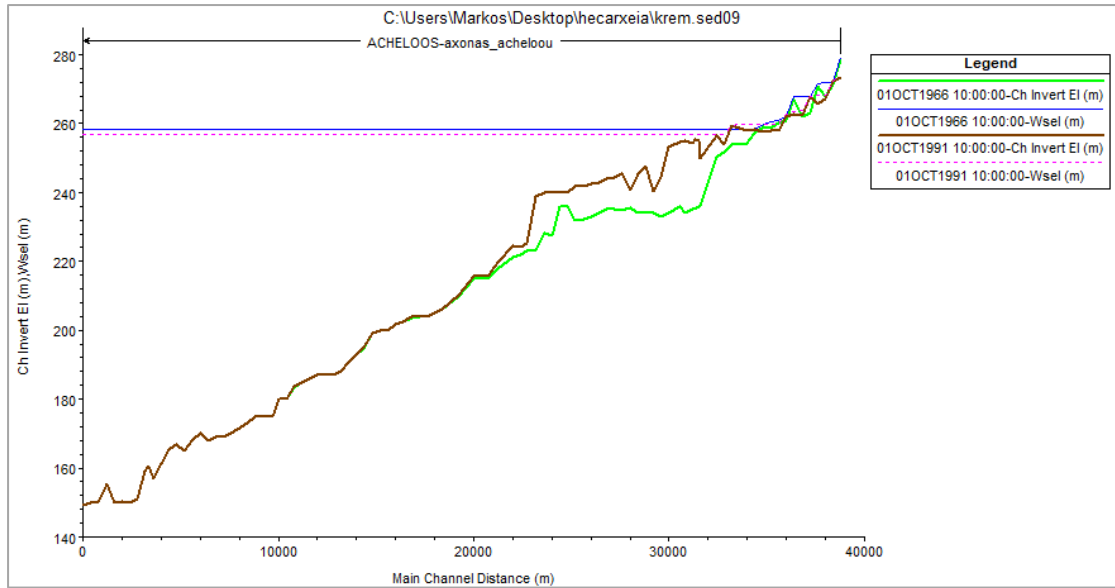


**Figure A.5:** Evolution of the deposits at Kremasta reservoir (Acheloo part) from 1966 to 1991 (HEC-RAS 5.0.7)

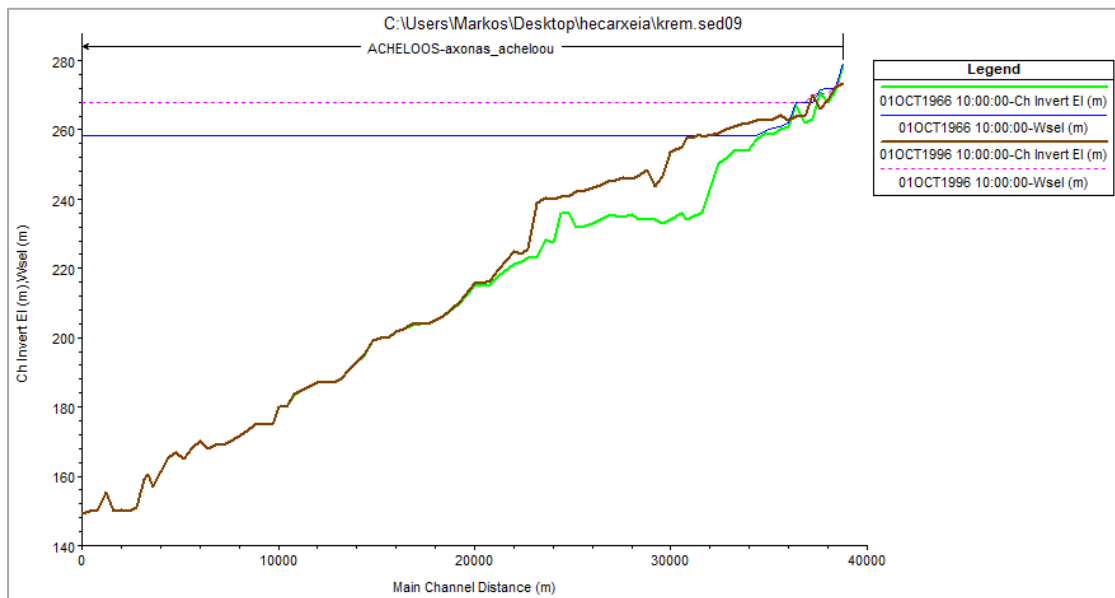


**Figure A.6:** Evolution of the deposits at Kremasta reservoir (Acheloo part) from 1966 to 1996 (HEC-RAS 5.0.7)

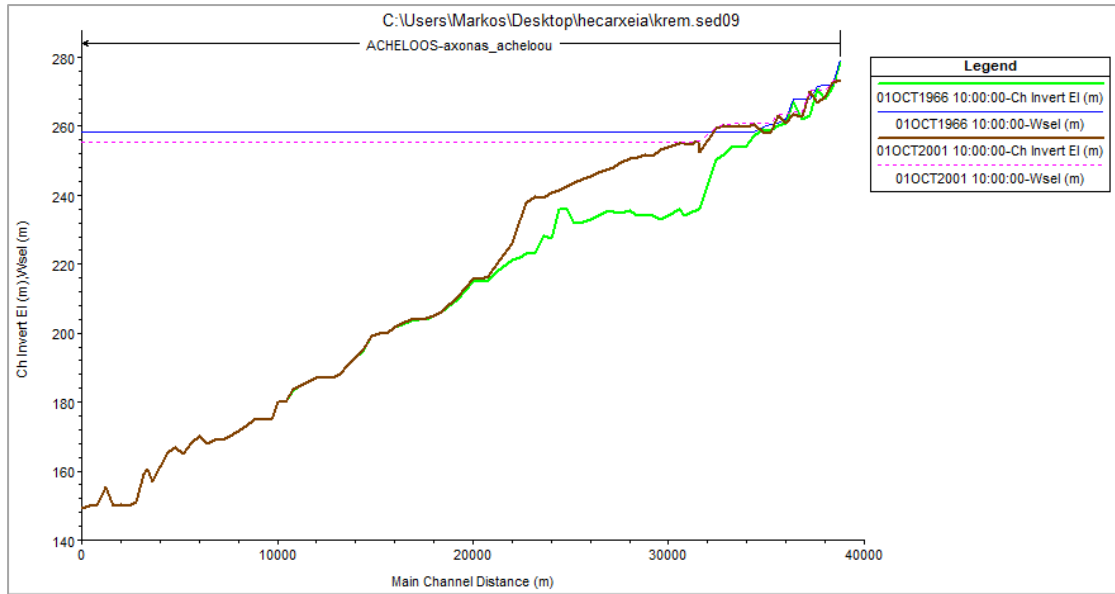


**Figure A.7:** Evolution of the deposits at Kremasta reservoir (Acheloo part) from 1966 to 2001 (HEC-RAS 5.0.7)

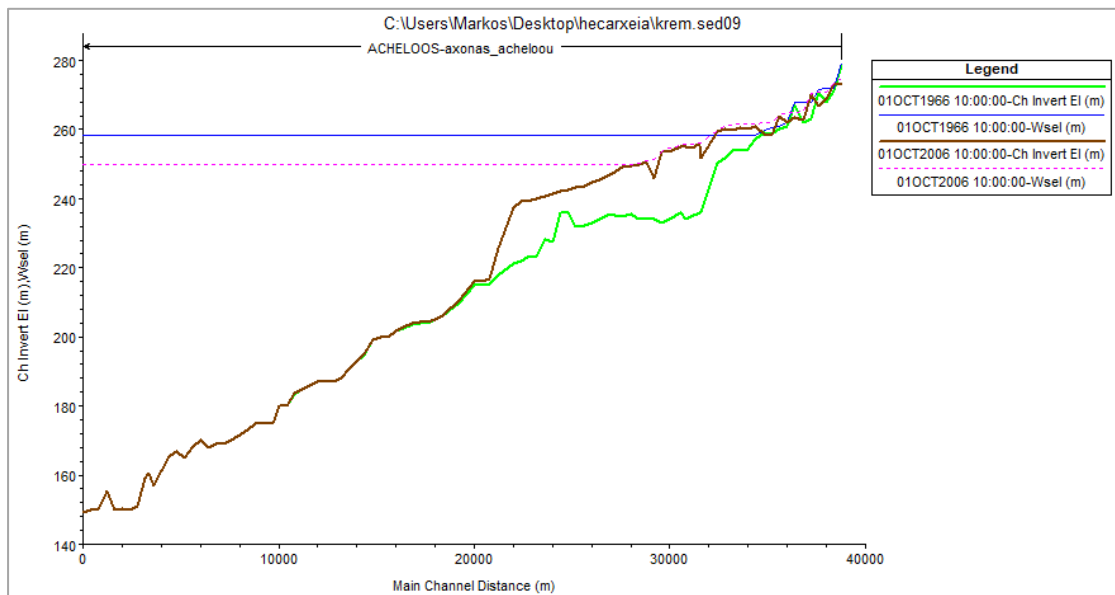


**Figure A.8:** Evolution of the deposits at Kremasta reservoir (Acheloo part) from 1966 to 2006 (HEC-RAS 5.0.7)

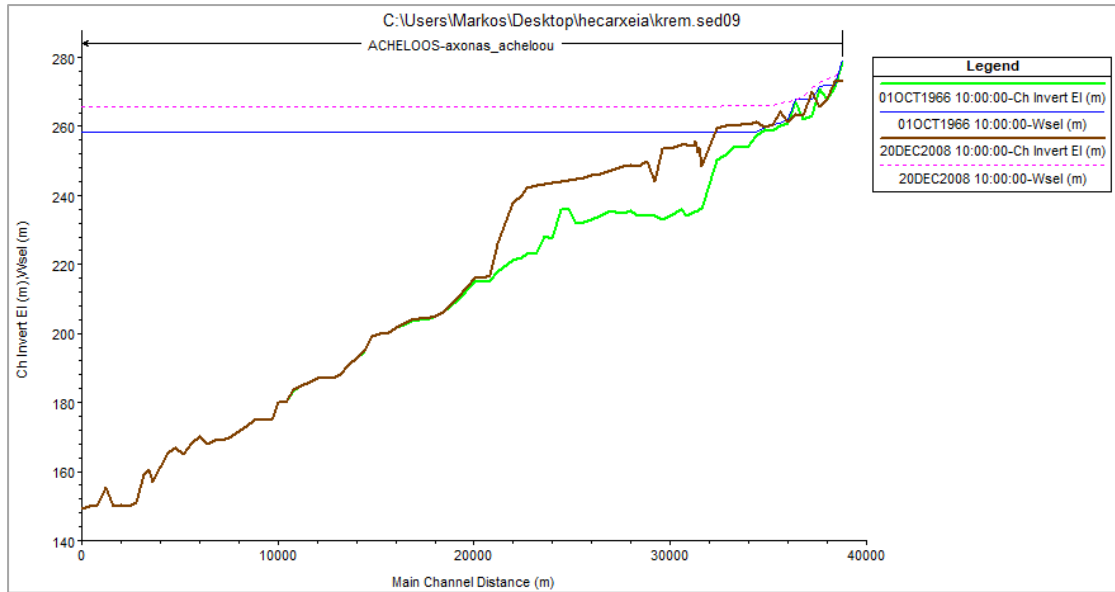


**Figure A.9:** Evolution of the deposits at Kremasta reservoir (Achelous part) from 1966 to 2008 (HEC-RAS 5.0.7)

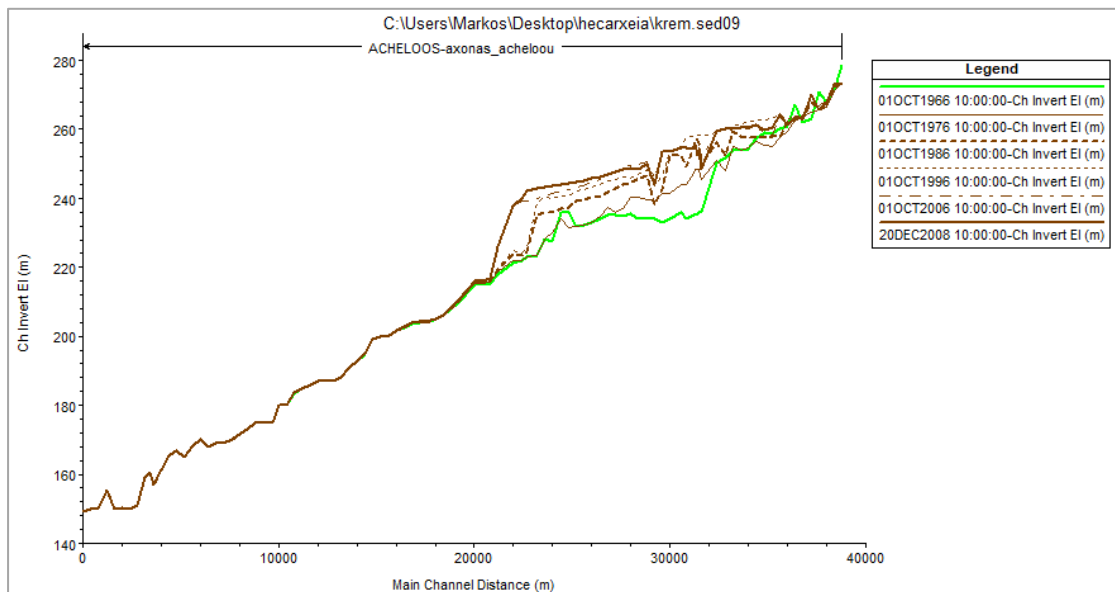


**Figure A.10:** Cumulative diagram of the bed changes from 1966 to 2008 (HEC-RAS 5.0.7)

**Table A.5:** Hydrodynamic characteristics of the first part of the reservoir at the day with the highest inflow (1136,7 m<sup>3</sup>/s) (HEC-RAS 5.0.7)

Reach	River Sta	Profile	Q Total (m <sup>3</sup> /s)	Min Ch El (m)	W.S. Elev (m)	Crit W.S. (m)	E.G. Elev (m)	E.G. Slope (m/m)	Vel Chnl (m/s)	Flow Area (m <sup>2</sup> )	Top Width (m)	Froude # Chl
axonas_achelooou	39200	05Dec1976 1000	1136.70	273.43	280.76	280.76	282.20	0.006859	5.32	213.74	74.84	1.00
axonas_achelooou	38800	05Dec1976 1000	1136.70	273.08	278.64		278.93	0.003096	2.37	478.76	325.40	0.63
axonas_achelooou	38400	05Dec1976 1000	1136.70	267.03	278.11		278.33	0.000836	2.08	546.68	153.77	0.35
axonas_achelooou	38000	05Dec1976 1000	1136.70	265.79	275.34	275.34	277.41	0.006748	6.38	178.19	43.74	1.01
axonas_achelooou	37600	05Dec1976 1000	1136.70	267.09	273.05		273.19	0.001155	1.67	681.09	369.04	0.39
axonas_achelooou	37200	05Dec1976 1000	1136.70	262.51	272.79		272.91	0.000455	1.57	724.67	213.47	0.27
axonas_achelooou	36800	05Dec1976 1000	1136.70	262.59	271.11		272.40	0.003540	5.04	225.56	39.29	0.67
axonas_achelooou	36400	05Dec1976 1000	1136.70	259.61	269.45		270.68	0.005222	4.92	230.88	64.91	0.83
axonas_achelooou	36000	05Dec1976 1000	1136.70	257.26	268.20		269.41	0.002113	4.88	232.97	24.43	0.50
axonas_achelooou	35600	05Dec1976 1000	1136.70	254.44	267.20		268.51	0.002347	5.08	223.73	22.31	0.51
axonas_achelooou	35200	05Dec1976 1000	1136.70	254.99	266.06		267.50	0.002644	5.32	213.84	22.63	0.55
axonas_achelooou	34800	05Dec1976 1000	1136.70	256.49	263.10	263.10	265.80	0.006548	7.27	156.26	29.01	1.00
axonas_achelooou	34400	05Dec1976 1000	1136.70	254.09	262.55		263.80	0.002345	4.95	229.75	28.82	0.56
axonas_achelooou	34000	05Dec1976 1000	1136.70	250.15	262.74		263.16	0.000537	2.89	393.39	36.23	0.28
axonas_achelooou	33600	05Dec1976 1000	1136.70	255.11	262.10		262.75	0.002356	3.56	319.14	91.12	0.61
axonas_achelooou	33200	05Dec1976 1000	1136.70	246.78	259.34		261.37	0.004281	6.31	180.13	17.81	0.63
axonas_achelooou	32800	05Dec1976 1000	1136.70	250.81	256.43	256.43	259.10	0.007362	7.24	157.09	29.40	1.00
axonas_achelooou	32000	05Dec1976 1000	1136.70	232.96	255.31		255.97	0.001136	3.61	314.65	19.65	0.29
axonas_achelooou	31900.0*	05Dec1976 1000	1136.70	251.26	255.39		255.77	0.001133	2.75	412.63	101.12	0.44
axonas_achelooou	31800.0*	05Dec1976 1000	1136.70	251.06	255.37		255.65	0.000769	2.34	486.45	113.06	0.36
axonas_achelooou	31700.0*	05Dec1976 1000	1136.70	251.06	255.34		255.56	0.000623	2.11	539.41	127.08	0.33
axonas_achelooou	31600	05Dec1976 1000	1136.70	248.08	253.57	253.16	255.28	0.004978	5.80	196.15	43.75	0.87
axonas_achelooou	31200	05Dec1976 1000	1136.70	242.17	253.74		254.06	0.001076	2.52	451.83	115.05	0.41
axonas_achelooou	30934.19	05Dec1976 1000	1136.70	243.48	253.27		253.80	0.000774	3.23	352.09	37.58	0.34
axonas_achelooou	30400	05Dec1976 1000	1136.70	241.13	252.85		253.27	0.001140	2.88	394.27	86.62	0.43
axonas_achelooou	30000	05Dec1976 1000	1136.70	242.08	252.43		252.71	0.001492	2.33	487.71	190.68	0.47
axonas_achelooou	29600	05Dec1976 1000	1136.70	241.16	252.00		252.19	0.001015	1.91	594.25	237.39	0.39
axonas_achelooou	29200	05Dec1976 1000	1136.70	241.34	251.82		251.92	0.000414	1.43	797.25	255.12	0.26
axonas_achelooou	28800	05Dec1976 1000	1136.70	241.61	251.78		251.83	0.000100	0.94	1208.26	250.15	0.14
axonas_achelooou	28400	05Dec1976 1000	1136.70	240.79	251.80		251.81	0.000008	0.34	3322.92	466.32	0.04
axonas_achelooou	28000	05Dec1976 1000	1136.70	237.27	251.80		251.81	0.000003	0.26	4336.92	465.42	0.03
axonas_achelooou	27600	05Dec1976 1000	1136.70	235.99	251.80		251.81	0.000002	0.21	5403.04	494.22	0.02
axonas_achelooou	27200	05Dec1976 1000	1136.70	237.46	251.80		251.81	0.000001	0.15	7691.21	644.66	0.01
axonas_achelooou	26800	05Dec1976 1000	1136.70	234.72	251.78		251.80	0.000015	0.68	1664.68	126.10	0.06
axonas_achelooou	26400	05Dec1976 1000	1136.70	233.01	251.78		251.79	0.000006	0.45	2545.77	184.77	0.04

**Table A.6:** Hydrodynamic characteristics of the second part of the reservoir at the day with the highest inflow (1136,7 m<sup>3</sup>/s) (HEC-RAS 5.0.7)

Reach	River Sta	Profile	Q Total (m <sup>3</sup> /s)	Min Ch El (m)	W.S. Elev (m)	Crit W.S. (m)	E.G. Elev (m)	E.G. Slope (m/m)	Vel Chnl (m/s)	Flow Area (m <sup>2</sup> )	Top Width (m)	Froude # Chl
axonas_acheloo	26000	05Dec1976 1000	1136.70	232.20	251.78		251.79	0.000006	0.47	2433.89	165.72	0.04
axonas_acheloo	25600	05Dec1976 1000	1136.70	231.96	251.77		251.79	0.000012	0.63	1814.70	139.73	0.06
axonas_acheloo	25200	05Dec1976 1000	1136.70	231.51	251.43		251.74	0.000393	2.49	456.31	44.70	0.25
axonas_acheloo	24800	05Dec1976 1000	1136.70	234.18	251.43		251.60	0.000172	1.87	608.45	55.04	0.18
axonas_acheloo	24400	05Dec1976 1000	1136.70	229.91	251.47		251.54	0.000044	1.14	1000.45	69.82	0.10
axonas_acheloo	24000	05Dec1976 1000	1136.70	228.12	251.50		251.52	0.000011	0.66	1722.25	101.15	0.05
axonas_acheloo	23600	05Dec1976 1000	1136.70	223.49	251.50		251.51	0.000004	0.48	2392.43	117.22	0.03
axonas_acheloo	23111.09	05Dec1976 1000	1136.70	222.97	251.49		251.51	0.000006	0.53	2128.69	114.52	0.04
axonas_acheloo	22800	05Dec1976 1000	1136.70	222.08	251.50		251.51	0.000002	0.37	3054.78	141.90	0.03
axonas_acheloo	22400	05Dec1976 1000	1136.70	221.84	251.50		251.50	0.000003	0.37	3034.43	150.01	0.03
axonas_acheloo	21600	05Dec1976 1000	1136.70	218.65	251.50		251.50	0.000000	0.03	34623.84	2019.96	0.00
axonas_acheloo	21200	05Dec1976 1000	1136.70	215.59	251.50		251.50	0.000000	0.02	54240.55	1868.49	0.00
axonas_acheloo	20800	05Dec1976 1000	1136.70	215.28	251.50		251.50	0.000000	0.02	70637.12	2486.34	0.00
axonas_acheloo	20400	05Dec1976 1000	1136.70	215.29	251.50		251.50	0.000000	0.02	65194.16	2067.59	0.00
axonas_acheloo	19600	05Dec1976 1000	1136.70	210.13	251.50		251.50	0.000000	0.02	55994.07	1760.61	0.00
axonas_acheloo	18800	05Dec1976 1000	1136.70	206.01	251.50		251.50	0.000000	0.02	48247.01	1927.12	0.00
axonas_acheloo	18400	05Dec1976 1000	1136.70	205.03	251.50		251.50	0.000000	0.04	31469.36	1518.02	0.00
axonas_acheloo	18000	05Dec1976 1000	1136.70	204.04	251.50		251.50	0.000000	0.02	54756.62	1809.97	0.00
axonas_acheloo	17600	05Dec1976 1000	1136.70	204.04	251.50		251.50	0.000000	0.02	54965.41	1693.20	0.00
axonas_acheloo	17200	05Dec1976 1000	1136.70	203.77	251.50		251.50	0.000000	0.02	51635.91	1787.26	0.00
axonas_acheloo	16800	05Dec1976 1000	1136.70	202.62	251.50		251.50	0.000000	0.03	36210.43	1372.49	0.00
axonas_acheloo	16400	05Dec1976 1000	1136.70	201.67	251.50		251.50	0.000000	0.04	31908.19	1060.31	0.00
axonas_acheloo	16000	05Dec1976 1000	1136.70	200.02	251.50		251.50	0.000000	0.03	38195.29	979.87	0.00
axonas_acheloo	15600	05Dec1976 1000	1136.70	200.01	251.50		251.50	0.000000	0.03	33617.82	1050.40	0.00
axonas_acheloo	15200	05Dec1976 1000	1136.70	199.06	251.50		251.50	0.000000	0.04	30704.16	947.09	0.00
axonas_acheloo	14800	05Dec1976 1000	1136.70	194.95	251.50		251.50	0.000000	0.03	34678.59	971.91	0.00
axonas_acheloo	14400	05Dec1976 1000	1136.70	193.01	251.50		251.50	0.000000	0.05	24801.80	690.94	0.00
axonas_acheloo	14000	05Dec1976 1000	1136.70	190.85	251.50		251.50	0.000000	0.18	6363.14	228.64	0.01
axonas_acheloo	13600	05Dec1976 1000	1136.70	188.00	251.50		251.50	0.000000	0.11	10535.40	256.59	0.01
axonas_acheloo	13200	05Dec1976 1000	1136.70	187.12	251.50		251.50	0.000000	0.16	7179.11	191.72	0.01
axonas_acheloo	12800	05Dec1976 1000	1136.70	187.00	251.50		251.50	0.000000	0.15	7447.88	188.63	0.01
axonas_acheloo	12400	05Dec1976 1000	1136.70	187.00	251.50		251.50	0.000000	0.15	7643.41	175.13	0.01
axonas_acheloo	12000	05Dec1976 1000	1136.70	185.90	251.50		251.50	0.000000	0.02	56602.86	1811.27	0.00
axonas_acheloo	11600	05Dec1976 1000	1136.70	184.85	251.50		251.50	0.000000	0.01	45645.90	3107.99	0.00
axonas_acheloo	11200	05Dec1976 1000	1136.70	183.56	251.50		251.50	0.000000	0.01	38419.10	2651.58	0.00
axonas_acheloo	10800	05Dec1976 1000	1136.70	180.02	251.50		251.50	0.000000	0.01	39161.90	3100.40	0.00
axonas_acheloo	10400	05Dec1976 1000	1136.70	180.01	251.50		251.50	0.000000	0.01	18727.50	2501.51	0.00
axonas_acheloo	10094.9	05Dec1976 1000	1136.70	175.01	251.50		251.50	0.000000	0.01	35469.80	2623.77	0.00
axonas_acheloo	9600	05Dec1976 1000	1136.70	174.83	251.50		251.50	0.000000	0.01	30613.10	2333.38	0.00
axonas_acheloo	9200	05Dec1976 1000	1136.70	174.86	251.50		251.50	0.000000	0.01	15168.90	2085.94	0.00
axonas_acheloo	8800	05Dec1976 1000	1136.70	173.04	251.50		251.50	0.000000	0.01	13321.40	2165.30	0.00
axonas_acheloo	8400	05Dec1976 1000	1136.70	171.45	251.50		251.50	0.000000	0.01	10942.20	2106.70	0.00
axonas_acheloo	8000	05Dec1976 1000	1136.70	170.00	251.50		251.50	0.000000	0.01	14804.10	2222.32	0.00
axonas_acheloo	7600	05Dec1976 1000	1136.70	169.00	251.50		251.50	0.000000	0.02	75279.65	1198.66	0.00
axonas_acheloo	7200	05Dec1976 1000	1136.70	169.00	251.50		251.50	0.000000	0.02	58006.13	964.58	0.00
axonas_acheloo	6800	05Dec1976 1000	1136.70	168.00	251.50		251.50	0.000000	0.01	78744.23	1313.08	0.00
axonas_acheloo	6400	05Dec1976 1000	1136.70	170.00	251.50		251.50	0.000000	0.02	70818.84	1301.53	0.00
axonas_acheloo	6000	05Dec1976 1000	1136.70	168.11	251.50		251.50	0.000000	0.01	78525.34	1345.95	0.00
axonas_acheloo	5600	05Dec1976 1000	1136.70	164.91	251.50		251.50	0.000000	0.02	65917.57	1488.48	0.00
axonas_acheloo	5200	05Dec1976 1000	1136.70	166.72	251.50		251.50	0.000000	0.01	93474.64	1546.74	0.00
axonas_acheloo	4800	05Dec1976 1000	1136.70	165.19	251.50		251.50	0.000000	0.01	36406.80	2590.92	0.00
axonas_acheloo	4400	05Dec1976 1000	1136.70	161.16	251.50		251.50	0.000000	0.01	75822.06	1748.91	0.00
axonas_acheloo	4000	05Dec1976 1000	1136.70	157.08	251.50		251.50	0.000000	0.01	66233.60	3742.87	0.00
axonas_acheloo	3797.35	05Dec1976 1000	1949.20	160.70	251.50		251.50	0.000000	0.01	55441.90	3348.29	0.00
axonas_acheloo	3547.46	05Dec1976 1000	1949.20	159.19	251.50		251.50	0.000000	0.01	125689.60	5005.65	0.00
axonas_acheloo	3200	05Dec1976 1000	1949.20	151.00	251.50		251.50	0.000000	0.01	52101.70	2524.93	0.00
axonas_acheloo	2800	05Dec1976 1000	1949.20	150.00	251.50		251.50	0.000000	0.03	74686.09	1323.31	0.00
axonas_acheloo	2400	05Dec1976 1000	1949.20	150.17	251.50		251.50	0.000000	0.09	22027.74	486.33	0.00
axonas_acheloo	2000	05Dec1976 1000	1949.20	150.00	251.50		251.50	0.000000	0.11	18247.27	329.29	0.00
axonas_acheloo	1600	05Dec1976 1000	1949.20	155.37	251.50		251.50	0.000000	0.12	16832.95	347.25	0.01
axonas_acheloo	1200	05Dec1976 1000	1949.20	149.94	251.50		251.50	0.000000	0.08	22990.04	383.75	0.00
axonas_acheloo	800	05Dec1976 1000	1949.20	150.00	251.50		251.50	0.000000	0.08	24388.97	454.32	0.00
axonas_acheloo	400	05Dec1976 1000	1949.20	149.10	251.50	154.44	251.50	0.000000	0.09	21365.94	404.10	0.00